5   *WATER QUALITY TRANSPORT EXAMPLES*

In this chapter, we are to present a total of 15 water quality transport problems: six examples for one-dimensional transport, four examples for two-dimensional transport, and five examples for three-dimensional transport.

5.1   One-Dimensional Examples

Six examples are used in this section. Two examples are compared with analytical solutions to verify the model and to emphasize the need of implementing various numerical options and coupling strategies to deal with different types of problems for different application circumstances. A hypothetical example with complexation, sorption and dissolution reactions is employed to demonstrate the capability of the model to handle complex reaction network involving both kinetic and equilibrium reactions. Two more example problems are employed to demonstrate the design capability of the model, in simulating sediment and chemical transport, chemicals in both mobile water phase and immobile water phase, and both kinetic and equilibrium reactions.

5.1.1   Comparison of Options to Solve Advective-dispersive Transport Equations

This example involves the transient simulation of chemical transport in a horizontally 50 km-long river/stream containing a uniform width of 10 m. The domain of interest is discretized into 1000 equal size elements (50 m each). We assume the water depth is 5 m and river/stream flow velocity is 0.4 m/s throughout the river/stream. There are two species, a dissolved chemical in the mobile water phase CMW and a dissolved chemical in the immobile water phase CIMW. The phase densities associated with both species are assumed to be 1.0. CMW and CIMW are considered to undergo the following equilibrium reaction.

$$\text{CMW} \rightleftharpoons \text{CIMW} \quad K_{eq} = 0.8 \qquad\qquad \textbf{(5.1.1)}$$

Initially, no chemical exists in the domain of interest. Variable boundary conditions are applied to both the upstream and downstream boundary nodes for mobile species CMW. At the upstream boundary node, the incoming concentration of CMW is 1 g/m^3. The molecular diffusion coefficient is assumed to be zero. Three cases with different dispersivities of 3.125 m, 62.5 m, and 1000 m (grid Peclet number Pe = $\Delta x/\alpha L$ = 16, 0.8 and 0.05 for case 1, 2, and 3, respectively) were considered. Simulations were performed with fixed time step size of 36 s (grid Courant number Cr = $V\Delta t/\Delta x$ = 0.288) and total simulation time of 1800 s. For case 2, two more simulations were performed with different time step size of 120 s and 180 s (Cr = 0.96 and 1.44) in case 4 and 5, respectively.

Using the same coupling strategy, the fully-implicit scheme, to deal with reactive chemistry, simulations were performed with the five numerical options to solve the advective-dispersive equation. In Figure 5.1-1, simulation results of CMW in cases 1 through 3 are compared with the analytical solutions given by Lindstrom and Freed, 1967. R^2 values based on simulations and analytical results are also calculated and listed in the figure. In Figure 5.1-2, simulation results of CMW in cases 4 and 5 are plotted. R^2 and CPU time are also listed in the figure.
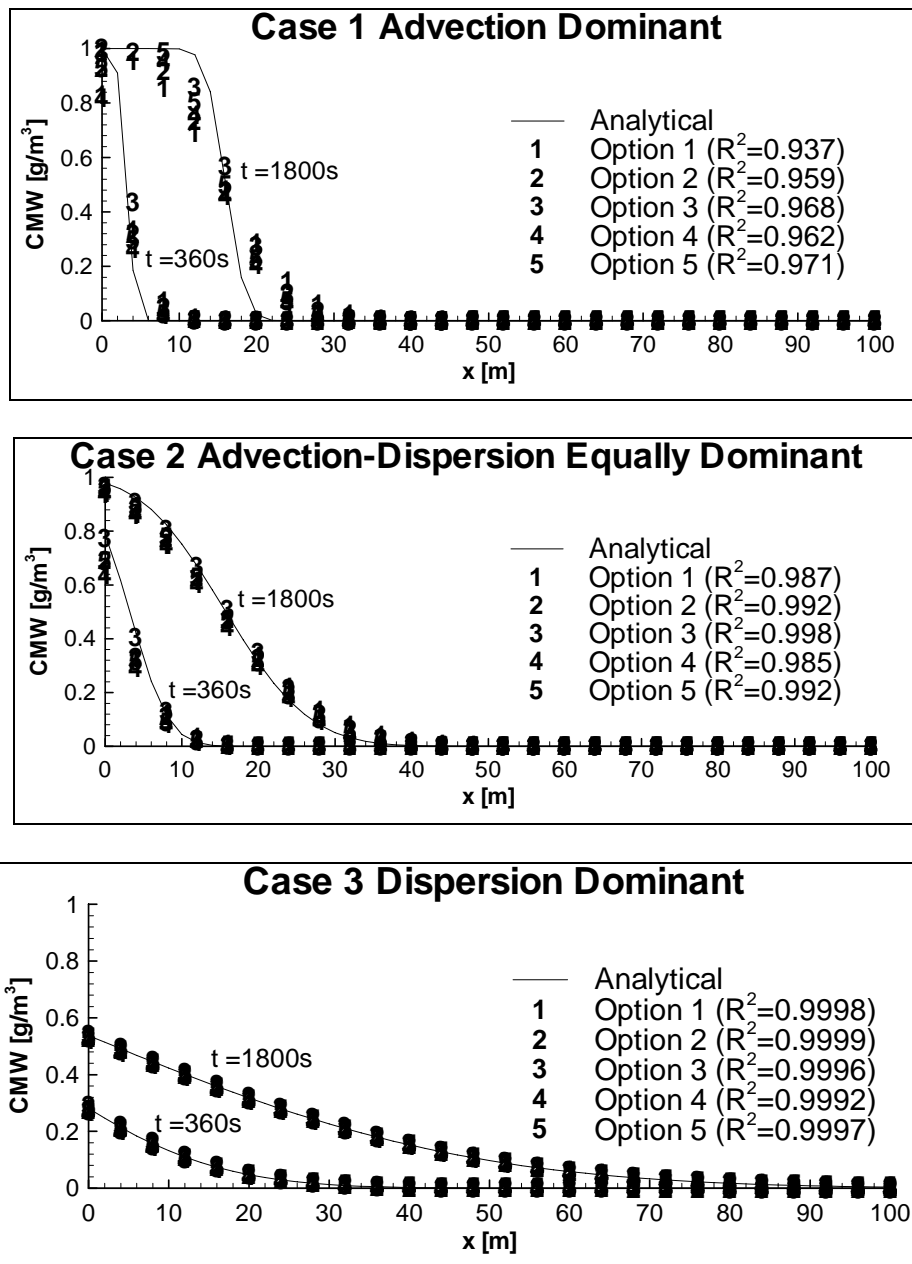
Fig. 5.1-1. Concentration Profiles of CMW in Cases 1, 2, and 3 of Example 5.1

It is seen that: (1) for advection dominant cases, Options 3 through 5 give more accurate simulation

than the other two; (2) for advection-dispersion equally-dominant cases, all five options yield almost same accurate results with Option 3 giving slightly better results than Option 2 and 5, and Option 2 and 5 yielding slightly better results than Option 1 and 4; (3) for dispersion dominant cases, all five options give approximately the same accurate simulation but with Option 1 and 2 giving slightly better results than the other three. Therefore, for advection dominant problems for research applications when accuracy is the primary concern, Options 3 through 5 are preferred. However, for dispersion dominant problems for research applications, Options 1 and 2 may be preferred. For practical applications when the efficiency is the primary concern, Option 3 is preferred under all transport conditions because it gives the most efficient computation in term of CPU time. The efficiency results from the fact that one can use a much larger time step size without having to worry about the limitation of time-step sizes imposed by advective transport. As shown in Figure 5.1-2, when the Courant number increases from 0.96 to1.44, Option 1 and 2 were not able to yield convergent solutions. Although, all of the other three options gave less accuracy results, only Option 3 yields accurate enough simulation. Since the time step size is enlarged, the total number of simulation time steps decreased, resulting in less CPU time.

Case 4 Time Step Size = 120s Courant Number = 0.96

Analytical
1 Option 1 (R^2=0.981 & CPU time=16s)
2 Option 2 (R^2=0.988 & CPU time=16s)
3 Option 3 (R^2=0.997 & CPU time=16s)
4 Option 4 (R^2=0.974 & CPU time=16s)
5 Option 5 (R^2=0.984 & CPU time=16s)

t =1800s
t =360s

Case 5 Time Step Size = 180s Courant Number = 1.44

Analytical
Option 1 (no convergent solution)
Option 2 (no convergent solution
3 Option 3 (R^2=0.992 & CPU time=11s)
4 Option 4 (R^2=0.962 & CPU time=11s)
5 Option 5 (R^2=0.974 & CPU time=11s)

t =1800s
t =360s

Fig. 5.1-2. Concentration Profiles of CMW in Cases 4 and 5 of Example 5.1

5.1.2 Comparison of Coupling Strategies to Deal with Reactive Chemistry

In this example, a horizontally 4 km-long river/stream containing a uniform width of 10 m is considered. The domain is discretized into 400 equal size elements (each 10 m). We assume the water depth is 2 m and river/stream flow velocity is 1.0 m/s throughout the river/stream. There are two species, a dissolved chemical in the mobile water phase CMW and a dissolved chemical in the

immobile water phase CIMW. The phase densities associated with both species are assumed to be 1.0. CMW and CIMW are considered to undergo the following reaction.

$$\text{Case1}: \text{CMW} \rightleftharpoons \text{CIMW} \quad K_{eq} = 1.0 \tag{5.1.2}$$

$$\text{Case2}: \text{CMW} \rightleftharpoons \text{CIMW} \quad K_f = 3h^{-1}, K_b = 3h^{-1} \tag{5.1.3}$$

$$\text{Case3}: \text{CMW} \rightleftharpoons \text{CIMW} \quad K_f = 1.0 \times 10^{-2}h^{-1}, K_b = 1.0 \times 10^{-2}h^{-1} \tag{5.1.4}$$
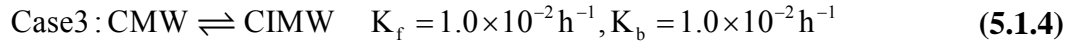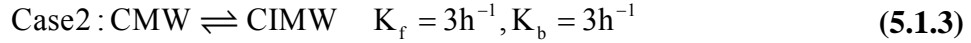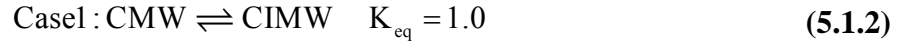
Initially, no chemical exists in the domain of interest. Dirichelet and Variable boundary conditions are applied to the upstream and downstream boundary nodes for mobile species CMW, respectively. At the upstream boundary node, the concentration of CMW is 1 mg/kg. Simulations were performed with fixed time step sizes of 360 s and total simulation time of 1800 s. The molecular diffusion coefficient and longitudinal dispersivity are assumed to be zero. Option 3 is used to solve the transport equations. With the grid size, time-step size and model parameters given above, the mesh Courant numbers are $Cr = V\Delta t/\Delta x = 36$. When the fully-implicit scheme with E_n^m written in terms of $(E_n^m/E_n) \cdot E_n$ is applied to Case 1, the mesh Courant number is $Cr = V/(1+K_{eq}) \cdot (\Delta t/\Delta x) = 18$. With integral mesh Courant numbers, the numerical error is zero in solving the advective transport equation, thus numerical errors due to coupling strategies are isolated.

Using the same numerical option, Option 3 – the Modified LE approach, to solve the advective-dispersive equation, simulations were performed with three coupling strategies to deal with the reactive chemistry. In Figure 5.1-3, simulation results of CMW in Case 1, 2, and 3 are compared with the analytical solutions (Quezada et al, 2004). It is seen that the fully-implicit strategy gives accurate enough solution for all three cases although solution for Case 2 is less accurate than the other two. However, simulation accuracy using the mixed predictor-corrector/operator-splitting and operator-splitting strategies varies for the three cases. For Case 1, in which an equilibrium reaction involves, calculation results of these two strategies are far from the analytical values. For Case 2, in which a kinetic reaction with faster rate (compared to Case 3) involves, simulations of these two strategies are close to the exact solution although less accurate than the fully-implicit strategy. For Case 3, in which a kinetic reaction with slower rate (compared to Case 2) involves, accurate simulations are obtained with these two strategies.

For problems with reaction network involving only kinetic reactions with slower rates, all the three strategies can generate accurate solution. Because the fully-implicit strategy takes more time to achieve convergent simulations due to iteration between the advective-dispersive transport step and the reactive chemistry step, the other two strategies are recommended under this situation. However, for problems with reaction network involving equilibrium reactions, the fully-implicit strategy is recommended for both research and practical applications because the other two strategies simply cannot give enough accurate simulations. For problems involving only kinetic reactions with faster rates, the fully-implicit strategy is recommended when accuracy is the primary concern; on the other hand, the mixed predictor-corrector/operator splitting strategy and the operator splitting strategy are recommended for practical applications when efficiency is the primary concern.
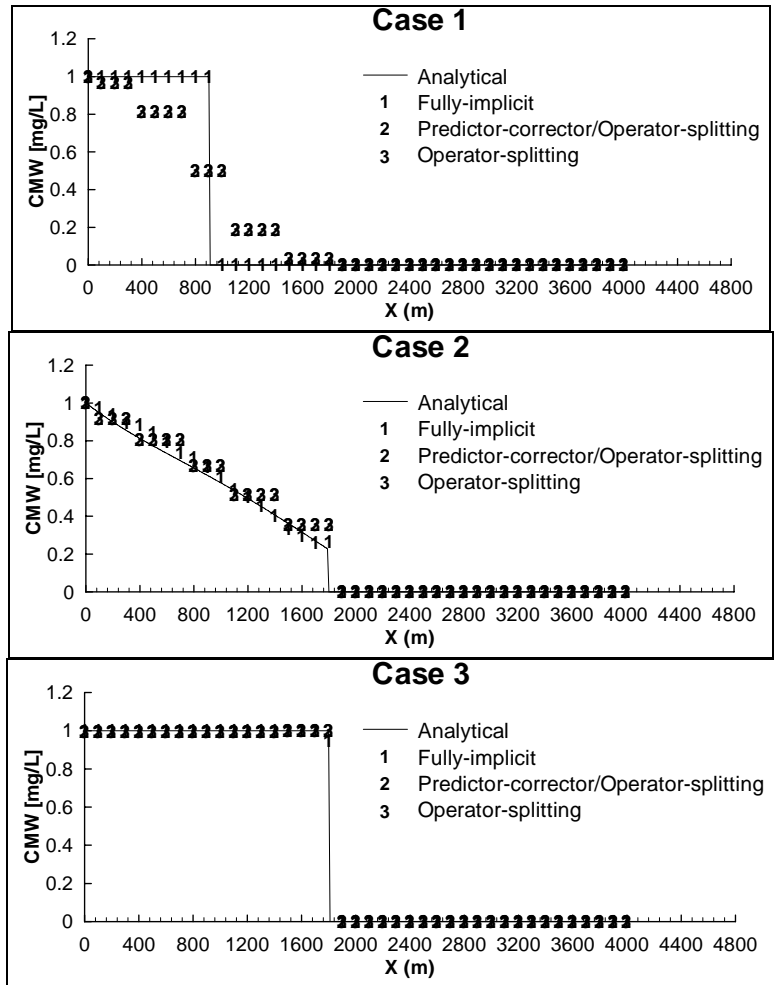
Fig. 5.1-3. Concentration Profiles of CMW in Cases 1, 2, and 3 of Example 5.2

5.1.3 Chemical Transport with Complexation, Sorption and Dissolution reactions

Reactive chemical transport, incorporating hypothetical aqueous complexation, sorption, and precipitate dissolution reactions in a system of mixed equilibrium and kinetic reactions, is simulated in this example. A horizontally 20 km-long river/stream containing a uniform width of 20 m is considered. The domain is discretized into 100 equal size elements (200 m each). To focus on transport, we assume water depth is 2 m and river/stream velocity is 1 m/s.

Forty-one chemical species are taken account, including 29 dissolved species in the mobile water phase ($C_1 \sim C_{27}$, C_{29}, and C_{30}), 1 bed precipitate (M), and 11 particulates sorbed onto bed sediment ($S_1 \sim S_8$, site-C_6, site-C_{29} and site-C_{30}). As shown in Table 5.1-1, the complex reaction network involves 33 reactions: including 1 dissolution reaction R1; 1 sorbing site forming reaction R2; 22 aqueous complexation reactions R3~R24; and 9 sorption reactions R25~R33.

Table 5.1-1   Reaction Network for Example 5.1-3

Reaction	Reaction parameters	No.
$M \leftrightarrow C_1 - 3C_2$	Rate= 5.787e-7M	R1
$M \leftrightarrow S_1$	$0.0047M = S_1 + S_2 + S_3 + S_4 + S_5 + S_6 + S_7 + S_8$	R2
$C_3 \leftrightarrow C_4 + C_5$	Log K_3^e = -17.97	R3
$C_6 + C_5 \leftrightarrow C_7$	Log K_4^e = 12.32	R4
$C_2 + C_5 + C_6 \leftrightarrow C_8$	Log K_5^e = 15.93	R5
$C_6 \leftrightarrow C_2 + C_9$	Log K_6^e = -12.6	R6
$C_1 + C_5 \leftrightarrow C_{10}$	Log K_7^e = 22.57	R7
$C_1 + C_2 + C_5 \leftrightarrow C_{11}$	Log K_8^e = 29.08	R8
$C_1 + C_5 \leftrightarrow C_2 + C_{12}$	Log K_9^e = 19.65	R9
$C_1 + C_5 \leftrightarrow 2\ C_2 + C_{13}$	Log K_{10}^e = -36.3	R10
$C_1 \leftrightarrow C_2 + C_{14}$	Log K_{11}^e = -2.19	R11
$C_1 \leftrightarrow 2C_2 + C_{15}$	Log K_{12}^e = -5.67	R12
$C_1 \leftrightarrow 3C_2 + C_{16}$	Log K_{13}^e = -13.6	R13
$C_1 \leftrightarrow 4C_2 + C_{17}$	Log K_{14}^e = -21.6	R14
$2C_1 \leftrightarrow 2C_2 + C_{18}$	Log K_{15}^e = -2.95	R15
$C_2 + C_4 + C_5 \leftrightarrow C_{19}$	Log K_{16}^e = 21.4	R16
$C_4 \leftrightarrow C_2 + C_{20}$	Log K_{17}^e = -9.67	R17
$C_4 \leftrightarrow 2C_2 + C_{21}$	Log K_{18}^e = -18.76	R18
$C_4 \leftrightarrow 3C_2 + C_{22}$	Log K_{19}^e = -32.23	R19
$C_2 + C_5 \leftrightarrow C_{23}$	Log K_{20}^e = 11.03	R20
$2C_2 + C_5 \leftrightarrow C_{24}$	Log K_{21}^e = 17.78	R21
$3C_2 + C_5 \leftrightarrow C_{25}$	Log K_{22}^e = 20.89	R22
$4C_2 + C_5 \leftrightarrow C_{26}$	Log K_{23}^e = 23.1	R23
$\leftrightarrow C_2 + C_{27}$	Log K_{24}^e = -14.0	R24
$S_1 \leftrightarrow S_2 + C_2$	Log K_{25}^e = -11.6	R25
$S_1 + C_2 \leftrightarrow S_3$	Log K_{26}^e = 5.6	R26
$S_1 + 3C_2 + C_5 \leftrightarrow S_4$	Log K_{27}^e = 30.48	R27
$S_1 + C_1 + C_2 + C_5 \leftrightarrow S_5$	Log K_{28}^e = 37.63	R28
$S_1 + C_2 + C_4 + C_5 \leftrightarrow S_6$	Log K_{29}^f = 25.0, Log K_{29}^b = -3.49	R29
$S_1 - C_2 + C_4 \leftrightarrow S_7$	Log K_{30}^f = -5.99, Log K_{30}^b = -3.30	R30
$S_1 + C_2 + C_5 + C_6 \leftrightarrow S_8$	Log K_{31}^f = 20.0, Log K_{31}^b = -3.81	R31
$C_{29} + 2\text{Site-}C_{30} \leftrightarrow \text{Site-}C_{29} + 2C_{30}$	Rate=$10^{-5.75}\ C_{29} \cdot (a_{30}\text{Site-}C_{30})^2 - 10^{-5.5} a_{29}\text{Site-}C_{29} \cdot C_{30}^2$ a_{29}= Site-C_{29}/(Site-C_6+Site-C_{29}+Site-C_{30}) a_{30}= Site-C_{30}/(Site-C_6+Site-C_{29}+Site-C_{30})	R32
$C_6 + 2\text{Site-}C_{30} \leftrightarrow \text{Site-}C_6 + 2C_{30}$	$a_6\text{Site-}C_6 \cdot C_{30}^2 = 10^{0.6} C_6 \cdot (a_{30}\text{Site-}C_{30})^2$ a_6= Site-C_6/(Site-C_6+Site-C_{29}+Site-C_{30}) a_{30}= Site-C_{30}/(Site-C_6+Site-C_{29}+Site-C_{30})	R33

Totally, we have 41 species, 28 equilibrium reactions, and 5 kinetic reactions. Thus, 13 kinetic-variable transport equations (Table 5.1-2) and 28 equilibrium reaction algebraic equations (Table 5.1-3) were set up through decomposition and solved for 41 species. Among the 13 kinetic-variables, the 6th, 7th, 9th, and 11th contain no mobile species and are thus not solved in the advective-dispersive transport step. Therefore, instead of solving 29 advective-dispersive transport equations for 29 mobile species in a primitive approach, we only need to solve 9 advective-dispersive transport equations for 9 kinetic-variables. Since the fast reaction is decoupled and not included in the transport equations any more, robust numerical integration can be achieved.

Table 5.1-2 Kinetic-variable Transport Equations for Example 5.1-3

Equations	No.
$\partial(AE_1)/\partial t + L(E_1{}^m) = A(-R31 + R32)$ where $E_1 = E_1{}^m = \rho_{C_6}C_6 + \rho_{C_7}C_7 + \rho_{C_8}C_8 + \rho_{C_9}C_9 + 0.5\rho_{C_{30}}C_{30}$	1
$\partial(AE_2)/\partial t + L(E_2{}^m) = A(-R29 - R30)$ where $E_2 = E_2{}^m = \rho_{C_3}C_3 + \rho_{C_4}C_4 + \rho_{C_{19}}C_{19} + \rho_{C_{20}}C_{20} + \rho_{C_{21}}C_{21} + \rho_{C_{22}}C_{22}$	2
$\partial(AE_3)/\partial t + L(E_3{}^m) = A(0.5R29 + 0.5R30 - R31)$ where $E_3 = -\rho_{C_1}C_1 - 0.5\rho_{C_2}C_2 - 1.5\rho_{C_4}C_4 + \rho_{C_5}C_5 + \rho_{C_7}C_7 + 0.5\rho_{C_8}C_8 + 0.5\rho_{C_9}C_9 - 0.5\rho_{C_{11}}C_{11}$ $+ 0.5\rho_{C_{12}}C_{12} + \rho_{C_{13}}C_{13} - 0.5\rho_{C_{14}}C_{14} + 0.5\rho_{C_{16}}C_{16} + \rho_{C_{17}}C_{17} - \rho_{C_{18}}C_{18} - \rho_{C_{19}}C_{19} - \rho_{C_{20}}C_{20}$ and $-0.5\rho_{C_{21}}C_{21} + 0.5\rho_{C_{23}}C_{23} - 0.5\rho_{C_{25}}C_{25} - \rho_{C_{26}}C_{26} + 0.5\rho_{C_{27}}C_{27} + 0.5\rho_M M + 0.5\rho_{S_1}S_1 + \rho_{S_2}S_2$ $E_3{}^m = -\rho_{C_1}C_1 - 0.5\rho_{C_2}C_2 - 1.5\rho_{C_4}C_4 + \rho_{C_5}C_5 + \rho_{C_7}C_7 + 0.5\rho_{C_8}C_8 + 0.5\rho_{C_9}C_9$ $-0.5\rho_{C_{11}}C_{11} + 0.5\rho_{C_{12}}C_{12} + \rho_{C_{13}}C_{13} - 0.5\rho_{C_{14}}C_{14} + 0.5\rho_{C_{16}}C_{16} + \rho_{C_{17}}C_{17} - \rho_{C_{18}}C_{18}$ $-\rho_{C_{19}}C_{19} - \rho_{C_{20}}C_{20} - 0.5\rho_{C_{21}}C_{21} + 0.5\rho_{C_{23}}C_{23} - 0.5\rho_{C_{25}}C_{25} - \rho_{C_{26}}C_{26} + 0.5\rho_{C_{27}}C_{27}$	3
$\partial(AE_4)/\partial t + L(E_4{}^m) = A(-R1 - 0.5R29 - 1.5R30 + R31)$ where $E_4 = \rho_{C_1}C_1 + 0.5\rho_{C_2}C_2 - 0.5\rho_{C_3}C_3 + 1.5\rho_{C_4}C_4 - 2\rho_{C_5}C_5 - 2\rho_{C_7}C_7 - 1.5\rho_{C_8}C_8 - 0.5\rho_{C_9}C_9$ $-\rho_{C_{10}}C_{10} - 0.5\rho_{C_{11}}C_{11} - 1.5\rho_{C_{12}}C_{12} - 2\rho_{C_{13}}C_{13} + 0.5\rho_{C_{14}}C_{14} - 0.5\rho_{C_{16}}C_{16} - \rho_{C_{17}}C_{17} + \rho_{C_{18}}C_{18}$ and $+\rho_{C_{20}}C_{20} + 0.5\rho_{C_{21}}C_{21} - 1.5\rho_{C_{23}}C_{23} - \rho_{C_{24}}C_{24} - 0.5\rho_{C_{25}}C_{25} - 0.5\rho_{C_{27}}C_{27} + 0.5\rho_M M + 0.5\rho_{S_1}S_1 + \rho_{S_3}S_3$ $E_4{}^m = \rho_{C_1}C_1 + 0.5\rho_{C_2}C_2 - 0.5\rho_{C_3}C_3 + 1.5\rho_{C_4}C_4 - 2\rho_{C_5}C_5 - 2\rho_{C_7}C_7 - 1.5\rho_{C_8}C_8$ $-0.5\rho_{C_9}C_9 - \rho_{C_{10}}C_{10} - 0.5\rho_{C_{11}}C_{11} - 1.5\rho_{C_{12}}C_{12} - 2\rho_{C_{13}}C_{13} + 0.5\rho_{C_{14}}C_{14} - 0.5\rho_{C_{16}}C_{16}$ $-\rho_{C_{17}}C_{17} + \rho_{C_{18}}C_{18} + \rho_{C_{20}}C_{20} + 0.5\rho_{C_{21}}C_{21} - 1.5\rho_{C_{23}}C_{23} - \rho_{C_{24}}C_{24} - 0.5\rho_{C_{25}}C_{25} - 0.5\rho_{C_{27}}C_{27}$	4
$\partial(AE_5)/\partial t + L(E_5{}^m) = AR1$ where $E_5 = \rho_{C_1}C_1 + \rho_{C_{10}}C_{10} + \rho_{C_{11}}C_{11} + \rho_{C_{12}}C_{12} + \rho_{C_{13}}C_{13} + \rho_{C_{14}}C_{14} + \rho_{C_{15}}C_{15} + \rho_{C_{16}}C_{16} + \rho_{C_{17}}C_{17} + 2\rho_{C_{18}}C_{18} + \rho_{S_5}S_5$ and $E_5{}^m = \rho_{C_1}C_1 + \rho_{C_{10}}C_{10} + \rho_{C_{11}}C_{11} + \rho_{C_{12}}C_{12} + \rho_{C_{13}}C_{13} + \rho_{C_{14}}C_{14} + \rho_{C_{15}}C_{15} + \rho_{C_{16}}C_{16} + \rho_{C_{17}}C_{17} + 2\rho_{C_{18}}C_{18}$	5
$\partial(AE_6)/\partial t + L(E_6{}^m) = AR29$ where $E_6 = \rho_{S_6}S_6$ and $E_6{}^m = 0$	6
$\partial(AE_7)/\partial t + L(E_7{}^m) = AR30$ where $E_7 = \rho_{S_7}S_7$ and $E_7{}^m = 0$	7
$\partial(AE_8)/\partial t + L(E_8{}^m) = A(-R1 - R29 - R31)$ where $E_8 = -\rho_{C_1}C_1 + \rho_{C_3}C_3 + \rho_{C_5}C_5 + \rho_{C_7}C_7 + \rho_{C_8}C_8 - \rho_{C_{14}}C_{14} - \rho_{C_{15}}C_{15} - \rho_{C_{16}}C_{16}$ and $-\rho_{C_{17}}C_{17} - 2\rho_{C_{18}}C_{18} + \rho_{C_{19}}C_{19} + \rho_{C_{23}}C_{23} + \rho_{C_{24}}C_{24} + \rho_{C_{25}}C_{25} + \rho_{C_{26}}C_{26} + \rho_{S_4}S_4$ $E_8{}^M = -\rho_{C_1}C_1 + \rho_{C_3}C_3 + \rho_{C_5}C_5 + \rho_{C_7}C_7 + \rho_{C_8}C_8 - \rho_{C_{14}}C_{14} - \rho_{C_{15}}C_{15} - \rho_{C_{16}}C_{16}$ $-\rho_{C_{17}}C_{17} - 2\rho_{C_{18}}C_{18} + \rho_{C_{19}}C_{19} + \rho_{C_{23}}C_{23} + \rho_{C_{24}}C_{24} + \rho_{C_{25}}C_{25} + \rho_{C_{26}}C_{26}$	8
$\partial(AE_9)/\partial t + L(E_9{}^m) = AR31$ where $E_9 = \rho_{S_8}S_8$ and $E_9{}^m = 0$	9
$\partial(AE_{10})/\partial t + L(E_{10}{}^m) = A(-R32)$ where $E_{10} = E_{10}{}^m = \rho_{C_{29}}C_{29}$	10
$\partial(AE_{11})/\partial t + L(E_{11}{}^m) = AR32$ where $E_{11} = \rho_{Site-C_{29}}Site-C_{29}$ and $E_{11}{}^m = 0$	11
$\partial(AE_{12})/\partial t + L(E_{12}{}^m) = 0$ where $E_{12} = \rho_{C_{30}}C_{30} + \rho_{Site-C_{30}}Site-C_{30}$ and $E_{12}{}^m = \rho_{C_{30}}C_{30}$	12

$$\partial(AE_{13})/\partial t + L(E_{13}{}^m) = A(-R32) \text{ where } E_{13} = -0.5\rho_{C_{30}}C_{30} + \rho_{Site-C_6}Site-C_6 \text{ and } E_{13}{}^m = -0.5\rho_{C_{30}}C_{30} \quad \boxed{13}$$

Note: $\rho_i = \rho_w$ for $C_1 \sim C_{27}$, C_{29}, and C_{30}; $\rho_i = Ph_b\rho_{wb}\theta_b/A$, for M; and $\rho_i = PBS/A$, for $S_1 \sim S_8$, site-C_6, site-C_{29} and site-C_{30} ($\rho_w = \rho_{wb} = 1.0$ kg/L, $h_b = 0.2$ m, $\theta_b = 0.6$, and BS = 1 kg/m^2).

Table 5.1-3 Equilibrium Reaction Algebraic Equations for Example 5.1-3

Equations	No.
$0.0047M = S_1 + S_2 + S_3 + S_4 + S_5 + S_6 + S_7 + S_8$	1
$Site\text{-}C_6{}^2 \cdot C_{30}{}^2 = 10^{0.6}C_6 \cdot Site\text{-}C_{30}{}^4 \big/ (Site\text{-}C_6 + Site\text{-}C_{29} + Site\text{-}C_{30})$	2
$C_4 = (K_{25}^e)^{1.5} \big/ \big[K_{19}^e (K_{26}^e)^{1.5} \big] \cdot C_{22}S_3^{1.5}/S_2^{1.5}$	3
$C_5 = (K_{26}^e)^2 \big/ (K_{25}^e K_{27}^e) \cdot S_2 S_4 / S_3^2$	4
$C_2 = (K_{25}^e)^{0.5} \big/ (K_{26}^e)^{0.5} \cdot S_3^{0.5}/S_2^{0.5}$	5
$C_7 = K_4^e (K_{26}^e)^2 \big/ (K_{25}^e K_{27}^e) \cdot C_6 S_2 S_4 / S_3^2$	6
$C_1 = K_{25}^e K_{27}^e \big/ (K_{26}^e K_{28}^e) \cdot S_3 S_5 / (S_2 S_4)$	7
$C_9 = K_6^e K_{26}^e \big/ (K_{25}^e)^{0.5} \cdot C_6 S_2^{0.5}/S_3^{0.5}$	8
$C_{10} = K_7^e K_{26}^e / K_{28}^e \cdot S_5 / S_3$	9
$C_{11} = K_8^e (K_{25}^e)^{0.5} (K_{26}^e)^{0.5} / K_{28}^e \cdot S_5 / (S_2^{0.5} S_3^{0.5})$	10
$C_8 = K_5^e (K_{26}^e)^{1.5} \big/ \big[(K_{25}^e)^{0.5} K_{27}^e \big] \cdot S_2^{0.5}S_4/S_3^{1.5}$	11
$C_{12} = K_9^e (K_{26}^e)^{1.5} \big/ \big[(K_{25}^e)^{0.5} K_{28}^e \big] \cdot S_2^{0.5}S_5/S_3^{1.5}$	12
$C_{14} = K_{11}^e (K_{25}^e)^{0.5} K_{27}^e \big/ \big[(K_{26}^e)^{0.5} K_{28}^e \big] \cdot S_3^{0.5}S_5/(S_2^{0.5}S_4)$	13
$C_{15} = K_{12}^e K_{27}^e / K_{28}^e \cdot S_5 / S_4$	14
$C_{16} = K_{13}^e (K_{26}^e)^{0.5} K_{27}^e \big/ \big[(K_{25}^e)^{0.5} K_{28}^e \big] \cdot S_2^{0.5}S_5/(S_3^{0.5}S_4)$	15
$C_{17} = K_{14}^e K_{26}^e K_{27}^e \big/ (K_{25}^e K_{28}^e) \cdot S_2 S_5 / (S_3 S_4)$	16
$C_{13} = K_{10}^e (K_{26}^e)^2 \big/ (K_{25}^e K_{28}^e) \cdot S_2 S_5 / S_3^2$	17
$C_3 = (K_{25}^e)^{0.5} (K_{26}^e)^{0.5} \big/ (K_3^e K_{19}^e K_{27}^e) \cdot C_{22}S_4/(S_2^{0.5}S_3^{0.5})$	18
$C_{20} = K_{17}^e K_{25}^e \big/ (K_{19}^e K_{26}^e) \cdot C_{22}S_3/S_2$	19
$C_{19} = K_{16}^e K_{25}^e \big/ (K_{19}^e K_{27}^e) \cdot C_{22}S_4/S_2$	20
$C_{21} = K_{18}^e (K_{25}^e)^{0.5} \big/ \big[K_{19}^e (K_{26}^e)^{0.5} \big] \cdot C_{22}S_3^{0.5}/S_2^{0.5}$	21
$C_{23} = K_{20}^e (K_{26}^e)^{1.5} \big/ \big[(K_{25}^e)^{0.5} K_{27}^e \big] \cdot S_2^{0.5}S_4/S_3^{1.5}$	22
$C_{24} = K_{21}^e K_{26}^e / K_{27}^e \cdot S_4 / S_3$	23
$C_{25} = K_{22}^e (K_{25}^e)^{0.5} (K_{26}^e)^{0.5} / K_{27}^e \cdot S_4 / (S_2^{0.5}S_3^{0.5})$	24
$S_1 = S_2^{0.5} S_3^{0.5} \big/ \big[(K_{25}^e)^{0.5} (K_{26}^e)^{0.5} \big]$	25
$C_{27} = K_{24}^e (K_{26}^e)^{0.5} \big/ (K_{25}^e)^{0.5} \cdot S_2^{0.5}/S_3^{0.5}$	26
$C_4 = K_{23}^e K_{25}^e / K_{27}^e \cdot S_4 / S_2$	27
$C_5 = K_{15}^e K_{25}^e (K_{27}^e)^2 \big/ \big[K_{26}^e (K_{28}^e)^2 \big] \cdot S_3 S_5^2 / (S_2 S_4^2)$	28

As simulation starts, variable boundary conditions are applied to both the upstream and downstream

boundary nodes. Initial and coming-in concentrations are listed in Table 5.1-4. The longitudinal dispersivity is 80 m. A 90,000-second simulation is performed with a fixed time step size of 150-second.

The concentration distributions of M, C_1, and S_1 at different simulation time are plotted in Figure 5.1-4. Due to the dissolution reaction R1, the bed precipitate M gradually dissolutes into dissolved chemical C_1 in the mobile water phase. Therefore, we observe decreasing concentration of M with time and increasing concentration of C_1 along the down stream direction. Due to the sorbing site forming reaction R2, the concentration of S_1 decreases with time as the surface area of M decreases along with dissolution. Since S_1 involves in seven sorption reactions R25~R31, its concentration distribution is also affected by these reactions and related species.

Table 5.1-4 Initial and Boundary Concentrations for Example 5.1-3

Species	Initial	Boundary
C_1	1.0e-7 mol/Kg	1.0e-7 mol/L
C_2	1.0e-5 mol/Kg	1.0e-5 mol/L
C_3	1.0e-7 mol/Kg	1.0e-4 mol/L
C_4	1.0e-5 mol/Kg	1.0e-5 mol/L
C_5	1.0e-5 mol/Kg	1.0e-5 mol/L
C_6	1.0e-5 mol/Kg	1.0e-4 mol/L
C_{10}	1.0e-5 mol/Kg	1.0e-5 mol/L
C_{29}	1.0e-5 mol/Kg	1.0e-5 mol/L
C_{30}	1.0e-5 mol/Kg	1.0e-4 mol/L
M	2.0e-5 mol/Kg	-
Site-C_6	1.4e-4 mol/g	-
Site-C_{29}	7.0e-4 mol/g	-
Site-C_{30}	1.5e-4 mol/g	-
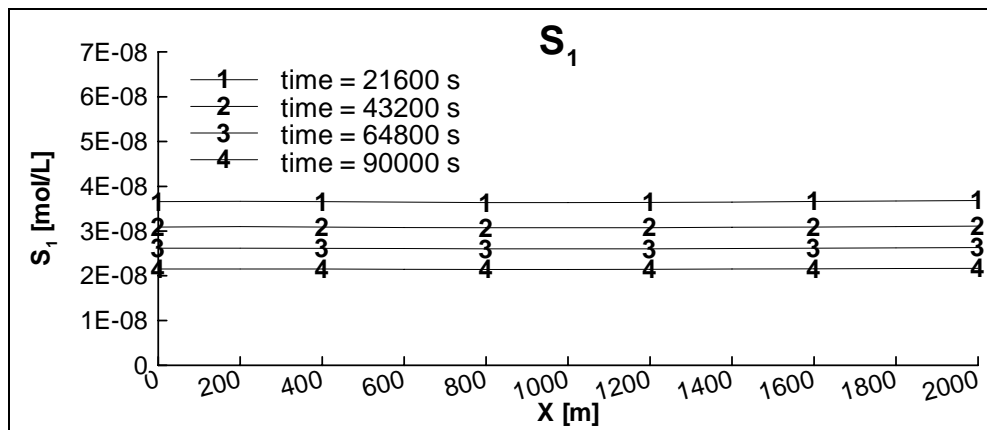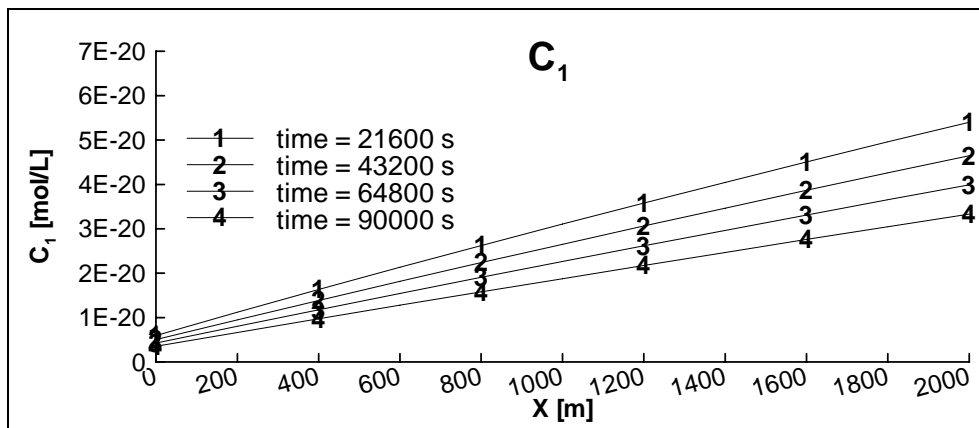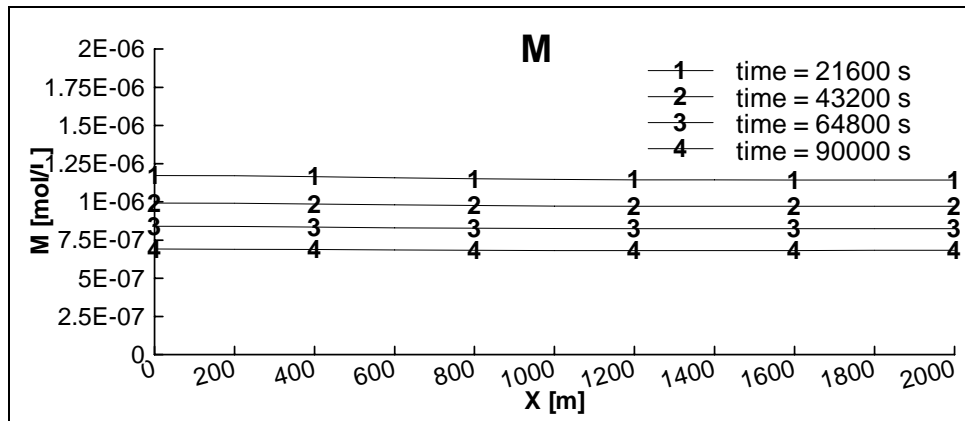
Fig. 5.1-4. Concentration Profiles for Species M, C_1, and S_1 for Example 5.1-3

5.1.4 River/Stream Transport with all Ten Types of Reactions

This example is to demonstrate the capability of the model in simulating sediment and reactive chemical transport subjected to all ten types of reactions presented in Figure 2.5-2.

A horizontally 20 km-long river/stream containing a uniform width of 20 m is considered. The domain is discretized into 100 equal size elements (200 m each). To focus on transport, we assume water depth is 2 m, and river/stream velocity is 1 m/s throughout the river/stream. Only one size of cohesive sediment is taken into account with settling speed of 1.0×10^{-6} m/s, erodibility of 0.15 $g/m^2/s$, critical shear stresses for deposition of 2.85 $g/m/s^2$, and critical shear stresses for erosion of 2.48 $g/m/s^2$. Manning's roughness is 0.02.

Fourteen chemical species are taken account including three dissolved chemicals in the mobile water phase (CMW1, CMW2, and CMW3), three dissolved chemicals in the immobile water phase (CIMW1, CIMW2, and CIMW3), three particulate chemicals in the suspended sediment phase (CS1, CS2, and CS3), three particulate chemicals in the bed sediment phase (CB1, CB2, and CB3), one suspension precipitate (SP3) and one bed precipitate (BP3). As shown in Table 5.1-5, these species are considered to undergo all ten types of reactions illustrated in Figure 2.5-2. Totally, there are twenty reactions, among which, R1 is an equilibrium aqueous complexation reaction among three dissolved chemicals in the mobile water phase; R2 through R4 are kinetic adsorption reactions of three dissolved chemicals in the mobile water phase onto the suspended sediment; R5 through R7 are kinetic adsorption reactions of three dissolved chemicals in the mobile water phase onto the bed sediment; R8 through R10 are kinetic sedimentation reactions of three particulates between suspended and bed sediment phases; R11 through R13 are kinetic diffusion of three dissolved chemicals between mobile and immobile water phases; R14 is a kinetic aqueous complexation reaction among three dissolved chemicals in the immobile water phase; R15 through R17 are kinetic adsorption reactions of three dissolved chemicals in the immobile water phase onto the bed sediment; R18 is a kinetic volatilization reaction of the second dissolved chemical in the mobile water phase; R19 is a kinetic precipitation/dissolution reaction between the third dissolved chemical in the mobile water phase and suspended precipitate; and R20 is a kinetic precipitation/dissolution reaction between the third dissolved chemical in the immobile water phase and bed precipitate;.

Totally, we have 14 species, one equilibrium reaction, and 19 kinetic reactions. Thus, 13 kinetic-variable transport equations and one equilibrium-reaction mass action equation were set up through decomposition and solved for 14 species (Table 5.1-6). Among the 13 kinetic-variables, the 6th through 11th and the 13th contain no mobile species and are thus not solved in the advective-dispersive transport step. Therefore, instead of solving seven advective-dispersive transport equations for mobile species in a primitive approach, we only need to solve six advective-dispersive transport equations for kinetic-variables. Since the fast reaction is decoupled and not included in the transport equations any more, robust numerical integration is enabled.

Table 5.1-5 Chemical Reactions Considered in Example 5.1.4

Reaction and rate parameter	Type	No.
$CMW1 + CMW2 \leftrightarrow CMW3$ ($k_{eq} = 0.4$ m^3/g)	1	R_1
$CMW1 + SS \leftrightarrow CS1 + SS$ $CMW2 + SS \leftrightarrow CS2 + SS$ $CMW3 + SS \leftrightarrow CS3 + SS$ ($k_f = 0.001$ m^3/gSS/s, $k_b = 0.0$ s^{-1})	2	R_2 R_3 R_4
$CMW1 + BS \leftrightarrow CB1 + BS$ $CMW2 + BS \leftrightarrow CB2 + BS$ $CMW3 + BS \leftrightarrow CB3 + BS$ ($k_f = 0.00001$ m^2/gBS/s, $k_b = 0.0$P/A m^{-1}s^{-1})	4	R_5 R_6 R_7
$CS1 \leftrightarrow CB1$ ($k_f = Depo_1$P/A gSS/m^3/s, $k_b = Eros_1$P/A gBS/m^3/s) $CS2 \leftrightarrow CB2$ ($k_f = Depo_2$P/A gSS/m^3/s , $k_b = Eros_2$P/A gBS/m^3/s) $CS3 \leftrightarrow CB3$ ($k_f = Depo_3$P/A gSS/m^3/s, $k_b = Eros_3$P/A gBS/m^3/s)	10	R_8 R_9 R_{10}
$CMW1 \leftrightarrow CIMW1$ $CMW2 \leftrightarrow CIMW2$ $CMW3 \leftrightarrow CIMW3$ ($k_f = 0.0001$ s^{-1}, $k_b = 0.0$Ph$_b\theta_b$/A s^{-1})	9	R_{11} R_{12} R_{13}
$CIMW1 + CIMW2 \leftrightarrow CIMW3$ ($k_f = 0.0002$Ph$_b\theta_b$/A m^3/g/s , $k_b = 0.0005$Ph$_b\theta_b$/A s^{-1})	5	R_{14}
$CIMW1 + BS \leftrightarrow CB1 + BS$ $CIMW2 + BS \leftrightarrow CB2 + BS$ $CIMW3 + BS \leftrightarrow CB3 + BS$ ($k_f = 0.00001$Ph$_b\theta_b$/A m^2/gBS/s, $k_b = 0.0$P/A m^{-1}s^{-1})	6	R_{15} R_{16} R_{17}
$CMW2 \leftrightarrow P$ ($k_f = 0.0002$ s^{-1}, $k_b = 0.02$ g/m^3/ATM/s, P=0.0025ATM)	8	R_{18}
$CMW3 \leftrightarrow SP3$ ($k_f = 0.001$ s^{-1}, $k_b = 0.000001$ s^{-1})	3	R_{19}
$CIMW3 \leftrightarrow BP3$ ($k_f = 0.0001$Ph$_b\theta_b$/A s^{-1}, $k_b = 0.0000001$Ph$_b\theta_b$/A s^{-1})	7	R_{20}

Note: the reaction types are defined in Figure 2.5-2.

Table 5.1-6 Equations Obtained through Decomposition in Example 5.1-4

Equations	Type
$\partial(AE_1)/\partial t + L(E_1{}^m) = A(-R_2 - R_4 - R_5 - R_7 - R_{11} - R_{13} - R_{19})$ where $E_1 = E_1{}^m = \rho_{CMW1}C_{CMW1} + \rho_{CMW3}C_{CMW3}$	1
$\partial(AE_2)/\partial t + L(E_2{}^m) = A(-R_3 - R_4 - R_6 - R_7 - R_{12} - R_{13} - R_{18} - R_{19})$ where $E_2 = E_2{}^m = \rho_{CMW2}C_{CMW2} + \rho_{CMW3}C_{CMW3}$	1
$\partial(AE_3)/\partial t + L(E_3{}^m) = A(R_2 - R_8)$ where $E_3 = E_3{}^m = \rho_{CS1}C_{CS1}$	1
$\partial(AE_4)/\partial t + L(E_4{}^m) = A(R_3 - R_9)$ where $E_4 = E_4{}^m = \rho_{CS2}C_{CS2}$	1
$\partial(AE_5)/\partial t + L(E_5{}^m) = A(R_4 - R_{10})$ where $E_5 = E_5{}^m = \rho_{CS3}C_{CS3}$	1
$\partial(AE_6)/\partial t + L(E_6{}^m) = A(R_5 + R_8 + R_{15})$ where $E_6 = \rho_{CB1}C_{CB1}$ and $E_6{}^m = 0$	1
$\partial(AE_7)/\partial t + L(E_7{}^m) = A(R_6 + R_9 + R_{16})$ where $E_7 = \rho_{CB2}C_{CB2}$ and $E_7{}^m = 0$	1
$\partial(AE_8)/\partial t + L(E_8{}^m) = A(R_7 + R_{10} + R_{17})$ where $E_8 = \rho_{CB3}C_{CB3}$ and $E_8{}^m = 0$	1
$\partial(AE_9)/\partial t + L(E_9{}^m) = A(R_{11} - R_{14} - R_{15})$ where $E_9 = \rho_{CIMW1}C_{CIMW1}$ and $E_9{}^m = 0$	1
$\partial(AE_{10})/\partial t + L(E_{10}{}^m) = A(R_{12} - R_{14} - R_{16})$ where $E_{10} = \rho_{CIMW2}C_{CIMW2}$ and $E_{10}{}^m = 0$	1
$\partial(AE_{11})/\partial t + L(E_{11}{}^m) = A(R_{13} + R_{14} - R_{17} - R_{20})$ where $E_{11} = \rho_{CIMW3}C_{CIMW3}$ and $E_{11}{}^m = 0$	1
$\partial(AE_{12})/\partial t + L(E_{12}{}^m) = AR_{19}$ where $E_{12} = E_{12}{}^m = \rho_{SP3}C_{SP3}$	1
$\partial(AE_{13})/\partial t + L(E_{13}{}^m) = AR_{20}$ where $E_{13} = \rho_{BP3}C_{BP3}$ and $E_{13}{}^m = 0$	1
$C_{CMW3} = 0.4C_{CMW1}C_{CMW2}$	2

Note: the equation type 1 is kinetic-variable transport equation and type 2 is equilibrium reaction mass action equation.
$\rho_i = \rho_w$ for CMW1~CMW3, and SP3; $\rho_i = $ SS for CS1~CS3; $\rho_i = Ph_b\rho_{wb}\theta_b/A$, for IMW1~CIMW3, and BP3; and $\rho_i = PBS/A$, for CB1~CB3 ($\rho_w = \rho_{wb} = 1.0$ kg/L, $h_b = 0.1$ m, and $\theta_b = 0.5$).

Initially, only sediment exists in the domain of interest with suspended concentration SS of 1 g/m^3 and bed concentration BS of 50 g/m^2. As simulation starts, Dirichlet boundary conditions are applied to the upstream boundary node, where suspended sediment has a constant concentration of 1 g/m^3 and dissolved chemicals in mobile water phase have constant concentrations of 1 mg/kg and all the other mobile chemicals have zero concentration. Out-flow variable boundary conditions are applied to the downstream boundary node. The longitudinal dispersivity is 80 m. A 90,000-second simulation is performed with a fixed time step size of 150-second. Simulation results are shown in Figure 5.1-5.

Figure 5.1-5 shows trend of increasing concentration of the suspended sediment along down stream direction, and depicts decrease of the bed sediment with increase of time. It indicates that deposition is less than erosion under the condition set for this example.
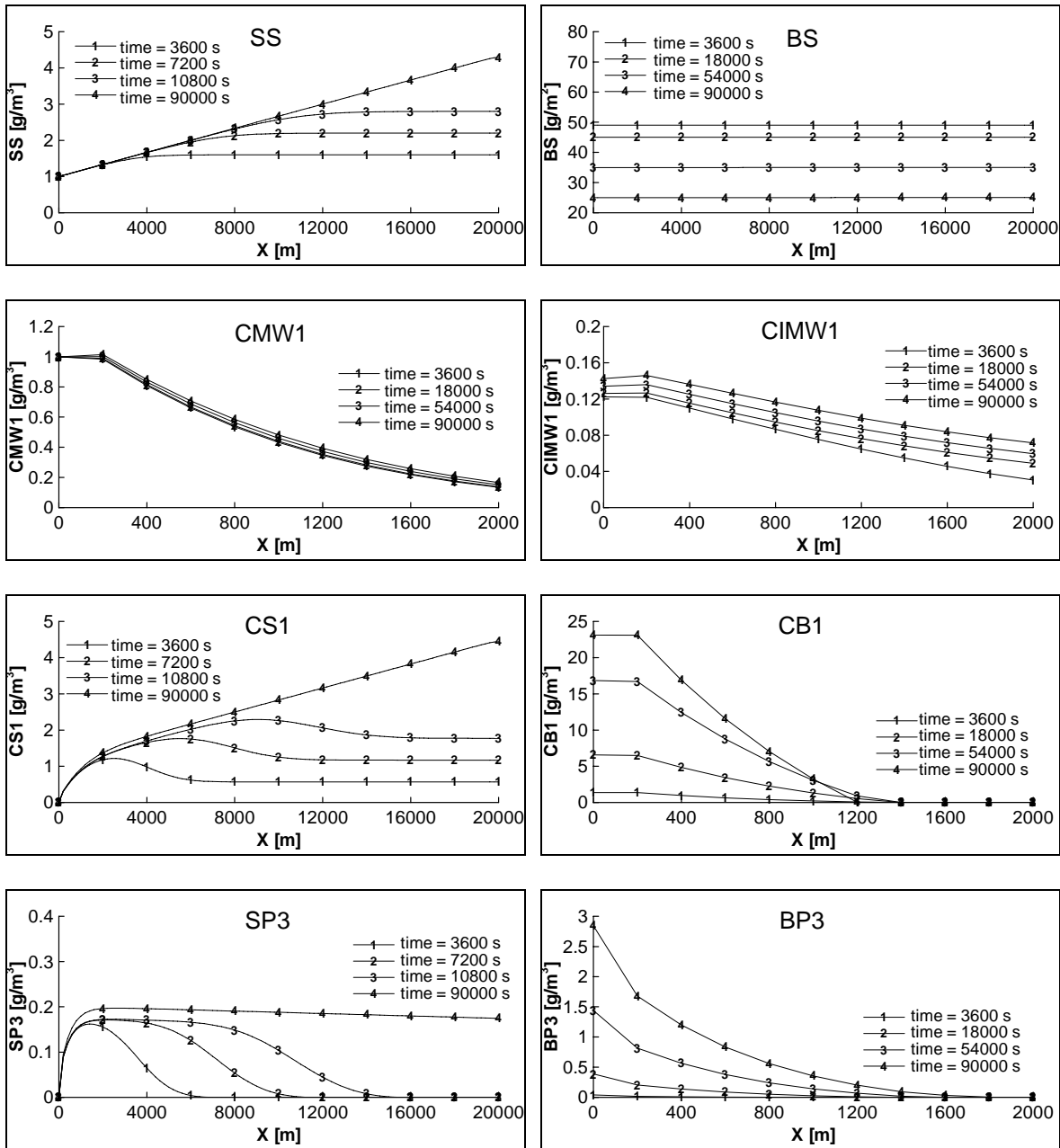
Fig. 5.1-5. Concentration Profiles of Various Species for Example 5.1-4

Figure 5.1-5 shows the decreasing concentration of CMW1 along the downstream direction. This is because we allow the adsorption to happen, but do not allow desorption from particulate chemicals to dissolved chemicals to occur. In the zone near the Dirichlet boundary, the concentration distribution curve of CMW1 is not smooth. Due to the fast reaction among the three dissolved chemicals in the mobile water phase, the concentration of CMW1 increases to its equilibrium value. The only source of dissolved chemicals in the immobile water phase is the corresponding dissolved chemicals in the mobile water phase. Therefore, concentration distribution of CIMW1 shows the similar pattern of CMW1.

Since the dissolved chemicals are little in the downstream region, the major source of chemicals is the particulate chemicals on suspended sediments that are transported from the upstream region along with water. Because erosion is greater than deposition, we observe increase of CS1 with time and decrease of CB1 along the downstream direction. Since the particulate chemicals on bed sediment result not only from dissolved chemicals in mobile water phase, but also from those in the immobile water phase, the decrease of CB1 along the downstream also reflects the similar pattern of CMW1 and CIMW1.

Since the major source of suspension precipitate in the downstream region is transported from the upstream region along with water, we observe an increase of suspension precipitate concentration with time. Since bed precipitate is involved in the precipitation reaction only, Figure 5.1-5 also shows decreasing bed precipitate concentration along the downstream direction reflecting the similar decrease of dissolved chemical concentration in the immobile phase.

5.1.5   River/Stream Transport with Eutrophication

This example is to demonstrate the capability of the model in simulating the chemical transport related to eutrophication reported in WASP5 (Ambrose et al., 1993).

WASP5, the Water quality Analysis Simulation Program, is a three-dimensional conventional water quality analysis simulation program. It is a group of mechanistic models capable of simulating water transport and fate and transport of water quality constituents and toxic organics for aquatic systems. Various components of WASP5 have been used to study a variety of river, lake, reservoir, and estuarine issues including ecological characterization, the effects of anthropogenic activities, and the impact of mitigation measures (Bierman and James, 1995; Lung and Larson, 1995; Tufford and McKellar, 1999; and Zheng et al., 2004).

EUTRO5 is a general operational WASP5 model used to simulate nutrient enrichment, eutrophication, and dissolved oxygen in the aquatic environment. It constitutes a complex of four interacting systems: dissolved oxygen, nitrogen cycle, phosphorus cycle, and phytoplankton dynamics. It can simulate up to eight eutrophication constituents in both water column and benthic layer, including: (1) Ammonia NH_3 and $NH_{3(b)}$, (2) Nitrate NO_3 and $NO_{3(b)}$, (3) Inorganic Phosphorus OPO_4 and $OPO_{4(b)}$, (4) Phytoplankton PHYT and $PHYT_{(b)}$, (5) Carbonaceous CH_2Ot and $CH2Ot_{(b)}$, (6) Oxygen O_2 and $O_{2(b)}$, (7) Organic Nitrogen ONt and $ONt_{(b)}$, and (8) Organic Phosphorus OPt and $OPt_{(b)}$, where 't' means total and '(b)' means benthic.

According to our definition of chemical phases and forms, the total concentration of a species is the sum of the dissolved chemical and the particulate sorbed onto sediments, such as $CH2Ot = CH_2O + CH2Op$, $CH2Ot_{(b)} = CH2O_{(b)} + CH2Op_{(b)}$, $ONt = ON + ONp$, $ONt_{(b)} = ON_{(b)} + ONp_{(b)}$, $OPt = OP + OPp$, and $OPt_{(b)} = OP(b) + OPp_{(b)}$), where 'p' means particulate. Therefore, the 16 species simulated in EUTRO5 were transformed into 22 chemical species listed in Table 5.1-7 and simulated in our model. The sixteen working equations of EUTRO5 were recast in terms of reaction network used in our eutrophication simulation. The reaction network includes 32 kinetic reactions and 6 equilibrium reactions (Zhang, 2005).

Table 5.1-7   Chemical Species in Example 5.1.5

Notation	Conc.	Initial Conditions	Boundary Conditions	ρ_i
NH_3	C_1	0.1 mg N/kg	1 mg N/kg	ρ_w
$NH_{3(b)}$	C_2	0.1 mg N/kg	-	$Ph_b\rho_{wb}\theta_b/A$
NO_3	C_3	0.1 mg N/kg	1 mg N/kg	ρ_w
$NO_{3(b)}$	C_4	0.1 mg N/kg	-	$Ph_b\rho_{wb}\theta_b/A$
OPO_4	C_5	0.01 mg P/kg	0.1 mg P/kg	ρ_w
$OPO_{4(b)}$	C_6	0.01 mg P/kg	-	$Ph_b\rho_{wb}\theta_b/A$
PHYT	C_7	0.2 mg C/kg	2 mg C/kg	ρ_w
$PHYT_{(b)}$	C_8	0.2 mg C/kg	-	$Ph_b\rho_{wb}\theta_b/A$
CH_2O	C_9	1.0 mg O_2/kg	10 mg O_2/kg	ρ_w
$CH_2O_{(p)}$	C_{10}	1.0 mg O_2/mg	10 mg O_2/mg	SS
$CH_2O_{(b)}$	C_{11}	1.0 mg O_2/kg	-	$Ph_b\rho_{wb}\theta_b/A$
$CH_2O_{(bp)}$	C_{12}	0.01 mg O_2/mg	-	PBS/A
O_2	C_{13}	0.2 mg O_2/kg	2 mg O_2/kg	ρ_w
$O_{2(b)}$	C_{14}	0.2 mg O_2/kg	-	$Ph_b\rho_{wb}\theta_b/A$
ON	C_{15}	0.2 mg N/kg	2 mg N/kg	ρ_w
$ON_{(p)}$	C_{16}	0.0 mg N/mg	0 mg N/mg	SS
$ON_{(b)}$	C_{17}	0.2 mg N/kg	-	$Ph_b\rho_{wb}\theta_b/A$
$ON_{(bp)}$	C_{18}	0.0 mg N/mg	-	PBS/A
OP	C_{19}	0.035 mg P/kg	0.35 mg P/kg	ρ_w
$OP_{(p)}$	C_{20}	0.015 mg P/mg	0.15 mg P/mg	SS
$OP_{(b)}$	C_{21}	0.035 mg P/kg	-	$Ph_b\rho_{wb}\theta_b/A$
$OP_{(bp)}$	C_{22}	0.00015 mg P/mg	-	PBS/A

Note: $\rho_w = \rho_{wb} = 1$ kg/L, $h_b = 0.12$ m, and $\theta_b = 0.6$

The canal considered is 4738 m-long with width of 4.6~12.2 m. It is descretized with nine elements of size of 515~549 m. The flow pattern was simulated using the flow module of WASH123D. The calculated water depth is 2.17~2.81 m and river/stream velocity is 0.06~0.88 m/s. To focus on reactive chemical transport, we assume that the temperature is 15°C, suspended sediment concentration SS is $1g/m^3$, and bed sediment concentration BS is 15 g/m^2 throughout the canal. Dirichlet boundary condition is applied to the upstream boundary node. Flow-out variable boundary condition is applied to the downstream boundary node. Initial concentrations of all species and Dirichlet boundary concentrations of mobile species are listed in Table 5.1-7. The longitudinal dispersivity is 90 m. A 12-day simulation is performed with a fixed time step size of 6 minutes.

Figure 5.1-6 plots the concentration distribution of phytoplankton and dissolved oxygen. The similar concentration pattern of PHYT and DO indicates that these mobile species concentration change is mainly controlled by the advective-dispersive transport rather than the biogeochemical reactions. However, the concentration change of immobile benthic species $PHYT_{(b)}$ and $DO_{(b)}$ is mainly affected by the biogeochemical reactions.

In the benthic immobile water phase, the concentration change of PHYT(b) is due to its decomposition and PHYT settling. Figure 5.1-6 shows increasing concentration of PHYT(b) with time, demonstrating that the settling rate of PHYT is greater than PHYT(b) decomposition rate. In the benthic immobile water phase, the concentration change of DO(b) is due to the consumption of oxidation and diffusion of DO. Figure 5.1-6 shows decreasing concentration of DO(b) at upstream. This indicates that at the upstream the diffusion rate of DO is less than the consumption rate of oxidation. As the simulation time increases, there is more DO at downstream. Figure 5.1-6 shows increasing concentration of DO(b) at downstream, demonstrating that the increased diffusion rate of DO is greater than the consumption rate of oxidation.
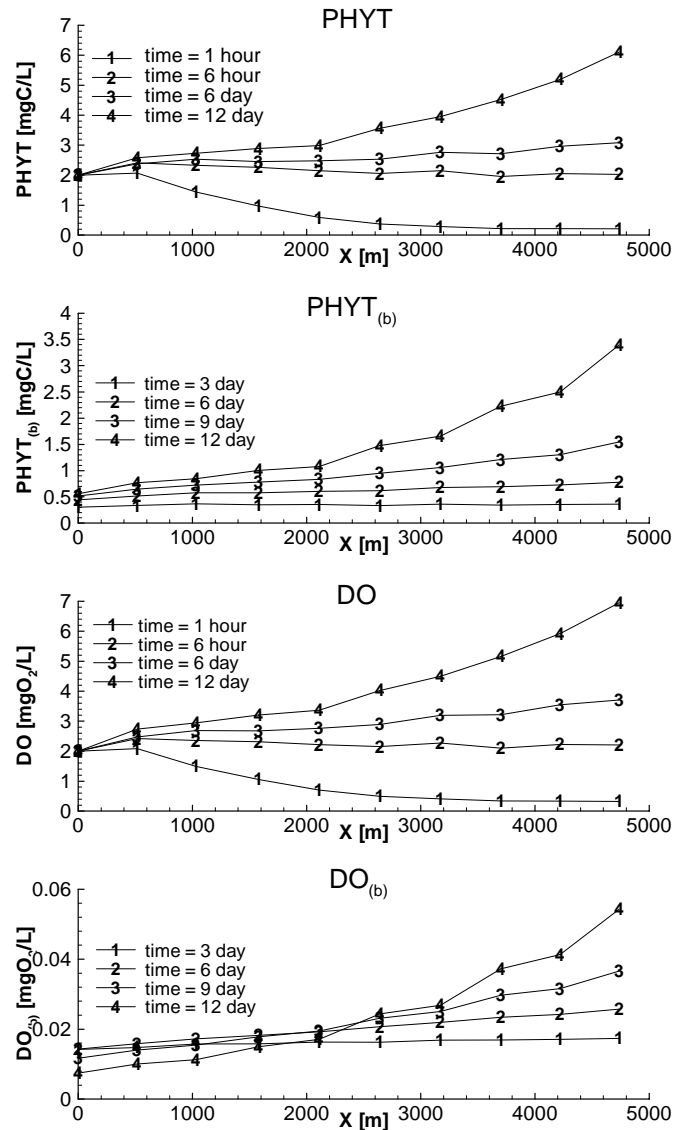
Fig. 5.1-6. Concentration Profiles of PHYT, PHYT$_{(b)}$, DO, and DO$_{(b)}$) for Example 5.1.5

5.1.6 River/Stream Transport with Junction

This example is to demonstrate the capability of the model in simulating sediment and chemical transport in river/stream network system with junction.

The system is composed of three river/stream reaches that are connected through a junction (figure 5.1-7). Each reach is 100 m long and is discretized with 11 nodes and 10 elements: Nodes 1 through 11 for Reach1, 12 through 22 for Reach 2, and 23 through 33 for Reach 3. Nodes 11, 12, and 23 coincide with one another and are located at the junction. The junction covers the area between

Node 11 and median of Nodes 10 and 11, Node 12 and median of Nodes 12 and 13, and Node 23 and median of Nodes 23 and 24.
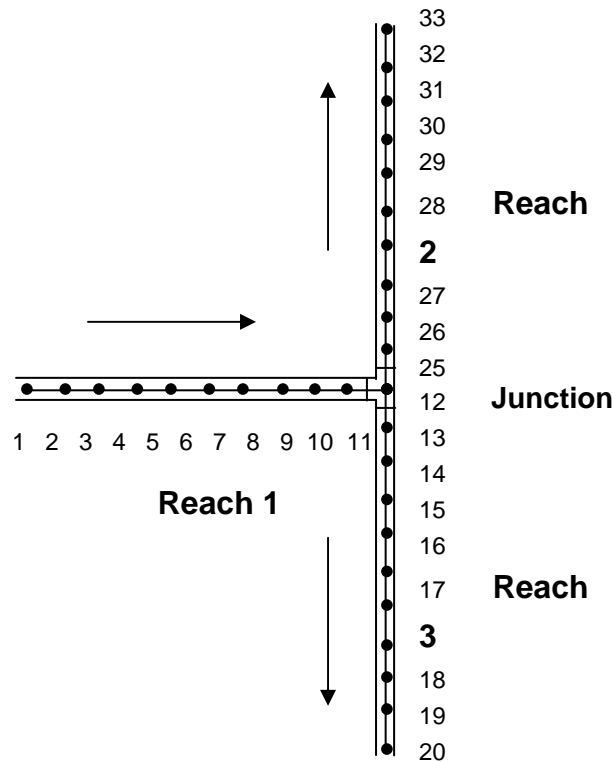
Fig. 5.1-7. River/stream Network for Example 5.1.6

Reach 1 has a uniform river/stream width of 2 m, while Reaches 2 and 3 contain a uniform river/stream width of 1 m. Manning's roughness is 0.028375 for all three reaches. To focus on transport, we assume water depth is 2 m and river/stream velocity is 1 m/s throughout the river/stream system under isotherm condition. Two dissolved chemicals are considered to undergo the following reaction:

$$CMW \rightleftharpoons CIMW \quad k_f = 0.001, \ k_b = 0 \tag{5.1.5}$$
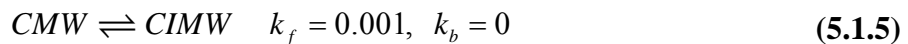
where CMW and CIMW represent dissolved chemicals in mobile water phase and immobile water phase, respectively.

Only one size of cohesive sediment is taken into account with settling speed of 1.2×10^{-6} m/s, critical shear stresses for deposition of 2.75 g/m/s^2 and critical shear stresses for erosion of 2.68 g/m/s^2. The following sorption reactions are included:

$$CMW + SS \rightleftharpoons CS + SS \quad k_f = 0.001, \quad k_b = 0 \tag{5.1.6}$$

$$CMW + BS \rightleftharpoons CB + BS \quad k_f = 0.0001, \quad k_b = 0 \tag{5.1.7}$$

$$CIMW + BS \rightleftharpoons CB + BS \quad k_f = 0.0001, \quad k_b = 0 \tag{5.1.8}$$
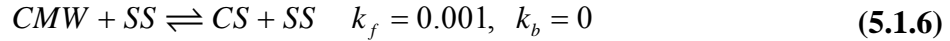
where SS is suspended sediment, BS is bed sediment, CS is particulate chemical associated with CMW on SS, and CB is particulate chemical associated with CMW or CIMW on BS. We have, therefore, 4 species and 4 kinetic reactions in total.

Initially, only bed sediment exists in the domain of interest with initial concentration of 50 g/m^2. Dirichlet boundary conditions are applied to the upstream boundary node, where dissolved chemical in mobile water phase has a constant concentration of 1 mg/kg, suspended sediment and particulate on suspended sediment have zero concentration at this boundary node. The longitudinal dispersivity is 10 m. A 1000 second simulation is performed with a fixed time step size of 2 seconds. A relative error of 10^{-4} is used to determine the convergence for iterations involved in the computation.

Figures 5.1-8 through 5.1.13 plot the numerical results at various time, for concentration distributions of (1) suspended sediment (Figure 5.1-8), (2) bed sediment (Figure 5.1-9), (3) dissolved chemical in mobile water phase (Figure 5.1-10), (4) dissolved chemical in immobile water phase (Figure 5.1-11), (5) particulate chemical on suspended sediment (Figure 5.1-12), and (6) particulate chemical on bed sediment (Figure 5.1-13). Since Reaches 2 and 3 are symmetric in geometry, have identical river/stream width, velocity, and Manning's roughness, and are given same initial and boundary conditions for both sediments and chemicals, they have identical sediment and chemical concentration distribution patterns. Sediment and chemical concentration distribution patterns in Reaches 1 and 2/3 are provided through figures 5.1-8 and 5.1-13, where Reach 1 is the region with x-coordinate ranging from 0m to 100 m and Reach 2/3 is the region with x-coordinate ranging from 100 m to 200 m.

Figure 5.1-8 shows the trend of increasing concentration of suspended sediment along the down stream direction in Reach 1, while Figure 5.1-9 depicts the concentration decrease of bed sediment in Reach 1 with the increase of time. Figures 5.1-8 and 5.1-9 tell that the deposition is less than the erosion in Reach 1 under the condition set for this example. Figure 5.1-8 shows no change of bed sediment concentration either with simulation time or along the river/stream in Reach 2. This indicates that there are same amount of deposition and erosion in Reach 2. Since all the suspended sediment in Reach 2 is transported from upstream, its concentration increases with the simulation time and is approaching a steady state shown in figure 5.1-8. This steady state is maintained until the bed sediment upstream is depleted and no more suspended sediment is transported. At the junction, Figure 5.1-8 and figure 5.1-9 show increasing and decreasing concentrations of suspended and bed sediment, respectively. This tells that erosion is greater than deposition at the junction.
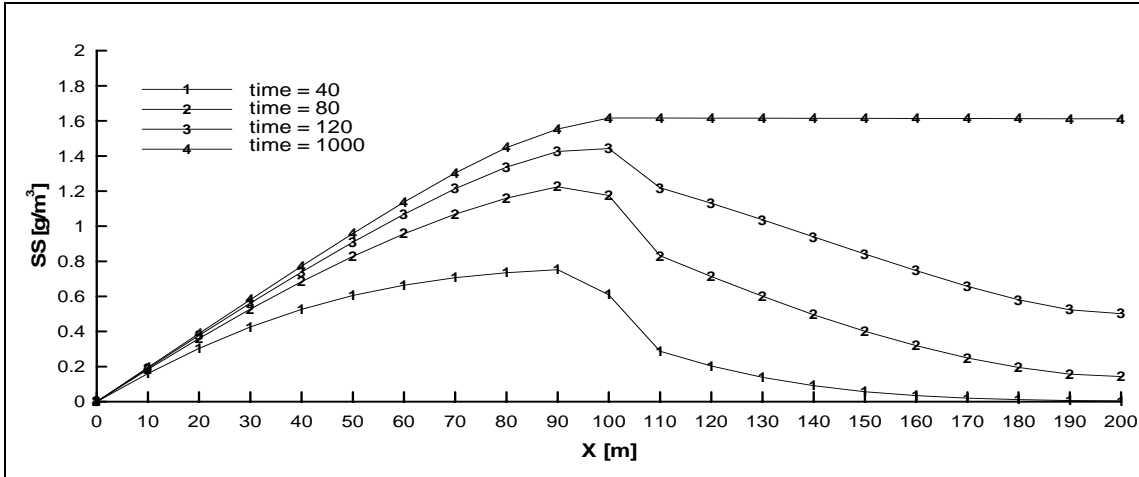
Fig. 5.1-8. Concentration of the Suspended Sediment for example 5.1.6
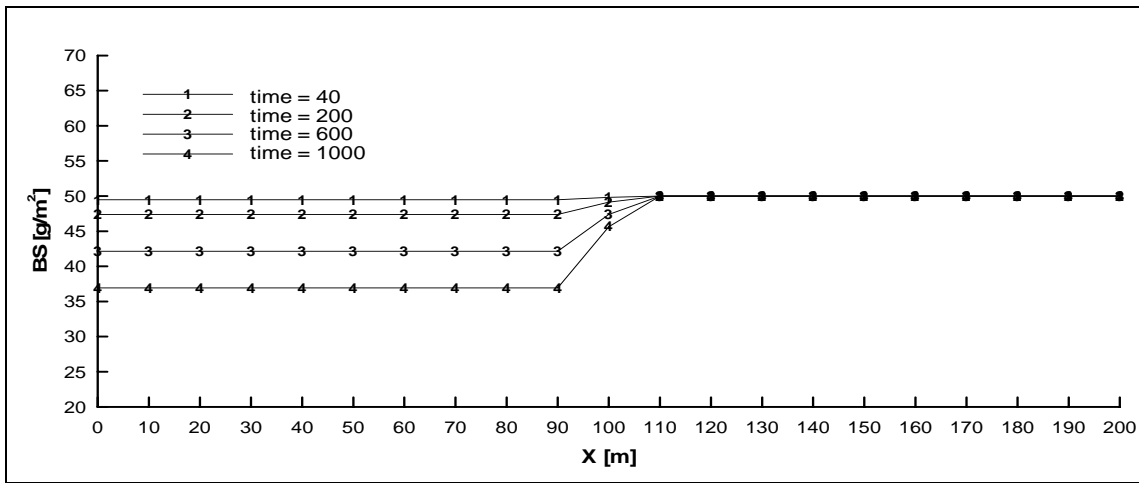
Fig. 5.1-9. Concentration of the Bed Sediment for Example 5.1.6

Figures 5.1-10 shows decreasing dissolved chemical concentration in mobile water phase along the downstream direction. This is because we allow the forward changing of dissolved chemical from mobile water phase to immobile water phase but not backward changing to occur (see equation 5.1.5), and the adsorption but not desorption from particulate chemicals to dissolved chemicals to happen (see equations 5.1.6 through 5.7.8). Due to the transform of dissolved chemical from mobile water phase into immobile water phase, the concentration of chemical in immobile water phase increases with time and shows similar pattern along the river/stream in figure 5.1.11 as that of chemical in mobile water phase. Since chemical in immobile water phase also involves in the reaction with bed sediment forming particulate on bed sediment, its concentration pattern in figure 5.111 also reflects this reaction. At the junction, figure 5.1-10 and figure 5.1-11 shows the decrease of chemical concentrations in both mobile and immobile water phase, due to the adsorption.
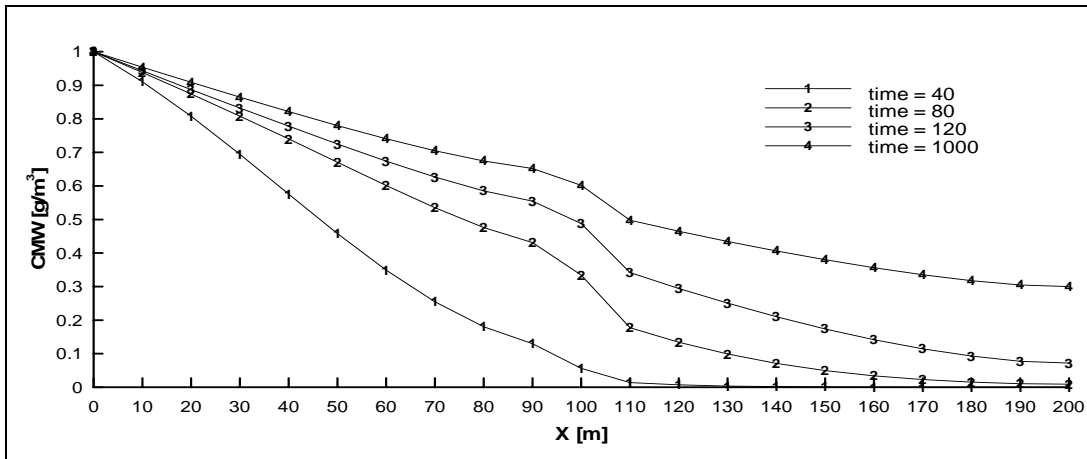
Fig. 5.1-10. Concentration of Dissolved Chemical in Mobile Water for Example 5.1.6
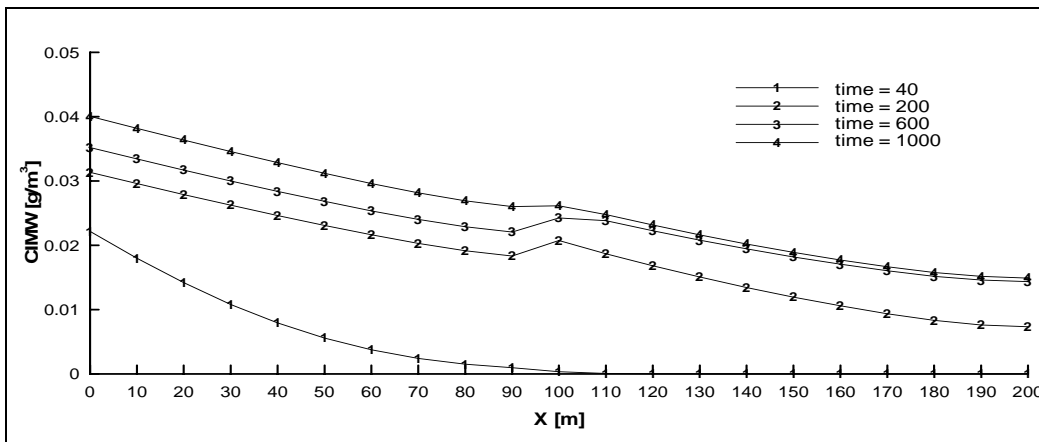
Fig. 5.1-11. Concentration of Dissolved Chemical in Immobile Water for Example 5.1.6

Particulate on suspended sediment results from adsorption/desorption, erosion/deposition, and transport. In reach 1, because erosion is greater than deposition, along the downstream direction, we observe an increase of particulate chemical on suspended sediments (figure 5.1-12). In Reach 2, erosion rate is the same as deposition rate and there is little dissolved chemical, so that most of the particulate on suspended sediment is transported from upstream and hardly transforms into particulate on bed sediment, and its concentration changes little along the reach (figure 5.1-12). At the junction, the increasing concentration of particulate chemical on suspended sediment (figure 5.1-12) is caused by not only adsorption but also erosion.

Particulate on bed sediment results from adsorption/desorption and erosion/deposition. In Reach 1, since deposition is less than erosion, the particulate on bed sediment is obtained from the adsorption of dissolved chemical in either mobile water phase or immobile water phase and reflects the same pattern in figure 5.1-13 as those of chemical in both mobile and immobile water phase (figure 5.1-10 and 5.1-11, respectively). In Reach 2, because erosion rate is the same as deposition rate, particulate on bed sediment is also formed through the adsorption and shows the same pattern in figure 5.1.13 as those of chemical in both mobile and immobile water phase (figure 5.1-10 and 5.1-11, respectively).

At the junction, the increasing concentration of particulate chemical on bed sediment (figure 5.1-12) indicates that its concentration increase due to adsorption is greater than the decrease caused by erosion.
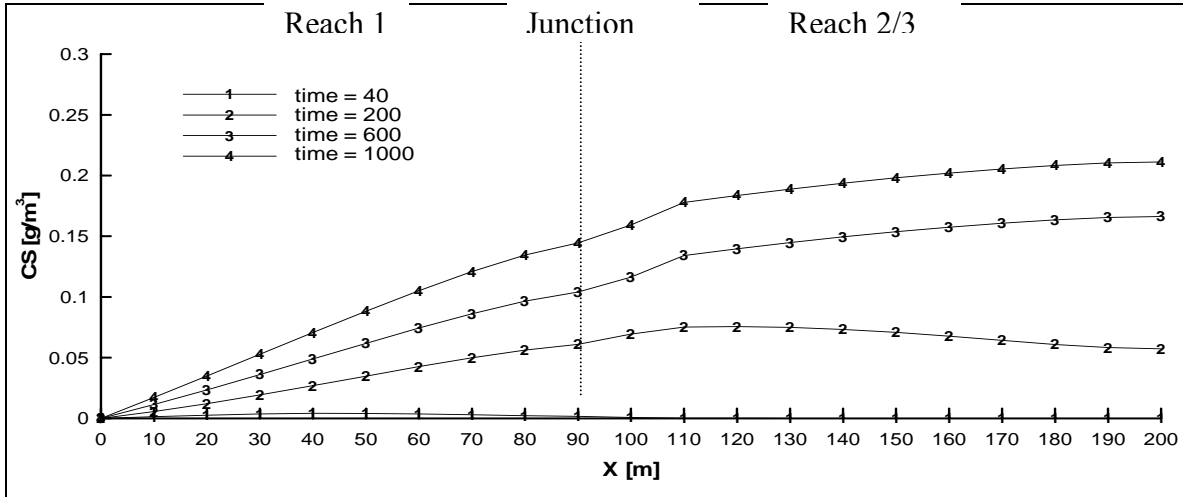
Fig. 5.1-12. Concentration of Particulate on Suspended Sediment for example 5.1.6
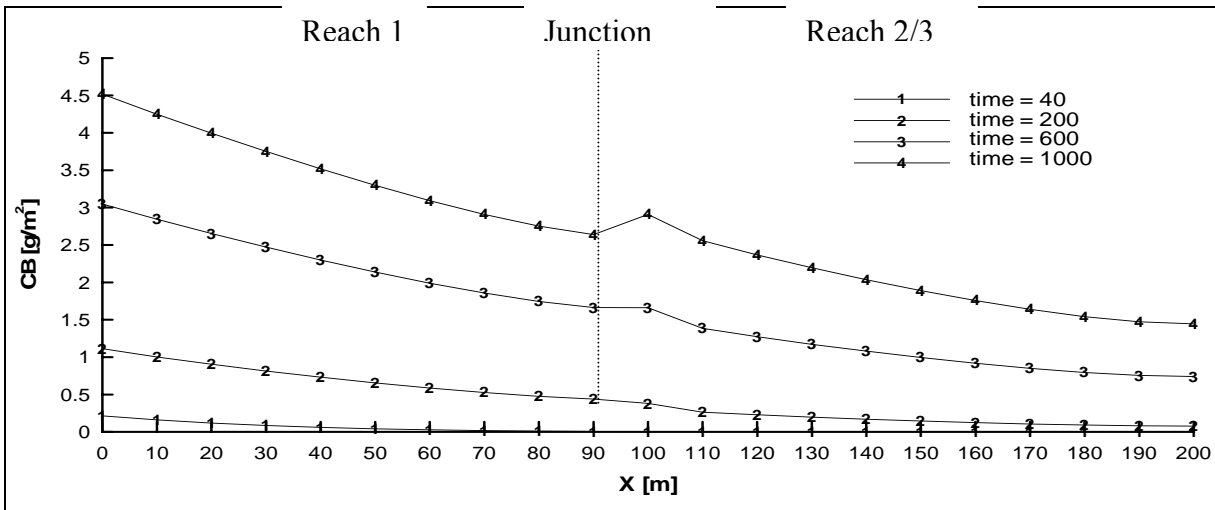
Fig. 5.1-13. Concentration of Particulate on Bed Sediment for example 5.1.6

5.2 Two-Dimensional Examples

Four examples are employed to demonstrate the design capability of the model in this section. The first example is used to demonstrate that the model can simulate all ten types of reactions described in Chapter 2. The second, third, and fourth examples are used to illustrate that the model has the design capability of simulate different eutrophication models reported in QUAL2E, WASP5, and CE-QUAL-ICM, respectively. Biogeochemical cycles, biota kinetics, and sediment-column water interactions in these eutrophication models have been successfully transformed into reaction networks. Based on the application of these eutrophication examples, the deficiency of current practices in water quality modeling is discussed and potential improvements over current practices using the current model are addressed.

5.2.1 Overland Transport with Ten Types of Reactions

This example is to demonstrate the capability of the model in simulating sediment and reactive chemical transport subject to complex reaction network involving both kinetic and equilibrium reactions, under the effect of temperature.

The domain of interest has covered a horizontal area of 5,000 m × 1,000 m and is discretized with 125 square elements of size 200 m × 200 m. To focus on transport, water depth is set to be 2.0 m, and flow velocity is 0.5 m/s in the x-direction and 0.0 m/s in the y-direction everywhere. Manning's roughness is 0.05. Two cases are considered with different temperature distribution. As shown in Figure 5.2-1, in case 1, temperature is set to be 15 °C throughout the region; and in case 2, temperature ranges from 15 °C to 25 °C at different locations.

One size of cohesive sediment is taken into account with settling speed of 1.2×0^{-6} m/s, critical shear stress for deposition of 4.15 g/m/s^2, critical shear stress for erosion of 4.08 g/m/s^2, and erodibility of 0.1 g/m^2/s. A reaction network of 20 reactions is considered for this example problem (Table 5.2-1). From the reaction network, it is seen that there are 14 species, including 3 dissolved chemicals in mobile water phase (CMW1, CMW2, and CMW3); 3 dissolved chemicals in immobile water phase (CIMW1, CIMW2, and CIMW3); 3 particulate chemicals sorbed onto suspended sediment (CS1, CS2, and CS3); 3 particulate chemicals sorbed onto bed sediment (CB1, CB2, and CB3); 1 suspension precipitate (SP3); and 1 bed precipitate (BP3).
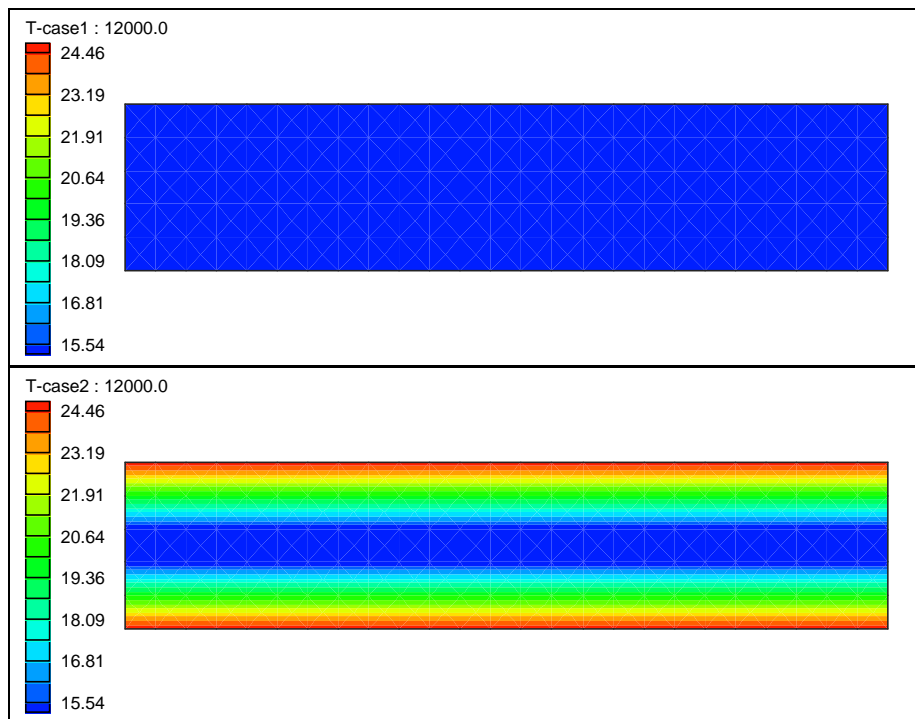
Fig. 5.2-1. Distribution of Temperature (ºC) for Example 5.2.1
Upper: case 1; Lower: case 2

As shown in Table 5.2-1, these species are considered to undergo all ten types of reaction illustrated in Figure 2.6-2, including aqueous complexation reactions, adsorption/desorption reactions, ion-exchange reactions, precipitation/dissolution reactions, volatilization reactions, diffusion reactions, and sedimentation reactions taking place between different chemical phases. Reaction rates of R11 through R13 are closely related to temperature (Table 5.2-1). Totally, we have 14 species, 1 equilibrium reaction, and 19 kinetic reactions. Thus, 13 kinetic-variable transport equations and 1 equilibrium reaction mass action equation were set up through decomposition and solved for 14 species, which are listed in Table 5.2-2. Among the 13 kinetic-variables, the 6th through 11th and the 13th contain no mobile species and are thus not solved in the advective-dispersive transport step. Therefore, instead of solving 7 advective-dispersive transport equations for mobile species in a primitive approach, we only need to solve 6 advective-dispersive transport equations for kinetic-variables. Since the fast reaction is decoupled and not included in the transport equations any more, robust numerical integration can be performed.

Initially, only bed sediments, BS, exist in the domain of interest. The initial concentration is 50 g/m^2 for the bed sediment. As the simulation starts, in-flow variable boundary conditions are applied to the upstream boundary sides, where all dissolved chemicals have a constant incoming concentration of 1 g/m^3 and all other mobile species and suspended sediment, SS, have zero incoming concentration. Out-flow variable boundary conditions are applied to the downstream boundary sides. The longitudinal dispersivity is 10.0 m. A 12,000-second simulation is performed with fixed time step size of 200 seconds. A relative error of 10^{-4} is used to determine the convergence for iterations involved in the computation.

Table 5.2-1 Chemical Reactions Considered in Example 5.2.1

Reaction type	Reaction and rate parameter	No.
Aqueous complexation reaction in mobile water phase	CMW1 + CMW2 $\leftrightarrow$ CMW3 (k_{eq} = 0.4 m^3/g)	R_1
Adsorption/desorption or ion-exchange reaction between mobile water and suspended sediment phases	CMW1+SS $\leftrightarrow$ CS1 + SS CMW2+SS $\leftrightarrow$ CS2 + SS CMW3+SS $\leftrightarrow$ CS3 + SS (k_f = 0.0001 m^3/g SS /s, k_b = 0.0 s^{-1})	R_2 R_3 R_4
Adsorption/desorption or ion-exchange reaction between mobile water and bed sediment phases	CMW1+BS $\leftrightarrow$ CB1 + BS CMW2+BS $\leftrightarrow$ CB2+ BS CMW3+BS $\leftrightarrow$ CB3 + BS (k_f = 0.00001 m^2/g BS /s, k_b = 0.0/h m^{-1}s^{-1})	R_5 R_6 R_7
Sedimentation of particulate chemical between suspended and bed sediment phases	CS1 $\leftrightarrow$ CB1 (k_f = Depo/h g SS/m^3/s , k_b = Eros/h g BS/m^3/s) CS2 $\leftrightarrow$ CB2 (k_f = Depo/h g SS/m^3/s , k_b = Eros/h g BS/m^3/s) CS3 $\leftrightarrow$ CB3 (k_f = Depo/h g SS/m^3/s , k_b = Eros/h g BS/m^3/s)	R_8 R_9 R_{10}
Diffusion of dissolved chemical between mobile and immobile water phases	CMW1 $\leftrightarrow$ CIMW1 CMW2 $\leftrightarrow$ CIMW2 CMW3 $\leftrightarrow$ CIMW3 (k_f = 0.00010$\theta^{T-15°C}$ s^{-1}, k_b = 0.0$h_b\theta_b$/h$\theta^{T-15°C}$ s^{-1}, θ = 1.2)	R_{11} R_{12} R_{13}
Aqueous complexation reaction in immobile water phase	CIMW1+ CIMW2 $\leftrightarrow$ CIMW3 (k_f = 0.002$h_b\theta_b$/h m^3/g /s, k_b = 0.005$h_b\theta_b$/h s^{-1})	R_{14}
Adsorption/desorption or ion-exchange reaction between immobile water and bed sediment phases	CIMW1+BS $\leftrightarrow$ CB1 + BS CIMW2+BS $\leftrightarrow$ CB2 + BS CIMW3+BS $\leftrightarrow$ CB3 + BS (k_f = 0.00001$h_b\theta_b$/h m^2/g BS/s, k_b = 0.0/h /m/s)	R_{15} R_{16} R_{17}
Volatilization reaction of dissolved chemical from mobile water phase	CMW2 $\leftrightarrow$ P (k_f = 0.00002 /s, k_b = 0.02 g/m^3/ATM/s) (P=0.0025ATM)	R_{18}
Precipitation/dissolution reaction between mobile water and suspension precipitate phases	CMW3 $\leftrightarrow$ SP3 (k_f = 0.0001 /s, k_b = 0.0000001 /s)	R_{19}
Precipitation/dissolution reaction between immobile water and bed precipitate phases	CIMW3 $\leftrightarrow$ BP3 (k_f = 0.0001 $h_b\theta_b$/h s^{-1}, k_b = 0.0000001 $h_b\theta_b$/h s^{-1})	R_{20}

Table 5.2-2 Equations Obtained through Decomposition in Example 5.2.1

Kinetic-Variable Transport Equations
$\dfrac{\partial(hE_1)}{\partial t} + L(E_1{}^m) = h\left(-R_2 - R_4 - R_5 - R_7 - R_{11} - R_{13} - R_{19}\right)$ where $E_1 = E_1{}^m = \rho_{CMW1}C_{CMW1} + \rho_{CMW3}C_{CMW3}$
$\dfrac{\partial(hE_2)}{\partial t} + L(E_2{}^m) = h\left(-R_3 - R_4 - R_6 - R_7 - R_{12} - R_{13} - R_{18} - R_{19}\right)$ where $E_2 = E_2{}^m = \rho_{CMW2}C_{CMW2} + \rho_{CMW3}C_{CMW3}$
$\dfrac{\partial(hE_3)}{\partial t} + L(E_3{}^m) = h\left(R_2 - R_8\right)$ where $E_3 = E_3{}^m = \rho_{CS1}C_{CS1}$
$\dfrac{\partial(hE_4)}{\partial t} + L(E_4{}^m) = h\left(R_3 - R_9\right)$ where $E_4 = E_4{}^m = \rho_{CS2}C_{CS2}$
$\dfrac{\partial(hE_5)}{\partial t} + L(E_5{}^m) = h\left(R_4 - R_{10}\right)$ where $E_5 = E_5{}^m = \rho_{CS3}C_{CS3}$
$\dfrac{\partial(hE_6)}{\partial t} + L(E_6{}^m) = h\left(R_5 + R_8 + R_{15}\right)$ where $E_6 = \rho_{CB1}C_{CB1}$ and $E_6{}^m = 0$
$\dfrac{\partial(hE_7)}{\partial t} + L(E_7{}^m) = h\left(R_6 + R_9 + R_{16}\right)$ where $E_7 = \rho_{CB2}C_{CB2}$ and $E_7{}^m = 0$
$\dfrac{\partial(hE_8)}{\partial t} + L(E_8{}^m) = h\left(R_7 + R_{10} + R_{17}\right)$ where $E_8 = \rho_{CB3}C_{CB3}$ and $E_8{}^m = 0$
$\dfrac{\partial(hE_9)}{\partial t} + L(E_9{}^m) = h\left(R_{11} - R_{14} - R_{15}\right)$ where $E_9 = \rho_{CIMW1}C_{CIMW1}$ and $E_9{}^m = 0$
$\dfrac{\partial(hE_{10})}{\partial t} + L(E_{10}{}^m) = h\left(R_{12} - R_{14} - R_{16}\right)$ where $E_{10} = \rho_{CIMW2}C_{CIMW2}$ and $E_{10}{}^m = 0$
$\dfrac{\partial(hE_{11})}{\partial t} + L(E_{11}{}^m) = h\left(R_{13} + R_{14} - R_{17} - R_{20}\right)$ where $E_{11} = \rho_{CIMW3}C_{CIMW3}$ and $E_{11}{}^m = 0$
$\dfrac{\partial(hE_{12})}{\partial t} + L(E_{12}{}^m) = hR_{19}$ where $E_{12} = E_{12}{}^m = \rho_{SP3}C_{SP3}$
$\dfrac{\partial(hE_{13})}{\partial t} + L(E_{13}{}^m) = hR_{20}$ where $E_{13} = \rho_{BP3}C_{BP3}$ and $E_{13}{}^m = 0$
Mass Action Equation
$C_{CMW3} = 0.4C_{CMW1}C_{CMW2}$

Note: $\rho_i = \rho_w$ for CMW1~CMW3, and SP3; $\rho_i = SS$ for CS1~CS3; $\rho_i = h_b\rho_{wb}\theta_b/h$, for CIMW1~CIMW3, and BP3; and $\rho_i = BS/h$, for CB1~CB3. ($\rho_w = \rho_{wb} = 1$ kg/L, $h_b = 0.2$ m, and $\theta_b = 0.5$)

Figures 5.2-2 through 5.2-4 depict the concentration contour at the end of simulation of SS, CMW1, and CIMW1, respectively. Figure 5.2.-2 shows trend of increasing concentration of the suspended sediment along down stream direction. It indicates that deposition is less than erosion under the condition set for this example. Because the reactive chemical transport was assumed having no effect on sediment transport, concentration distribution of SS in case 1 is the same as case 2. Figure 5.2-3 shows a decreasing concentration of CMW1 along the downstream direction. This is because we allow the adsorption to happen, but do not allow desorption from particulate chemicals to dissolved chemicals to occur. The only source of dissolved chemicals in the immobile water phase is the corresponding dissolved chemicals in the mobile phase. Therefore, Figure 5.2-4 also shows decreasing concentration of CIMW1 along the downstream direction.

Due to the temperature factor $\theta^{T-15^{\circ}C}$ in Table 5.2-1, reaction rates of R11 through R13 increase 6.19 times as temperature increases from 15°C at the center of the domain to 25°C at the top and bottom edges for case 2. Increase of these reaction rates means more dissolved chemicals will diffuse from mobile water phase to immobile water phase, therefore, we observe greater CMW1 concentration at the center than at the edges in Figure 5.2-3 and less CIMW1 at the center than at the edges in Figure 5.2-4.

Animations showing the spatial-temporal distribution of suspended sediment SS (Figure 5.2-2_case 1.avi and Figure 5.2-2_Case 2.avi), dissolved Chemical No. 1 in mobile water CMW1 (Figure 5.2-3_Case 1.avi and Figure 5.2-3_Case 2.avi), and dissolved Chemical No. 1 in immobile water CIMW1 (Figure 5.2-4_Case 1.avi and Figure 5.2-4_Case 2.avi), respectively, are attached in Appendix A. Readers can visualize these moves by clicking the file contained in the attached CD.
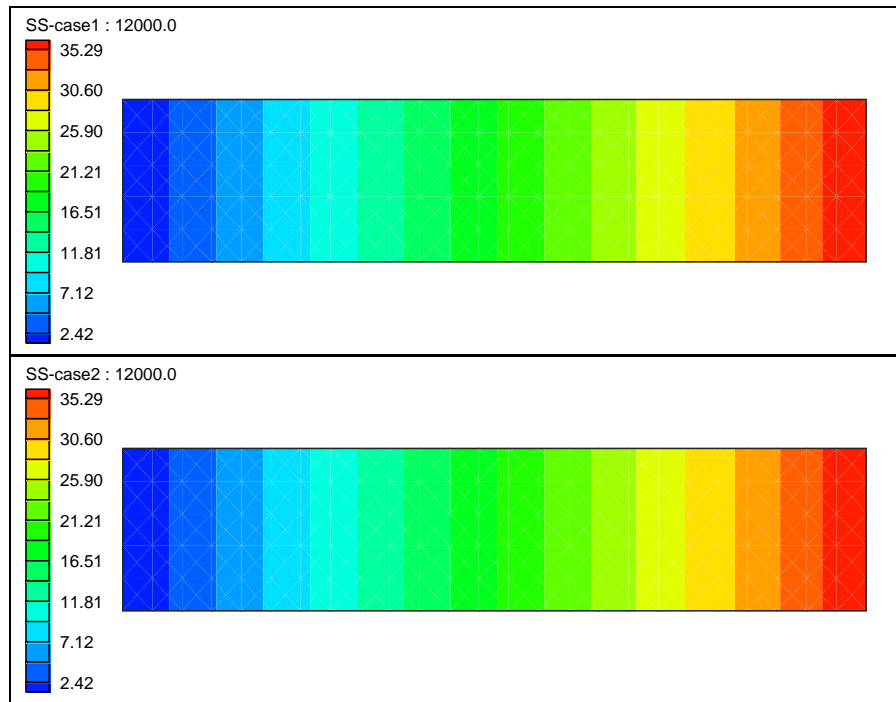
Fig. 5.2-2. Concentration of SS (g/m^3) for Example 5.2.1 Upper: case 1; Lower: case 2
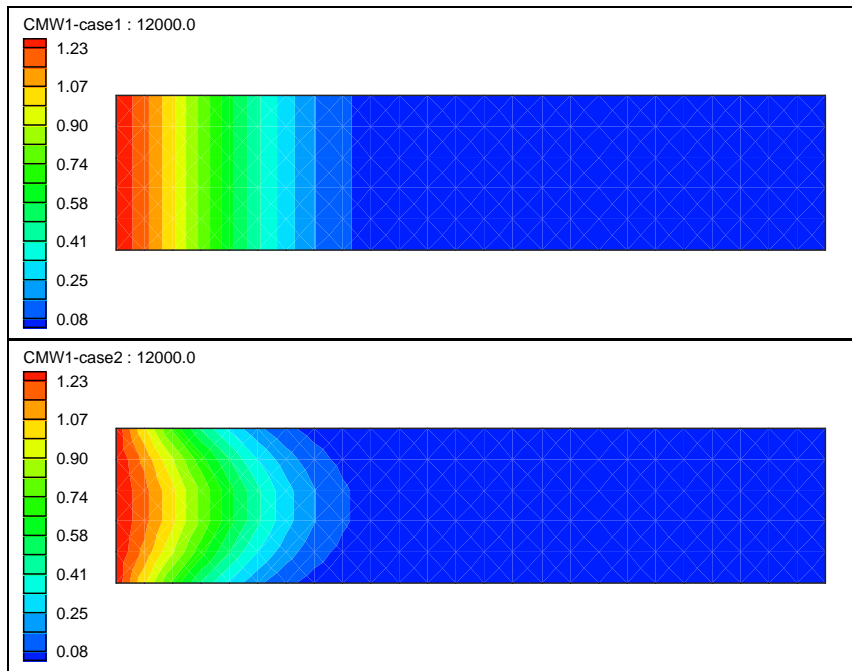
Fig. 5.2-3. Concentration of CMW1 (g/m^3) for Example 5.2.1
Upper: case 1; Lower: case 2
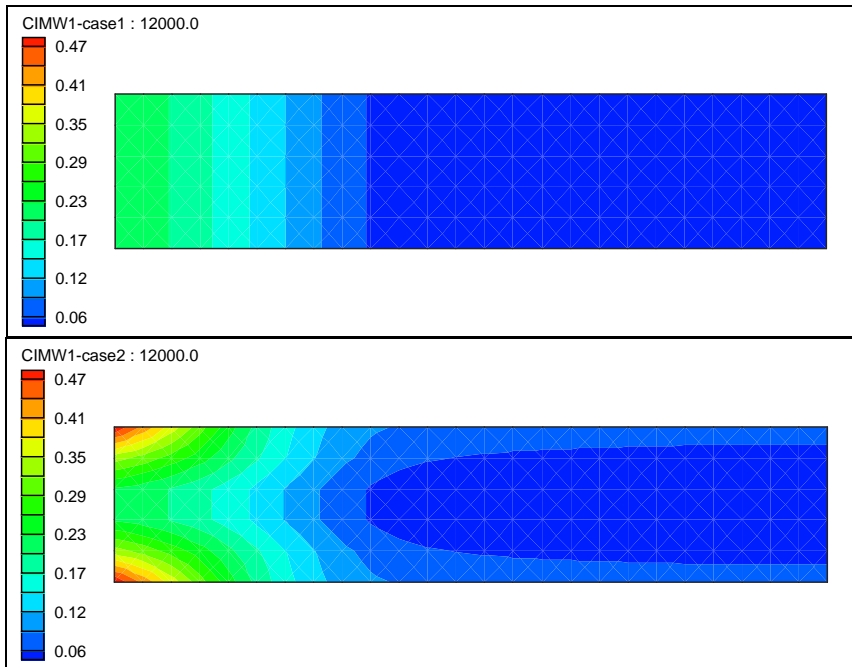
Fig. 5.2-4. Concentration of CIMW1 (g/m^3) for Example 5.2.1
Upper: case 1; Lower: case 2

5.2.2 Overland Transport with Eutrophication in QUAL2E

The Stream Water Quality Model QUAL2E (Brown and Barnwell, 1987) is a typical eutrophication model for stream systems. It is the most recent version of the model QUAL-II (Roesner et al., 1981), which was developed from the model QUAL-I in the 1960s. QUAL2E was first released in 1985 (Brown and Barnell, 1985) and has been successfully applied in many water quality studies since then (Lung, 1986; Wagner et al., 1996; Yang et al., 2000; Ning et al., 2001; Park and Lee, 2002; McAvoy et al., 2003; Ng and Perera, 2003; and Park et al., 2003). In QUAL2E, nine working equations were used to solve for nine water qualities (state variables) that related to eutrophication kinetics (Table 5.2-3).

Table 5.2-3   QUAL2E Original Working Equations

No.	Species	Notation	Working Equations
1	Dissolved Oxygen	O	$\dfrac{dO}{dt} = K_2\theta^{T-20}\left(O^* - O\right) + \left(\alpha_3\mu\theta^{T-20} - \alpha_4\rho\theta^{T-20}\right)\dfrac{Chl\underline{a}}{\alpha_0} - K_1\theta^{T-20}L$ $\qquad - K_4\theta^{T-20}/d - \alpha_5\beta_1 CORDO\theta^{T-20}N_1 - \alpha_6\beta_2 CORDO\theta^{T-20}N_2$
2	Biochemical oxygen demand	L	$\dfrac{dL}{dt} = -K_1\theta^{T-20}L - K_3\theta^{T-20}L$
3	Chlorophyll a	$Chl\underline{a}$	$\dfrac{dChl\underline{a}}{dt} = \mu\theta^{T-20}Chl\underline{a} - \rho\theta^{T-20}Chl\underline{a} - \dfrac{\sigma_1}{d}\theta^{T-20}Chl\underline{a}$
4	Organic nitrogen	N_4	$\dfrac{dN_4}{dt} = \alpha_1\rho\theta^{T-20}\dfrac{Chl\underline{a}}{\alpha_0} - \beta_3\theta^{T-20}N_4 - \sigma_4\theta^{T-20}N_4$
5	Ammonia nitrogen	N_1	$\dfrac{dN_1}{dt} = \beta_3\theta^{T-20}N_4 - \beta_1 CORDO\theta^{T-20}N_1 + \sigma_3\theta^{T-20}/d - F\alpha_1\mu\theta^{T-20}\dfrac{Chl\underline{a}}{\alpha_0}$
6	Nitrite nitrogen	N_2	$\dfrac{dN_2}{dt} = \beta_1 CORDO\theta^{T-20}N_1 - \beta_2 CORDO\theta^{T-20}N_2$
7	Nitrate nitrogen	N_3	$\dfrac{dN_3}{dt} = \beta_2 CORDO\theta^{T-20}N_2 - \left(1-F\right)\alpha_1\mu\theta^{T-20}\dfrac{Chl\underline{a}}{\alpha_0}$
8	Organic phosphorus	P_1	$\dfrac{dP_1}{dt} = \alpha_2\rho\theta^{T-20}\dfrac{Chl\underline{a}}{\alpha_0} - \beta_4\theta^{T-20}P_1 - \sigma_5\theta^{T-20}P_1$
9	Dissolved phosphorous	P_2	$\dfrac{dP_2}{dt} = \beta_4\theta^{T-20}P_1 + \sigma_2\theta^{T-20}/d - \alpha_2\mu\theta^{T-20}\dfrac{Chl\underline{a}}{\alpha_0}$

The eutrophication model of QUAL2E is recast in terms of a network of 16 reactions involving 19 reaction constituents (O, L, Chla, N_4, N_1, N_2, N_3, P_1, P_2, $O_{(b)}$, $L_{(b)}$, $Chla_{(b)}$, $N_{4(b)}$, $N_{(1b)}$, $P_{(1b)}$, $P_{(2b)}$, CO_2, H_2O, and $O_{2(g)}$) in this report (Table 5.2-4). These 16 reactions (Table 5.2-4) address four interacting biogeochemical processes: algae growth kinetics (Reactions R1 through R4), nitrogen cycles (Reactions R5 through R9), phosphorus cycle (Reactions R10 through R12), and carbon cycles (Reactions R13 through R16).

Table 5.2-4   QUAL2E Eutrophication Model Cast in Reaction Network

No.	Mechanism	Reaction	Rate
1	Algae growth	$\alpha_1 N_1 + \alpha_2 P_2 + H_2O + CO_{2(g)} \rightarrow$ $\alpha_0 Chl\underline{a} + \alpha_3 O + (\alpha_4 - \alpha_3)O_{(g)}$	$R = \dfrac{\mu}{\alpha_0}\theta^{T-20}Chl\underline{a}$
2	Diatom growth related nitrate reduction	$N_3 + 1.5H_2O \rightarrow N_1 + (\alpha_5 + \alpha_6)O_{(g)}$	$R = (1-F)\alpha_1\dfrac{\mu}{\alpha_0}\theta^{T-20}Chl\underline{a}$
3	Algae respiration	$\alpha_0 Chl\underline{a} + \alpha_4 O \rightarrow$ $\alpha_1 N_4 + \alpha_2 P_1 + H_2O + CO_{2(g)}$	$R = \dfrac{\rho}{\alpha_0}\theta^{T-20}Chl\underline{a}$
4	Algae settling	$Chl\underline{a} \rightarrow Chl\underline{a}_{(b)}$	$R = \dfrac{\sigma_1}{d}\theta^{T-20}Chl\underline{a}$
5	Mineralization of organic nitrogen	$N_4 \rightarrow N_1$	$R = \beta_3\theta^{T-20}N_4$
6	Organic nitrogen settling	$N_4 \rightarrow N_{4(b)}$	$R = \sigma_4\theta^{T-20}N_4$
7	Biological oxidation of ammonia nitrogen	$N_1 + \alpha_5 O \rightarrow N_2 + 1.5H_2O$	$R = \beta_1 CORDO\theta^{T-20}N_1$
8	Benthos source to ammonia nitrogen	$N_{1(b)} \rightarrow N_1$	$R = \sigma_3\theta^{T-20}/d$
9	Oxidation of nitrate nitrogen	$N_2 + \alpha_6 O \rightarrow N_3$	$R = \beta_2 CORDO\theta^{T-20}N_2$
10	Organic phosphorus decay	$P_1 \rightarrow P_2$	$R = \beta_4\theta^{T-20}P_1$
11	Organic phosphorus settling	$P_1 \rightarrow P_{1(b)}$	$R = \sigma_5\theta^{T-20}P_1$
12	Benthos source to dissolved phosphorus	$P_{2(b)} \rightarrow P_2$	$R = \sigma_2\theta^{T-20}/d$
13	Deoxygenating of BOD	$O + L \rightarrow CO_{2(g)} + H_2O$	$R = K_1\theta^{T-20}L$
14	BOD settling	$L \rightarrow L_{(b)}$	$R = K_3\theta^{T-20}L$
15	Re-aeration	$O_{(g)} \rightarrow O$	$R = K_2\theta^{T-20}(O^* - O)$
16	Sediment oxygen demand	$O \rightarrow O_{(b)}$	$R = K_4\theta^{T-20}/d$

The aforementioned 16 reactions are characterized by seven reaction stoichiometries (Table 5.2-5) and a total of 36 reaction parameters (Table 5.2-6).

Table 5.2-5   QUAL2E Example Reaction Coefficients

Variable	Description	Value	Unit
α_0	Ratio of chlorophyll-a to algae biomass	55	μg-Chl$\underline{a}$ / mg-A
α_1	Fraction of algae mass that is nitrogen	0.08	mg-N / mg-A
α_2	Fraction of algae mass that is phosphorus	0.015	mg-P / mg-A
α_3	O_2 production per unit of algae growth	1.6	mg-O / mg-A
α_4	O_2 uptake per unit of algae respired	1.95	mg-O / mg-A
α_5	O_2 uptake per unit of NH_3 oxidation	3.5	mg-O / mg-N
α_6	O_2 uptake per unit of NO_2 oxidation	1.0	mg-O / mg-N

Table 5.2-6   QUAL2E Example Reaction Rate Parameters

Variable	Description	Value	Unit
M	Algae growth rate	μ_{max}(FL) (FN) (FP)	day^{-1}
μ_{max}	Maximum algae growth rate	2.0	day^{-1}
FL	Algae growth limitation factor for light	$\min\{(1/\lambda d)\ln[(K_L+I)/(K_L+Ie^{-\lambda d})],1\}$	-
λ	Light extinction coefficient	2.0	ft^{-1}
d	Depth of flow	Variable	ft
K_L	Half saturation light intensity	5	Btu/ft^2-hr
I	Surface light intensity	5	Btu/ft^2-hr
FN	Algae growth limitation factor for N	$(N_1+N_3)/(N_1+N_3+K_N)$	-
K_N	Half saturation constant for N	0.155	mg-N/L
FP	Algae growth limitation factor for P	$P_2/(P_2+K_P)$	-
K_P	Half saturation constant for P	0.0255	mg-P/L
θ_μ	Temperature correction for algae growth	1.047	-
F	Fraction of algae N taken from ammonia	$P_NN_1/[P_NN_1+ (1-P_N)N_3]$	-
P_N	Preference factor for ammonia nitrogen	0.5	-
ρ	Algae respiration rate	0.275	day^{-1}
θ_ρ	Temperature correction for algae respiration	1.047	-
σ_1	Algae settling rate	3.25	ft/day
$\theta_{\sigma1}$	Temperature correction for algae settling	1.024	-
β_3	Rate constant for organic N decay	0.21	day^{-1}
$\theta_{\beta3}$	Temperature correction for organic N decay	1.047	-
σ_4	Organic N settling rate	0.0505	day^{-1}
$\theta_{\sigma4}$	Temperature correction for organic N settling	1.024	-
β_1	Rate constant for ammonia oxidation	0.55	day^{-1}
CORDO	Nitrification rate correction factor	$1-e^{-KNITRF*O}$	-

$\theta_{\beta1}$	Temperature correction for ammonia oxidation	1.083	-
KNITRF	First order nitrification inhibition coefficient	0.65	L/mg
σ_3	Benthic source rate for ammonia	0	$mg\text{-}N/ft^2/day$
$\theta_{\sigma3}$	Temperature correction for ammonia source	1.074	-
β_2	Rate constant for nitrite oxidation	1.10	day^{-1}
$\theta_{\beta2}$	Temperature correction for nitrite oxidation	1.047	-
β_4	Rate constant for organic P decay	0.355	day^{-1}
$\theta_{\beta4}$	Temperature correction for organic P decay	1.047	-
σ_5	Organic P settling rate	0.0505	day^{-1}
$\theta_{\sigma5}$	Temperature correction for organic P settling	1.024	-
σ_2	Benthic source rate for dissolved P	0	$mg\text{-}P/ft^2/day$
$\theta_{\sigma2}$	Temperature correction for dissolved P source	1.074	-
K_1	BOD deoxygenating rate constant	1.71	day^{-1}
θ_{K1}	Temperature correction for BOD decay	1.047	-
K_3	BOD settling rate constant	0	day^{-1}
θ_{K3}	Temperature correction for BOD settling	1.024	-
K_2	Re-aeration rate constant	$Min(5.026u^{0.969}d^{-1.673}2.31,10)$	day^{-1}
U	Flow velocity	Variable	ft/day
O^*	Equilibrium oxygen concentration	$e^{-139.3441+1.575701\times10^5/T_k-6.642308\times10^7/T_k^2+1.2438\times10^{10}/T_k^3-8.621949\times10^{11}/T_k^4}$	mg/l
T_k	Temperature	T+273.15	°K=°C+273.15
θ_{K2}	Temperature correction for re-aeration	1.024	-
K_4	Benthic oxygen uptake	0	$mg\text{-}O/ft^2/day$
θ_{K4}	Temperature correction for SOD uptake	1.060	-

An incomplete decomposition of the QUAL2E reaction network would result a total of 19 reaction-extent equations. Because reaction rates of all 16 reactions are function of only the first nine constituents (O, L, Chla, N_4, N_1, N_2, N_3, P_1, and P_2), the governing equations for these nine constituents are decoupled from those for the other 10 constituents ($O_{(b)}$, $L_{(b)}$, $Chla_{(b)}$, $N_{4(b)}$, $N_{(1b)}$, $P_{(1b)}$, $P_{(2b)}$, CO_2, H_2O, and $O_{2(g)}$). These equations are listed in Table 5.2-7. It is noted that because there is no fast reaction involved in the reaction network of QUAL2E, the incompletely decomposed equations of new paradigm are reduced to the generally used primitive reaction-based working equations.

Table 5.2-7   New Paradigm Working Equations for QUAL2E

No.	Species	Notation	Working Equations
1	Dissolved Oxygen	O	$d[O]/dt = \alpha_3 R_1 - \alpha_4 R_3 - \alpha_5 R_7 - \alpha_6 R_9 - R_{13} + R_{15} - R_{16}$
2	Biochemical oxygen demand	L	$d[L]/dt = -R_{13} - R_{14}$
3	Chlorophyll a	$Chl\underline{a}$	$d[Chla]/dt = \alpha_o R_1 - \alpha_o R_3 - R_4$
4	Organic nitrogen	N_4	$d[N_4]/dt = \alpha_1 R_3 - R_5 - R_6$
5	Ammonia nitrogen	N_1	$d[N_1]/dt = -\alpha_1 R_1 + R_2 + R_5 - R_7 + R_8$
6	Nitrite nitrogen	N_2	$d[N_2]/dt = R_7 - R_9$
7	Nitrate nitrogen	N_3	$d[N_3]/dt = -R_2 + R_9$
8	Organic phosphorus	P_1	$d[P_1]/dt = \alpha_2 R_3 - R_{10} - R_{11}$
9	Dissolved phosphorous	P_2	$d[P_2]/dt = -\alpha_2 R_1 + R_{10} + R_{12}$

As shown in Figure 5.2-5, the domain of interest is a shallow water body discretized with 462 elements and 275 nodes. Region A, B, and C are illustrated for simulation results discussion. The flow is allowed to reverse direction every 12 hours (T = 12 hours). The flow pattern was simulated with a flow-reversal boundary condition implemented on the open boundary side and with the rest of the boundary treated as closed. It was also assumed subject to 10 point sources each with an injection rate of 1 m^3/s. As shown in Figure 5.2-6, water depth varies from 0.7 m to 10.3 m during one flow-reversal cycle. The calculated flow velocity ranges from 0.02 m/s to 1.6 m/s at various times during one flow-reversal cycle (Fig. 5.2-7).

To focus on transport, we assume that the temperature is 15 ^{o}C throughout the simulation region. Variable boundary conditions are applied to the open boundary sides. Initial and variable boundary incoming concentrations of the 9 simulated constituents are listed in Table 5.2-8. The dispersion coefficient is 5.2 m^2/s. Each point source injected the biochemical oxygen demand L at a rate of 20.0 g/m^2/s. A 30-day simulation is performed with a fixed time step size of 10 minutes.

Figure 5.2-8 plots the concentration contours of L and Chla at different simulation time. It is seen that at the point sources, the concentration of L increases due to injection, and at the open boundary, the concentration of L decreases due to the low incoming concentration. According to the reaction network of QUAL2E, the source of Chla is algae growth, and the sink of Chla includes algae respiration and settling. The Chla concentration decrease shown in Figure 5.2-8 indicates that the source is less than the sink. Because the settling rate of algae increases when water depth decreases, settling rate in region A is greater than in region C and settling rate in region C is greater than in region B. Therefore, we observe less Chla concentration in region A than in region C and less Chla concentration in region C than in region B. As the simulation time increases, when only small amount of Chla is left, the concentration distribution is mainly affected by advective-dispersive transport rather than reactions.
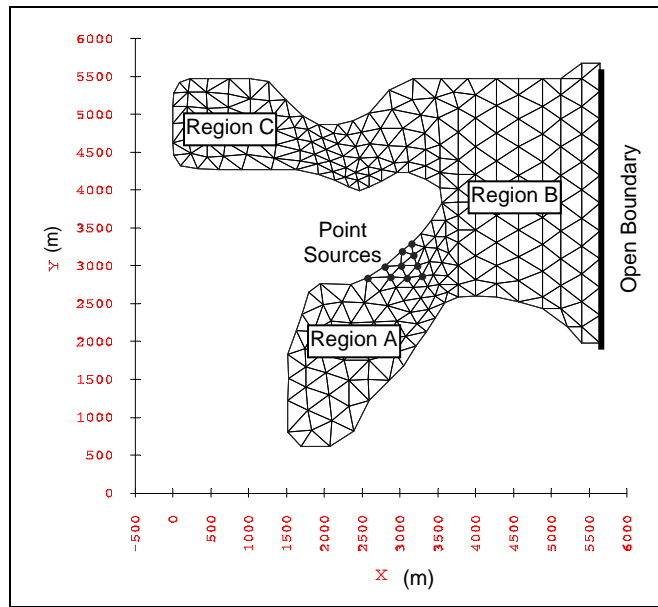
Fig. 5.2-5.   Simulation Domain Descretization for Example 5.2.2
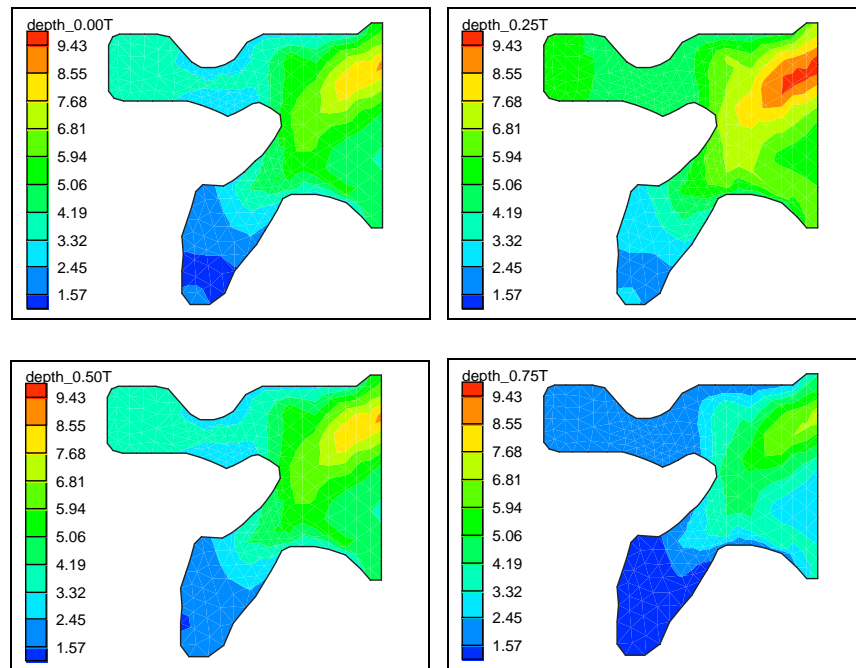
Fig. 5.2-6.   Water Depth (m) at Various Times for Example 5.2.2:
0 T (upper left), 0.25T (upper right), 0.5T (lower left), and 1.0T (lower right)
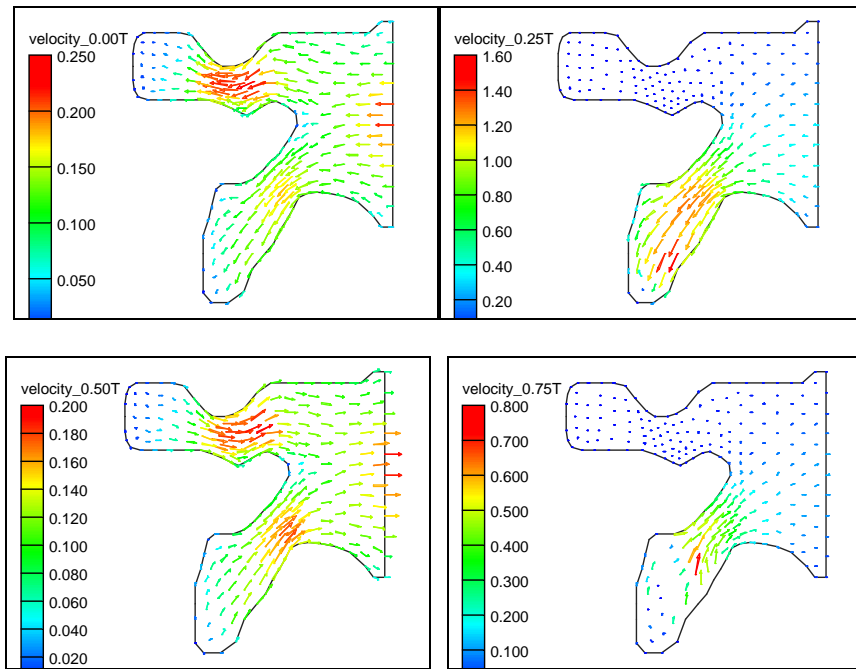
Fig. 5.2-7.   Flow Velocity (m/s) at Various Times for Example 5.2.2:
0 h (upper left), 3 h (upper right), 6 h (lower left), and 12 h (lower right)

Table 5.2-8   Initial and Boundary Concentration in Example 5.2.2

No.	Species	Notatio	Initial	Boundary	ρ_i
1	Dissolved oxygen	O	5 mg-O_2 /kg	0.5 mg-O_2 /L	$\rho_w = 1$ kg/L
2	Biochemical oxygen	L	0.8 mg-O_2 /kg	0.08 mg-O_2 /L	$\rho_w = 1$ kg/L
3	Algae as chlorophyll a	Chla	20.0 µg-	2.0 µg-Chla/L	$\rho_w = 1$ kg/L
4	Organic nitrogen as N	N_4	2.0 mg-N /kg	0.2 mg-N /L	$\rho_w = 1$ kg/L
5	Ammonia as N	N_1	1.0 mg-N /kg	0.1 mg-N /L	$\rho_w = 1$ kg/L
6	Nitrite as N	N_2	0.1 mg-N /kg	0.01 mg-N /L	$\rho_w = 1$ kg/L
7	Nitrate as N	N_3	1.0 mg-N /kg	0.1 mg-N /L	$\rho_w = 1$ kg/L
8	Organic phosphorus as P	P_1	0.5 mg-P /kg	0.05 mg-P /L	$\rho_w = 1$ kg/L
9	Dissolved phosphorus as P	P_2	0.1 mg-P /kg	0.01 mg-P /L	$\rho_w = 1$ kg/L
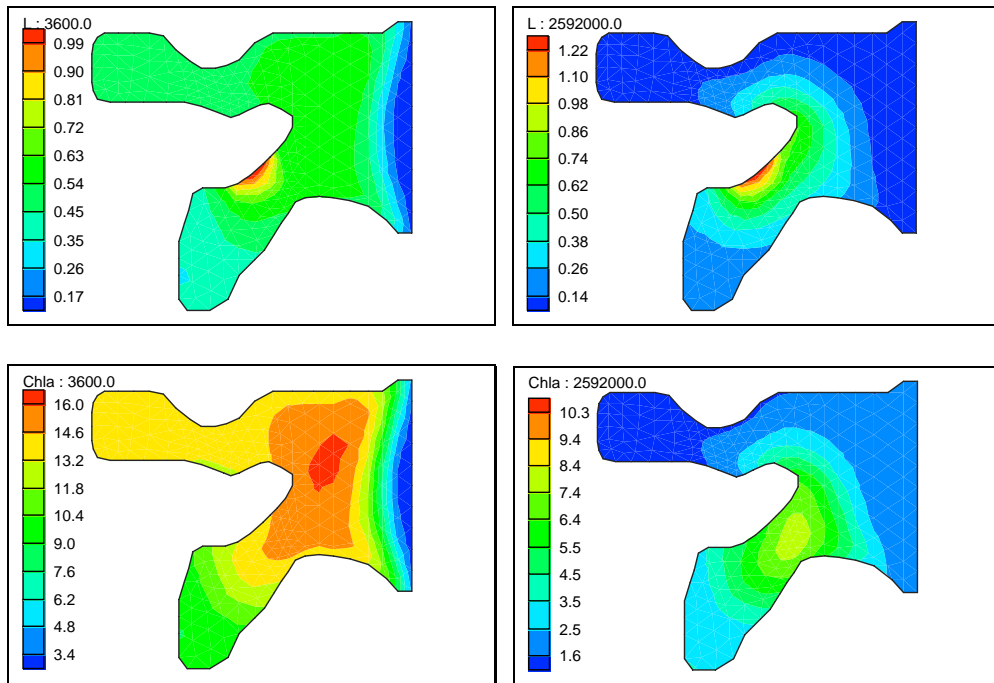
Fig. 5.2-8.   Concentration Contours at 1hour (left) and 720 h (right) in Example 5.2.2:
Upper: L (mg-O_2/L); Lower: Chla (μg-Chla/L)

Animations showing the spatial-temporal distribution of BOD (File Name: QUAL2E BOD.avi) and Chla (File Name: QUAL2E Algae.avi), respectively, are attached in Appendix A.   Readers can visualize these moves by clicking the file contained in the attached CD.

5.2.3   Overland Transport with Eutrophication in WASP5

WASP5, the Water quality Analysis Simulation Program (Ambrose et al., 1993), is a three-dimensional conventional water quality analysis simulation program. It is a group of mechanistic models capable of simulating water transport and fate and transport of water quality constituents and toxic organics for aquatic systems. Various components of WASP5 have been used to study a variety of lake, reservoir, and estuarine issues including ecological characterization, the effects of anthropogenic activities, and the impact of mitigation measures (Bierman and James, 1995; Lung and Larson, 1995; Tufford and McKellar, 1999; Carroll et al., 2004; and Zheng et al., 2004). EUTRO5 is a general operational WASP5 model used to simulate nutrient enrichment, eutrophication, and dissolved oxygen in the aquatic environment. Sixteen working equations were used in EUTRO5 to simulate 16 state variables (NH_3, $NH_{3(b)}$, NO_3, $NO_{3(b)}$, OPO_4, $OPO_{4(b)}$, $PHYT$, $PHYT_{(b)}$, CH_2Ot, $CH_2Ot_{(b)}$, O_2, $O2_{(b)}$, ONt, $ONt_{(b)}$, OPt, and $OPt_{(b)}$) related to eutrophication kinetics (Zhang, 2005).

The eutrophication model of WASH5 was recast in terms of a network of 38 reactions involving 27 reaction constituents (NH_3, $NH_{3(b)}$, NO_3, $NO_{3(b)}$, OPO_4, $OPO_{4(b)}$, $PHYT$, $PHYT_{(b)}$, CH_2O, CH_2Op,

$CH_2O_{(b)}$, $CH_2Op_{(b)}$, O_2, $O_{2(b)}$, ON, ONp, $ON_{(b)}$, $ONp_{(b)}$, OP, OPp, $OP_{(b)}$, $OPp_{(b)}$, CO_2, H_2O, H^+, N_2, and $O_{2(g)}$). Details of these reactions can be found elsewhere (Zhang, 2005). These 38 reactions address sediment-biogeochemical interactions and four interacting biogeochemical processes: phytoplankton growth kinetics, nitrogen cycles, phosphorus cycle, and carbon cycles (Zhang, 2005). They are characterized by three reaction stoichiometries and a total of 66 reaction parameters (Zhang, 2005).

The simulation domain, descretization, flow field and temperature distribution are same as example 5.2.2. Variable boundary conditions are applied to the open boundary sides. Initial concentrations of the 22 simulated species and variable boundary incoming concentrations of mobile species are listed in Table 5.2-9. It is noted that only 22 species out of 27 species are simulated because the governing equations for CO_2, H_2O, H^+, N_2, and $O_{2(g)}$ are decoupled from those for the other 22 species. The decoupling of two sets of state variable is due to the formulation of rate equations that depend on only 22 species.

Table 5.2-9 Species Initial and Boundary Concentration in Example 5.2.3

No.	Species	Notation	Initial	Boundary	ρ_i
1	NH_3	C_1	1 mg N/kg	0.1 mg N/L	ρ_w
2	NO_3	C_3	1 mg N/kg	0.1 mg N/L	ρ_w
3	OPO_4	C_5	0.1 mg P/kg	0.01 mg P/L	ρ_w
4	PHYT	C_7	2 mg C/kg	0.2 mg C/L	ρ_w
5	CH_2O	C_9	10 mg O_2/kg	1.0 mg O_2/L	ρ_w
6	O_2	C_{13}	2 mg O_2/kg	0.2 mg O_2/L	ρ_w
7	ON	C_{15}	2 mg N/kg	0.2 mg N/L	ρ_w
8	OP	C_{19}	0.35 mg P/kg	0.035 mg P/L	ρ_w
9	$CH_2O_{(p)}$	C_{10}	0.2 mg O_2/mg	1.0 mg O_2/L	SS
10	$ON_{(p)}$	C_{16}	0.0 mg N/mg	0 mg N/L	SS
11	$OP_{(p)}$	C_{20}	0.003 mg P/mg	0.015 mg P/L	SS
12	$NH_{3(b)}$	C_2	1 mg N/kg	-	$h_b\rho_{wb}\theta_b$/
13	$NO_{3(b)}$	C_4	1 mg N/kg	-	$h_b\rho_{wb}\theta_b$/
14	$OPO_{4(b)}$	C_6	0.1 mg P/kg	-	$h_b\rho_{wb}\theta_b$/
15	$PHYT_{(b)}$	C_8	2 mg C/kg	-	$h_b\rho_{wb}\theta_b$/
16	$CH_2O_{(b)}$	C_{11}	10 mg O_2/kg	-	$h_b\rho_{wb}\theta_b$/
17	$O_{2(b)}$	C_{14}	2 mg O_2/kg	-	$h_b\rho_{wb}\theta_b$/
18	$ON_{(b)}$	C_{17}	2 mg N/kg	-	$h_b\rho_{wb}\theta_b$/
19	$OP_{(b)}$	C_{21}	0.35 mg P/kg	-	$h_b\rho_{wb}\theta_b$/
20	$CH_2O_{(bp)}$	C_{12}	0.002 mg O_2/mg	-	BS/h
21	$ON_{(bp)}$	C_{18}	0.0 mg N/mg	-	BS/h
22	$OP_{(bp)}$	C_{22}	0.00003 mg P/mg	-	BS/h

The dispersion coefficient was 5.2 m^2/s. Each point source injected NO_3 at a rate of 10.0 g/m^2/s. A 30-day (60T) simulation is performed with a fixed time step size of 10 minutes. A relative error of 10^{-4} is used to determine the convergence for iterations involved in the computation.

Figure 5.2-9 plots the concentration contours of NO_3 and PHYT at different simulation time. It is seen that at the point sources, the concentration of NO_3 increases due to the injection, and at the

open boundary, the concentration of NO_3 decreases due to the low incoming concentration. According to the reaction network of WASP5, PHYT growth consumes NO_3. Due to the light effect, the depth averaged growth rate of PHYT increases when water depth decreases. Thus, NO_3 consumed in region A is greater than in region C and NO_3 consumed in region C is greater than in region B. Therefore, we observe less NO_3 concentration in region A than in region C and less NO_3 concentration in region C than in region B.

According to the reaction network, the source of PHYT is its growth, and the sink of PHYT includes its death and settling. The PHYT concentration decrease shown in Figure 5.2-8 indicates that the source is less than the sink. Comparing the concentration distributions of PHYT (Figure 5.2-9) and Chla (Figure 5.2-8), we can see that relative decreasing rate of Chla (compared to the concentration) is greater than that of PHYT. This indicates that the rate of (algae respiration + settling – growth) in the QUAL2E example is greater than the rate of (PHYT death + settling – growth) in this example. The rate difference is due to the different rate formulation and parameterization of the two models.
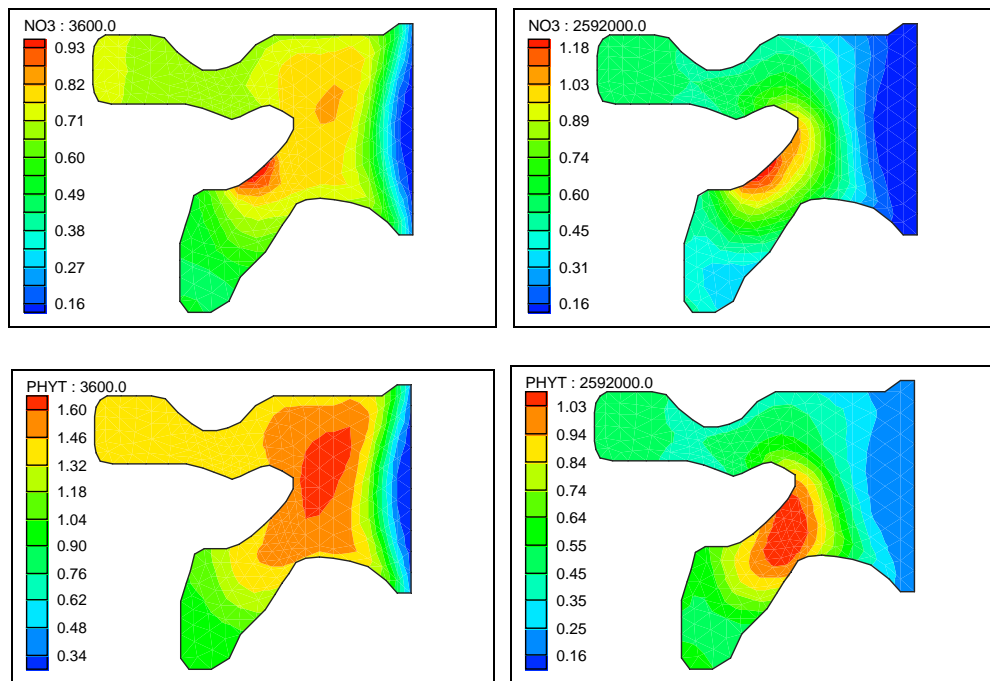
Fig. 5.2-9.   Concentration Contours at 1hour (left) and 60T (right) in Example 5.2.3
Upper: NO_3 (mg-N/L); Lower: PHYT (mg-C/L)

Animations showing the spatial-temporal distribution of nitrate (File Name: WASP5 Nitrogen.avi) and phytoplankton (File Name: WASP5 PHYT.avi), respectively, are attached in Appendix A. Readers can visualize these moves by clicking the file contained in the attached CD.

5.2.4 Overland Transport with Eutrophication in CE-QUAL-ICM

The CE-QUAL-ICM (Cerco and Cole, 1995) water quality model was developed as one component of a model package employed to study eutrophication processes in Chesapeake Bay (Cerco and Cole, 1993; and Cerco and Cole, 2000). Eutrophication processes modeled with the CE-QUAL-ICM were also used to study phosphorus dynamics for the St. Johns River (Cerco and Cole, 2004). Fourty one working equations were used in CE-QUAL-ICM to simulate 41 state variables (Bc, Bd, Bg, DOC, LPOC, RPOC, NH_4, NO_3, DON, LPON, RPON, PO_4t, DOP, LPOP, RPOP, COD, DO, SU, SA, TAM, $POC_{(1b)}$, $POC_{(2b)}$, $POC_{(3b)}$, $NH_{4(1b)}$, $NH_{4(2b)}$, $NO_{3(1b)}$, $NO_{3(2b)}$, $PON_{(1b)}$, $PON_{(2b)}$, $PON_{(3b)}$, $PO_{4(1b)}$, $PO_{4(2b)}$, $POP_{(1b)}$, $POP_{(2b)}$, $POP_{(3b)}$, $COD_{(1b)}$, $COD_{(2b)}$, $SU_{(1b)}$, $SU_{(2b)}$, $SA_{(1b)}$, and $SA_{(2b)}$) related to eutrophication kinetics (Zhang, 2005).

The CE-QUAL-ICM eutrophication model was recast in terms of a network of 90 reactions involving 66 reaction constituents (Bc, Bd, Bg, DOC, LPOC, RPOC, NH_4, NO_3, DON, LPON, RPON, PO_4d, PO_4p, DOP, LPOP, RPOP, COD, DO, SU, SAd, SAp, TAMd, TAMp, $POC_{(1b)}$, $POC_{(2b)}$, $POC_{(3b)}$, $NH_{4(1b)}$, $NH_{4(2b)}$, $NO_{3(1b)}$, $NO_{3(2b)}$, $PON_{(1b)}$, $PON_{(2b)}$, $PON_{(3b)}$, $PO_{4d(1b)}$, $PO_{4p(1b)}$, $PO_{4d(2b)}$, $PO_{4p(2b)}$, $POP_{(1b)}$, $POP_{(2b)}$, $POP_{(3b)}$, $COD_{(1b)}$, $COD_{(2b)}$, $SU_{(1b)}$, $SU_{(2b)}$, $SAd_{(1b)}$, $SAp_{(1b)}$, $SAd_{(2b)}$, $SAp_{(2b)}$, CO_2, H_2O, N_2, $O_{2(g)}$, $Bc_{(b)}$, $Bd_{(b)}$, $Bg_{(b)}$, $TAMp_{(b)}$, BPOC, BNH$_4$, BNO$_3$, BPON, BPO$_4$, BPOP, BCOD, BSU, BSA, and BTAM). Eighty seven of the 90 reactions were considered slow/kinetic reactions and the other seven were fast/equilibrium reactions. Details of these reactions can be found elsewhere (Zhang, 2005). These 90 reactions address sediment-biogeochemical interactions and 6 interacting biogeochemical processes: plant and bacterial growth kinetics, nitrogen cycles, phosphorus cycle, carbon cycles, silica cycles, and metal cycles (Zhang, 2005). They are characterized by 45 reaction stoichiometries and a total of 86 reaction parameters (Zhang, 2005).

The simulation domain, descretization, flow field and temperature distribution are same as example 5.2.2. Variable boundary conditions are applied to the open boundary sides. Initial concentrations of the 48 simulated species and variable boundary incoming concentrations of mobile species are listed in Table 5.2-10. It is noted that only 48 species out of 66 species are simulated because the governing equations for CO_2, H_2O, N_2, $O_{2(g)}$, $Bc_{(b)}$, $Bd_{(b)}$, $Bg_{(b)}$, $TAMp_{(b)}$, BPOC, BNH$_4$, BNO$_3$, BPON, BPO$_4$, BPOP, BCOD, BSU, BSA, and BTAM are decoupled from those for the other 48 species. The decoupling of two sets of state variable is due to the formulation of rate equations that depend on only 48 species.

The dispersion coefficient was 5.2 m^2/s. Each point source injected PO_4d with a rate of 5.0 g/m^2/s. A 2.5-day (5T) simulation is performed with a fixed time step size of 10 minutes. A relative error of 10^{-4} is used to determine the convergence for iterations involved in the computation.

Table 5.2-10 Species Initial and Boundary Concentration in Example 5.2.4

No.	Species	Notati	Initial	Boundary	ρ_i
1	Cyan bacteria	Bc	0.1 mg-C/kg	0.01 mg-C/m^3	ρ_w
2	Diatoms	Bd	1.0 mg-C/kg	0.1 mg-C/m^3	ρ_w
3	Green algae	Bg	2.0 mg-C/kg	0.2 mg-C/m^3	ρ_w
4	Dissolved organic carbon	DOC	5.0 mg-C/kg	0.5 mg-C/m^3	ρ_w
5	Dissolved organic phosphorus	DOP	0.5 mg-P/kg	0.05 mg-P/m^3	ρ_w
6	Dissolved phosphate	PO$_4$d	0.05 mg-P/kg	0.005 mg-	ρ_w
7	Dissolved organic nitrogen	DON	2.0 mg-N/kg	0.2 mg-N/m^3	ρ_w
8	Ammonium	NH$_4$	1.0 mg-N/kg	0.1 mg-N/m^3	ρ_w
9	Nitrate	NO$_3$	1.0 mg-N/kg	0.1 mg-N/m^3	ρ_w
10	Dissolved available silica	SAd	1.0 mg-Si/kg	0.1 mg-Si/m^3	ρ_w
11	Chemical oxygen demand	COD	2.0 mg-O$_2$/kg	0.2 mg-O$_2$/m^3	ρ_w
12	Dissolved oxygen	DO	8.0 mg-O$_2$/kg	0.8 mg-O$_2$/m^3	ρ_w
13	Dissolved active metal	TAMd	0.000005 mol	0.0000005	SS
14	Labile particulate organic carbon	LPOC	0.02 mg-C/mg	0.1 mg-C/m^3	SS
15	Refractory particulate organic	RPOC	0.02 mg-C/mg	0.1 mg-C/m^3	SS
16	Labile particulate organic	LPOP	0.004 mg-P/mg	0.02 mg-P/m^3	SS
17	Refractory particulate organic	RPOP	0.004 mg-P/mg	0.02 mg-P/m^3	SS
18	Particulate phosphate	PO$_4$p	0.00006 mg-	0.0003 mg-	SS
19	Labile particulate organic nitrogen	LPON	0.0002 mg-	0.001 mg-	SS
20	Refractory particulate organic	RPON	0.0002 mg-	0.001 mg-	SS
21	Particulate available silica	SAp	0.0012 mg-	0.006 mg-	SS
22	Particulate biogenic silica	SU	0.0002 mg-Si/mg	0.01 mg-Si/m^3	SS
23	Particulate active metal	TAMp	0.0002 mol /mg	0.001 mol /m^3	SS
24	Benthic dissolved phosphate	PO$_4$d$_{(1)}$	0.9 mg-P/kg	-	$h_b\rho_{wb}\theta_b/h$
25	Benthic dissolved phosphate	PO$_4$d$_{(2)}$	1.8 mg-P/kg	-	$h_b\rho_{wb}\theta_b/h$
26	Benthic ammonium layer 1	NH$_{4(1b)}$	1.0 mg-N/kg	-	$h_b\rho_{wb}\theta_b/h$
27	Benthic ammonium layer 2	NH$_{4(2b)}$	2.0 mg-N/kg	-	$h_b\rho_{wb}\theta_b/h$
28	Benthic nitrate layer 1	NO$_{3(1b)}$	1.0 mg-N/kg	-	$h_b\rho_{wb}\theta_b/h$
29	Benthic nitrate layer 2	NO$_{3(2b)}$	2.0 mg-N/kg	-	$h_b\rho_{wb}\theta_b/h$
30	Benthic dissolved available silica	SAd$_{(1b)}$	0.6 mg-Si/kg	-	$h_b\rho_{wb}\theta_b/h$
31	Benthic dissolved available silica	SAd$_{(2b)}$	1.2 mg-Si/kg	-	$h_b\rho_{wb}\theta_b/h$
32	Benthic chemical oxygen demand	COD$_{(1)}$	2.0 mg-O$_2$/kg	-	$h_b\rho_{wb}\theta_b/h$
33	Benthic chemical oxygen demand	COD$_{(2)}$	4.0 mg-O$_2$/kg	-	$h_b\rho_{wb}\theta_b/h$
34	Benthic particulate organic carbon	POC$_{(1b)}$	0.0195 mg-C/mg	-	BS/h
35	Benthic particulate organic carbon	POC$_{(2b)}$	0.0075 mg-C/mg	-	BS/h
36	Benthic particulate organic carbon	POC$_{(3b)}$	0.003 mg-C/mg	-	BS/h
37	Benthic particulate organic	POP$_{(1b)}$	0.0039 mg-P/mg	-	BS/h
38	Benthic particulate organic	POP$_{(2b)}$	0.0015 mg-P/mg	-	BS/h
39	Benthic particulate organic	POP$_{(3b)}$	0.0006 mg-P/mg	-	BS/h
40	Benthic particulate phosphate layer	PO$_4$p$_{(1)}$	0.0000099 mg-	-	BS/h
41	Benthic particulate phosphate layer	PO$_4$p$_{(2)}$	0.0000198 mg-	-	BS/h
42	Benthic particulate organic nitrogen	PON$_{(1b)}$	0.000195 mg-N/mg	-	BS/h
43	Benthic particulate organic nitrogen	PON$_{(2b)}$	0.000084 mg-N/mg	-	BS/h
44	Benthic particulate organic nitrogen	PON$_{(3b)}$	0.000021 mg-N/mg	-	BS/h
45	Benthic particulate available silica	SAp$_{(1b)}$	0.0000066 mg-	-	BS/h
46	Benthic particulate available silica	SAp$_{(2b)}$	0.0000132 mg-	-	BS/h
47	Benthic particulate biogenic silica	SU$_{(1b)}$	0.003 mg-Si/mg	-	BS/h
48	Benthic particulate biogenic silica	SU$_{(2b)}$	0.006 mg-Si/mg	-	BS/h

Figure 5.2-10 plots the concentration contours of PO$_4$d at different simulation time. It is seen that at the point sources, concentration of PO$_4$d increases due to the injection, and at the open boundary, concentration of PO$_4$d decreases due to the low incoming concentration.
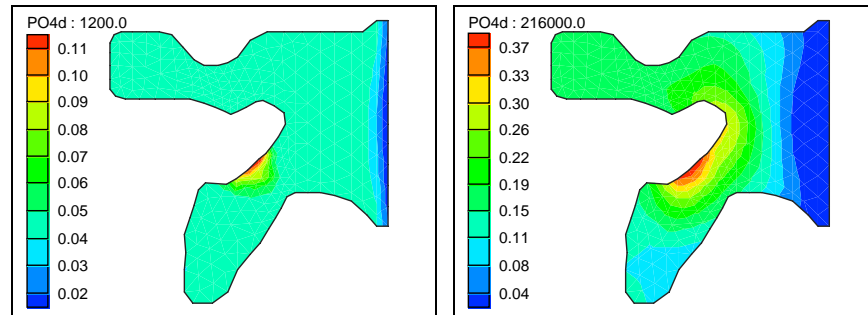
Fig. 5.2-10.   Concentration of PO$_4$d (mg-P/L) in Example 5.2.4
Left: 20 minutes; Right: 5T

Figure 5.2-11 plots the concentration contours of Bc, Bd, and Bg. According to the reaction network of CE-QUAL-ICM, the source of Bc, Bd, and Bg is the growth, and the sink of Bc, Bd, and Bg includes basal metabolism, predating, and settling. The concentration decrease of Bc, Bd, and Bg shown in the Figure 5.2-11 indicates that the source is less than the sink. Among these three groups of algae, Bd has special need of silica to form cell walls. The similar concentration distribution of Bc, Bd, and Bg indicates that under the condition set for this example, there is enough silica, which does not limit the growth of Bd.

Comparing the concentration distributions of Bc (bacteria), Bd (diatom), and Bg (green alage) (Figure 5.2-11), PHYT (Figure 5.2-9) and Chla (Figure 5.2-8), we can see that relative decreasing rate of Chla is greater than Bc, Bd, Bg, and PHYT. This indicates that the rate of (algae respiration + settling – growth) in the QUAL2E example is greater than the rate of (PHYT death + settling – growth) in the WASP5 example and the rate of (Bc, Bd, and Bg basal metabolism + predating + settling – growth) in this example. The rate difference is due to the different rate formulation and parameterization of the models. For example, in QUAL2E, there is only transfer of chemicals from water column to bed. However, WASP5 and CE-QUAL-ICM include both column and benthic interactions. Thus, the algae settling speed in QUAL2E example is greater than the PHYT settling speed in WASP5 example and the Bc, Bd, and Bg settling speeds in CE-QUAL-ICM example.

Animations showing the spatial-temporal distribution of dissolved phosphorus (File Name: CE-QUAL-ICM PO4d.avi), bacteria (File Name: CE-QUAL-ICM Bc Bacteria.avi), diatom (File Name: CE-QUAL-ICM Bd diatom.avi), and green alage (File Name: CE-QUAL-ICM Bg Green algae.avi), respectively, are attached in Appendix A. Readers can visualize these moves by clicking the file contained in the attached CD.
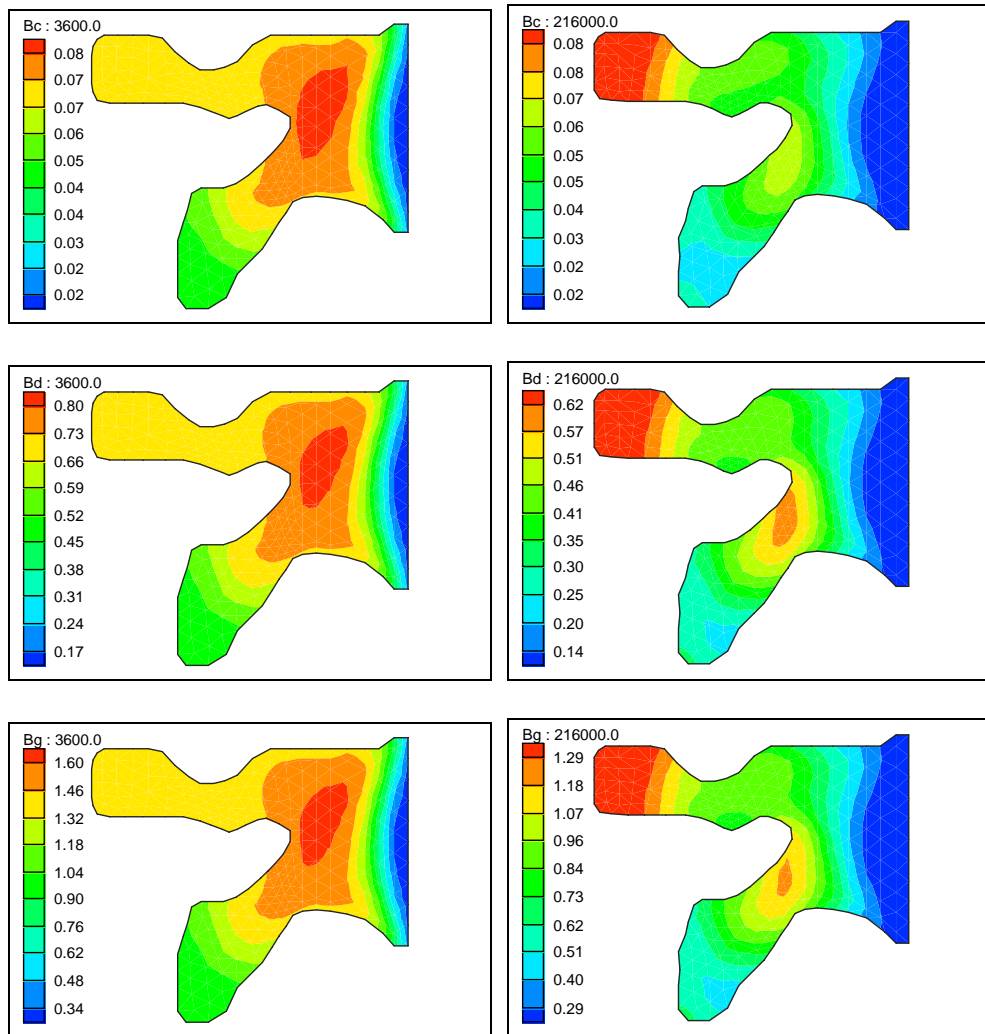
Fig. 5.2-11. Concentration of Algae (mg-C/L) at 1 hour (Left) and 5T (Right)
in Example 5.2.4: Upper: Bc; Middle: Bd; Lower: Bg

5.2.5   Discussions on Diagonalization Approaches to Water Quality Modeling

To demonstrate flexibility of the general paradigm to model water quality, the eutrophication
kinetics in three widely used models, QUAL2E, WASP5, and CE-QUAL-ICM, were recast in the
mode of reaction networks and employed as examples. Table 5.2-11 lists the comparison of the
three models via a reaction point of view.

Table 5.2-11   Comparison of QUAL2E, WASP5, and CE-QUAL-ICM

Model	QUAL2E	WASP5	CE-QUAL-ICM
Number and types of reactions	**16 kinetic reactions and 0 equilibrium reactions:** Algal kinetics: 4 Dissolved Oxygen Balance: 4 Nitrogen Cycle: 5 Phosphorus Cycle: 3	**32 kinetic reactions and 6 equilibrium reactions:** Phytoplankton Kinetics: 11 Dissolved Oxygen Balance: 9 Nitrogen Cycle: 11 Phosphorus Cycle: 7	**83 kinetic reactions and 7 equilibrium reactions:** Plant and bacterial Kinetics: 14 Dissolved Oxygen Balance: 16 Nitrogen Cycle: 20 Phosphorus Cycle: 21 Silica Cycle: 16 Metal Cycle: 3
No. of reactive water quality related to eutrophication kinetics in the report	**9** O, L, Chla, N_4, N_1, N_2, N_3, P_1, and P_2.	**16** NH_3, $NH_{3(b)}$, NO_3, $NO_{3(b)}$, OPO_4, $OPO_{4(b)}$, PHYT, $PHYT_{(b)}$, CH_2Ot, $CH_2Ot_{(b)}$, O_2, $O2_{(b)}$, ONt, $ONt_{(b)}$, OPt, and $OPt_{(b)}$.	**41** Bc, Bd, Bg, DOC, LPOC, RPOC, NH_4, NO_3, DON, LPON, RPON, PO_4t, DOP, LPOP, RPOP, COD, DO, SU, SA, TAM, $POC_{(1b)}$, $POC_{(2b)}$, $POC_{(3b)}$, $NH_{4(1b)}$, $NH_{4(2b)}$, $NO_{3(1b)}$, $NO_{3(2b)}$, $PON_{(1b)}$, $PON_{(2b)}$, $PON_{(3b)}$, $PO_{4(1b)}$, $PO_{4(2b)}$, $POP_{(1b)}$, $POP_{(2b)}$, $POP_{(3b)}$, $COD_{(1b)}$, $COD_{(2b)}$. $SU_{(1b)}$, $SU_{(2b)}$, $SA_{(1b)}$, and $SA_{(2b)}$
No. of water quality from the reaction point of view	**19** (first 9 modeled) O, L, Chla, N_4, N_1, N_2, N_3, P_1, P_2, $O_{(b)}$, $L_{(b)}$, $Chla_{(b)}$, $N_{4(b)}$, $N_{(1b)}$, $P_{(1b)}$, $P_{(2b)}$, CO_2, H_2O, and $O_{2(g)}$	**27** (first 22 modeled) NH_3, $NH_{3(b)}$, NO_3, $NO_{3(b)}$, OPO_4, $OPO_{4(b)}$, PHYT, $PHYT_{(b)}$, CH_2O, CH_2Op, $CH_2O_{(b)}$, $CH_2Op_{(b)}$, O_2, $O_{2(b)}$, ON, ONp, $ON_{(b)}$, $ONp_{(b)}$, OP, OPp, $OP_{(b)}$, $OPp_{(b)}$, CO_2, H_2O, H^+, N_2, and $O_{2(g)}$.	**66** (first 48 modeled) Bc, Bd, Bg, DOC, LPOC, RPOC, NH_4, NO_3, DON, LPON, RPON, PO_4d, PO_4p, DOP, LPOP, RPOP, COD, DO, SU, SAd, SAp, TAMd, TAMp, $POC_{(1b)}$, $POC_{(2b)}$, $POC_{(3b)}$, $NH_{4(1b)}$, $NH_{4(2b)}$, $NO_{3(1b)}$, $NO_{3(2b)}$, $PON_{(1b)}$, $PON_{(2b)}$, $PON_{(3b)}$, $PO_4d_{(1b)}$, $PO_4p_{(1b)}$, $PO_4d_{(2b)}$, $PO_4p_{(2b)}$, $POP_{(1b)}$, $POP_{(2b)}$, $POP_{(3b)}$, $COD_{(1b)}$, $COD_{(2b)}$, $SU_{(1b)}$, $SU_{(2b)}$, $SAd_{(1b)}$, $SAp_{(1b)}$, $SAd_{(2b)}$, $SAp_{(2b)}$, CO_2, H_2O, N_2, $O_{2(g)}$, $Bc_{(b)}$, $Bd_{(b)}$, $Bg_{(b)}$, $TAMp_{(b)}$, BPOC, BNH_4, BNO_3, BPON, BPO_4, BPOP, BCOD, BSU, BSA, and BTAM
No. Reaction Parameters	**36**	**66**	**86**

In the context of reaction network, there are 16, 38, and 90 biogeochemical reactions included in QUAL2E, WASP5, and CE-QUAL-ICM, respectively. All three models include the major interactions of the nutrient cycles; algae kinetics modified by temperature, light, and nutrient limitation; and dissolved oxygen balance under the effect of benthic oxygen demand, carbonaceous oxygen uptake, and atmospheric aeration. Therefore, under the similar conditions set for three eutrophication examples, we obtained similar algae concentration distributions in Figures 5.2-8, 5.2-9, and 5.2-11, for QUAL2E, WASP5, and CE-QUAL-ICM, respectively.

In QUAL2E, sediment-biogeochemical interactions are not considered. However, WASP5 and CE-QUAL-ICM include both column and benthic interactions. In QUAL2E, there is transfer of chemicals from water column to bed, but no chemicals transferred from benthic bed to column. In WASP5 and CE-QUAL-ICM, dissolved fractions are subject to diffusion, particulate fractions can settle and re-suspend, and inorganic nutrients can also enter into column water by benthic release.

In QUAL2E and WASP5 model, nutrient cycles include nitrogen cycles and phosphorus cycles. In addition to these two nutrient cycles, CE-QUAL-ICM also includes silica cycle and metal cycle. Consideration of silica cycle makes it possible to include kinetics of diatoms, which are distinguished by their requirement of silica as a nutrient. In QUAL2E and WASP5, all algae or phytoplankton are simulated as one group. However, in CE-QUAL-ICM, algae are grouped in to three classes: cyan bacteria, diatoms, and greens. Therefore, concentration distributions of three algae groups rather than one are plotted in Figure 5.2-11 for CE-QUAL-ICM.

In the original reports, there are 9, 16, and 41 water quality state-variables related to eutrophication kinetics simulated in QUAL2E, WASP5, and CE-QUAL-ICM, respectively. In the context of reaction network, there are 19, 27, and 66 constituents involved in QUAL2E, WASP5, and CE-QUAL-ICM, respectively. In the case of QUAL2E, all 16 rate equations depend only on the first nine constituents; thus, the other 10 constituents can be decoupled from the first 9 in any simulation. Had evidence indicated that the rate formulation of the 16 kinetic reactions also depended on the other 10 constituents in a system, all 19 constituents would have been modeled simultaneously. Therefore, when QUAL2E is applied to any system, the first order of business is to check if the rate formulation for the 16 kinetic reactions is valid. If it is, then one can consider other issues involved in applying the model to the system. If any of the 16 rate equations is invalid, then one should not apply the model to the system.

In the case of WASP5, rates of the 32 kinetic reactions were assumed not affected by the last 5 constituents. Thus, these 5 constituents can be decoupled from the other 22. Therefore, one only needs to simulate 22 constituents simultaneously from the reaction point of view. The question is then why WASP5 only considered 16 water quality state-variables. Examination of 6 fast equilibrium reactions would reveal that the adsorption reactions of aqueous CH_2O, $CH_2O_{(b)}$, ON, $ON_{(b)}$, OP, and $OP_{(b)}$ onto sediments were formulated with a simple partition. Furthermore, rate equations are only functions of the aqueous fractions of CH_2Ot ($=CH_2O + CH_2Op$), $CH_2Ot_{(b)}$ ($=CH_2O_{(b)} + CH_2Op_{(b)}$), ONt ($=ON + ONp$), $ONt_{(b)}$($= ON_{(b)} + ONp_{(b)}$), OPt ($=OP + OPp$), and $OPt_{(b}$($=OP_{(b)} + OPp_{(b)}$); not functions of 12 individual species in the parentheses. Thus, if we eliminate these 12 species using the 6 partition equations and 6 equations defining the total, the reaction-based approach would yield 16 identical equations as those in the WASP5 report. In our reaction-based approach, we prefer to model all 22 species. This allows us, if necessary, the flexibility of more mechanistically modeling the sorption reactions and formulating the rate equations as functions of all individual species. Similarly, for CE-QUAL-ICM, we prefer to model 48 species out of the total 66 species, rather than 41 constituents. This reaction-based approach alleviates the need of modeling 7 sorption reactions with a simple partition. In the decomposition of reaction-matrix, the elimination of 7 fast equilibrium reactions is performed automatically rather then manually. Ideally, one should model all of the 66 species if any of the reaction rates is affected by the other 18 species.

No attempts were made to compare the simulation results with field measurements because this is not the main objective of this report. It is almost certain that the simulations presented above will not match with field measurements using all reaction parameters reported in QUAL2E, WASP5, or CE-QUAL-ICM. The important question then is what we should do to calibrate the model. There may be three ways out. Take QUAL2E as an example. First we can abuse the model by optimizing all 36 rate parameters characterizing 16 reaction rate equations with the best optimization technique disregarding the physics involved in the system. Second we can justify the model by fine-tuning some of the 36 rate parameters or better reformatting some of the rate equations based on our understanding of the system. Third, we can wise the model by researching if there are new mechanisms that are operating in the system under investigation but not included in QUAL2E. In order not to abuse the model, a general paradigm is developed that has the design capability to include any number of reactions involving any number of species and that provides a protocol for formulating the rates of reactions and discovering the assumptions and limitations of the model employed.

The reaction network for QUAL2E system includes 16 kinetic reactions involving 19 species. Substitution of this reaction network into Equation (2.6.30) results in 19 ordinary differential equations for 19 species in a well-mixed system. Because the rates of all 16 reactions depend on only the first 9 species, equations governing the last 10 species are decoupled from the equations governing the first 9 species. Thus, only the first 9 species were considered in QUAL2E. The exclusion of the last 10 species has an important implication when QUAL2E is applied to a new system other than the one QUAL2E was developed for.

In a "true" reaction-based approach, governing equations for all species involved in the reaction network must be considered. The diagonalization of the reaction matrix for all 19 species would result in a set of 15 kinetic-variable equations [Equations (1) through (9) and (14) through (19) in Table 5.2-12] and 4 component equations [Equations (10) through (13) in Table 5.2-12].

If we substitute Equations (14) through (19) into Equations (1) through (9) in Table 5.2-12, the resulting first 9 equations are then decoupled from the last 10 equations. Once the resulting 9 equations are solved for C_1 through C_9, Equations (14) through (19) are used to calculated the dynamics of $Chl\underline{a}_{(b)}$, $N_{4(b)}$, $P_{2(b)}$, $L_{(b)}$, $O_{2(g)}$, and $O_{(b)}$, and Equations (10) through (13) can be used to calculate the amount of H_2O, CO_2, $N_{1(b)}$, and $P_{1(b)}$ that must be supplied to maintain the conservation principle for water, carbon dioxide, benthic organic nitrogen, and benthic organic phosphorus. In a large water body, the amount of water needed to maintain its conservation due to biogeochemical processes can be met without much problem. The nagging question is what would be the source of CO_2, $N_{1(b)}$, and $P_{1(b)}$ to maintain their conservation with respective to reactions. For any system, if this nagging question cannot be answered, then the partial pressure of CO_2 and the concentrations of $N_{1(b)}$ and $P_{1(b)}$ would probably be important factors in controlling reaction rates and inducing additional biogeochemical processes. Under such circumstances, one probably has to revisit the rate equations and to conduct research to uncover additional reaction networks for the system under investigations.

Table 5.2-12 Governing Equations for the Reaction-based Diagonalization Approach

Decomposition Equations	No.
$dE_1/dt = d\left[0.00027\left(C_3 + Chla_{(b)}\right) + C_9 + P_{2(b)}\right]/dt = -0.015R_3 + R_{10}$	(1)
$dE_2/dt = d\left[C_9 + P_{2(b)}\right]/dt = -0.015R_1 + R_{10}$	(2)
$dE_3/dt = d\left[-0.21\left(C_1 - C_2 + O_{2(g)} + O_{(b)} - L_{(b)}\right) + 0.0078\left(C_3 + Chla_{(b)}\right) - 0.77C_6 - C_7 + 5.1\left(C_9 + P_{2(b)}\right)\right]/dt = R_2 + 5.1R_{10}$	(3)
$dE_4/dt = d\left[0.00032\left(C_3 + Chla_{(b)}\right) + 0.22\left(C_4 + N_{4(b)}\right) + 1.2\left(C_9 + P_{2(b)}\right)\right]/dt = -0.22R_5 + 1.2R_{10}$	(4)
$dE_5/dt = d\left[-0.22\left(C_1 - C_2 + O_{2(g)} + O_{(b)} - L_{(b)}\right) + 0.0078\left(C_3 + Chla_{(b)}\right) + 0.23C_6 + 5.1\left(C_9 + P_{2(b)}\right)\right]/dt = R_7 + 5.11R_{10}$	(5)
$dE_6/dt = d\left[0.0094\left(C_1 - C_2 + O_{2(g)} + O_{(b)}\right) - 0.00033\left(C_3 + Chla_{(b)}\right) + 0.033C_6 - 0.22\left(C_9 + P_{2(b)}\right)\right]/dt = -0.043R_9 - 0.22R_{10}$	(6)
$dE_7/dt = d\left[0.0015\left(C_3 + Chla_{(b)}\right) + C_4 + C_5 + C_6 + C_7 + N_{4(b)}\right]/dt = R_8$	(7)
$dE_8/dt = d\left[0.00027\left(C_3 + Chla_{(b)}\right) + C_8 + C_9 + P_{2(b)}\right]/dt = -R_{11}$	(8)
$dE_9/dt = d\left(C_2 + L_{(b)}\right)/dt = -R_{13}$	(9)
$dT_1/dt = d\left(C_2 + L_{(b)} + H_2O\right)/dt = 0$	(10)
$dT_2/dt = d\left(C_2 + L_{(b)} + CO_2\right)/dt = 0$	(11)
$dT_3/dt = d\left[0.0015\left(C_3 + Chla_{(b)}\right) + C_4 + C_5 + C_6 + C_7 + N_{1(b)} + N_{4(b)}\right]/dt = 0$	(12)
$dT_4/dt = d\left[0.00027\left(C_3 + Chla_{(b)}\right) + C_8 + C_9 + P_{1(b)} + P_{2(b)}\right]/dt = 0$	(13)
$dE_{10}/dt = dChla_{(b)}/dt = R_4$	(14)
$dE_{11}/dt = dN_{4(b)}/dt = R_6$	(15)
$dE_{12}/dt = dP_{2(b)}/dt = -R_{12}$	(16)
$dE_{13}/dt = dL_{(b)}/dt = R_{14}$	(17)
$dE_{14}/dt = dO_{2(g)}/dt = -R_{15}$	(18)
$dE_{15}/dt = dO_{(b)}/dt = R_{16}$	(19)

$C_1 = O$, $C_2 = L$, $C_3 = \underline{Chla}$, $C_4 = N_4$, $C_5 = N_1$, $C_6 = N_2$, $C_7 = N_3$, $C_8 = P_1$, and $C_9 = P_2$

The use of diagonalization approaches allows one to formulate some rate equations one by one. For example, the reaction rate R_8 can be calculated by plotting the concentration of E_7 versus time in which E_7 is the linear combination of C_3, C_4, C_5, C_6, C_7, $Chla_{(b)}$ and $P_{2(b)}$ [see Equation (7) in Table 5.2-12]. Similarly, reaction rates R_{11}, R_{13}, R_4, R_6, R_{12}, R_{14}, R_{15}, and R_{16} can be calculated from the dynamics of E_8 through E_{15}, respectively [see Equations (8), (9) and (14) through (19) in Table 5.2-12]. Because linearly dependent reactions are present in the system, one cannot formulate all rate equations independently. To do so, one has to design an experimental system such that only linearly independent reactions are present to individually and mechanistically formulate rate equations.

5.3 Three-Dimensional Examples

Three examples are employed in this section. The first two examples involving simulations of uranium transport in soil columns are presented to evaluate the ability of the model to simulate reactive transport with reaction networks involving both kinetically and equilibrium-controlled reactions. The third example is a hypothetical three-dimensional problem and is presented to demonstrate the model application to a field-scale problem involving reactive transport with a complex reaction network.

5.3.1 Packed Column Breakthrough Curve Simulation for Uranium (VI) Sorption

A glass column of approximately one cm in diameter by 3 cm long was filled with 2.483 g crushed and sieved (< 2 mm) soil material with a porosity of 0.66. The soil contained 1.9 percent Fe oxides on a mass basis. A solution with 10 μM U(VI) and 50 mM $NaNO_3$ was injected at a specific discharge of 1.235 cm/h until breakthrough was observed. The inlet solution was switched to a U(VI) free solution after 614.7 PV (Pace et al., 2005).

In the simulation, the column is discretized with 20 nodes and 4 equal size elements (0.886 cm × 0.886 cm × 0.779 cm each) (Fig. 5.3-1). Other parameters for the experiments are summarized in Figure 5.3-1. The simulation was performed for a total duration of 2,500 hours with a constant time-step size of 0.25 hour.

Packed Column Parameters

Total volume: 2.45 cm³
Cross section area: 0.785 cm²
Total length: 3.12 cm
Pore volume (PV): 1.62 cm³
Porosity: 0.66 cm³/cm³
Mass of solids: 2.48 g
Bulk Density: 1.02 g/cm³
Flow rate: 0.97 cm³/hour
Darcy velocity: 1.24 cm/hour
Pulse duration: 615 PV
Total duration: 1493 PV
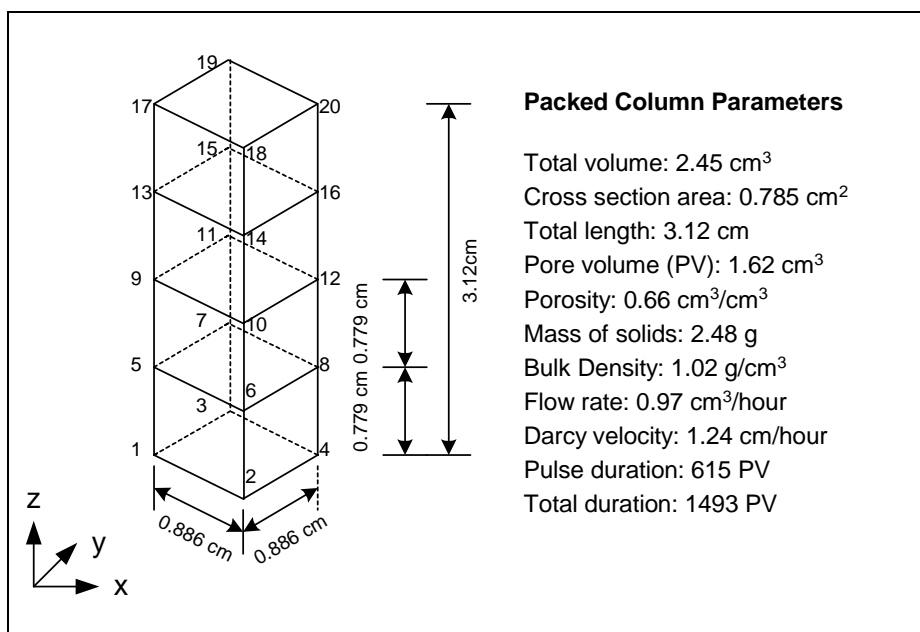
Fig. 5.3-1. Simulation Domain and Descretization for Example 5.3.1
Note: the column parameters are from Pace et al. (2005)

The reaction network utilized in the model is described in Table 5.3-1 (Lindsay, 1979, Brooks, 2001, Waite et al., 1994, and Langmuir, 1997), which utilizes 46 species and 39 equilibrium reactions. Because the activity of H_2O is assumed to be 1.0, it is decoupled from the system; hence only 45 chemical species are considered. The system involves 6 kinetic-variable transport equations (Table 5.3-2) and 39 equilibrium reaction mass action equations or user specified nonlinear algebraic equations (Table 5.3-3) set up through decomposition for 45 species.

Among the kinetic-variables, the fifth involves no mobile species and is not solved in the advection-dispersion transport step. Therefore, instead of solving 27 advection-dispersion transport equations for mobile species in a primitive approach, we only solve 5 advection-dispersion transport equations for kinetic-variables. Furthermore, one of the kinetic variables, E_6, involves only mobile species, which makes its transport equation linear allowing its solution to be solved outside the nonlinear iteration loop between transport and reactions when the fully-implicit scheme is used to deal with reactive chemistry. Since all reactions are equilibrium reactions, kinetic-variables are equivalent to components.

The experimental data and simulation results are shown in Figure 5.3-1. The simulation results closely follow the data, reflecting retardation due to reactions on both the leading and tailing portions of the breakthrough curve. The results provide validation of the reaction network employed to simulate uranium (VI) transport and the numerical implementation.
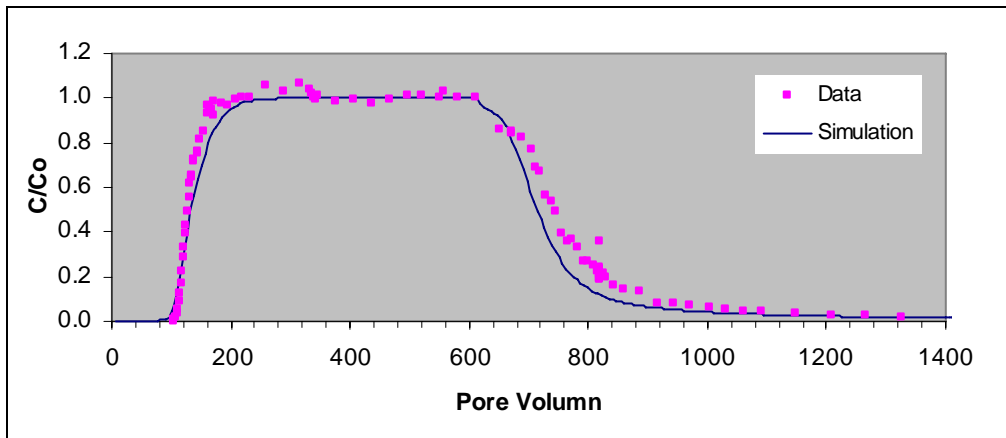
Fig. 5.3-2. U(VI) Breakthrough Curve for the Packed Column
Note: the experiment data are from Pace et al. (2005)

Table 5.3-1   Chemical Reactions Considered in Example 5.3.1

Reactions and Parameters	No.
$Fe(OH)_3 + 3H^+ = Fe^{3+} + 3H_2O$ logK = 2.7	(1)
$UO_2^{2+} + H_2O = UO_2OH^+ + H^+$ logK = -5.2	(2)
$UO_2^{2+} + 2H_2O = UO_2(OH)_{2(aq)} + 2H^+$ logK = -10.3	(3)
$UO_2^{2+} + 3H_2O = UO_2(OH)_3^- + 3H^+$ logK = -19.2	(4)
$UO_2^{2+} + 4H_2O = UO_2(OH)_4^{2-} + 4H^+$ logK = -33.0	(5)
$2UO_2^{2+} + H_2O = (UO_2)_2OH^{3+} + H^+$ logK = -2.7	(6)
$2UO_2^{2+} + 2H_2O = (UO_2)_2(OH)_2^{2+} + 2H^+$ logK = -5.62	(7)
$3UO_2^{2+} + 4H_2O = (UO_2)_3(OH)_4^{2+} + 4H^+$ logK = -11.9	(8)
$3UO_2^{2+} + 5H_2O = (UO_2)_3(OH)_5^+ + 5H^+$ logK = -15.5	(9)
$3UO_2^{2+} + 7H_2O = (UO_2)_3(OH)_7^- + 7H^+$ logK = -31.0	(10)
$UO_2^{2+} + CO_3^{2-} = UO_2CO_{3(aq)}$ logK = 9.68	(11)
$UO_2^{2+} + 2CO_3^{2-} = UO_2(CO_3)_2^{2-}$ logK = 16.94	(12)
$UO_2^{2+} + 3CO_3^{2-} = UO_2(CO_3)_3^{4-}$ logK = 21.6	(13)
$3UO_2^{2+} + 6CO_3^{2-} = (UO_2)_3(CO_3)_6^{6-}$ logK = 54.0	(14)
$2UO_2^{2+} + 4H_2O + CO_{2(g)} = (UO_2)_2CO_3(OH)_3^- + 5H^+$ logK = -19.01	(15)
$> Fe_sOH + H^+ + CO => Fe_sOH_2^+$ logK = 6.51	(16)
$> Fe_sOH => Fe_sO^- + H^+ + CO$ logK = -9.13	(17)
$> Fe_s(OH)_2 + UO_2^{2+} = (> Fe_sO_2)UO_2 + 2H^+$ logK = -2.57	(18)
$> Fe_w(OH)_2 + UO_2^{2+} = (> Fe_wO_2)UO_2 + 2H^+$ logK = -6.28	(19)
$> Fe_sOH + H_2CO_3 => Fe_sCO_3H + H_2O$ logK = 2.90	(20)
$> Fe_sOH + H_2CO_3 => Fe_sCO_3^- + H_2O + H^+ + CO$ logK = -5.09	(21)
$> Fe_s(OH)_2 + UO_2^{2+} + H_2CO_3 = (> Fe_sO_2)UO_2CO_3^{2-} + 4H^+ + 2CO$ logK $= -13.0$	(22)
$> Fe_w(OH)_2 + UO_2^{2+} + H_2CO_3 = (> Fe_wO_2)UO_2CO_3^{2-} + 4H^+ + 2CO$ logK $= -17.10$	(23)
$FeOH^{2+} + H^+ = Fe^{3+} + H_2O$ logK = 2.19	(24)
$Fe(OH)_2^+ + 2H^+ = Fe^{3+} + 2H_2O$ logK = 5.67	(25)
$Fe(OH)_3^0 + 3H^+ = Fe^{3+} + 3H_2O$ logK = 12.56	(26)
$Fe(OH)_4^- + 4H^+ = Fe^{3+} + 4H_2O$ logK = 21.6	(27)
$H_2O + CO_{2(g)} = H_2CO_3^0$ logK = -1.47	(28)
$H_2CO_3^0 = H^+ + HCO_3^-$ logK = -6.35	(29)
$HCO_3^- = H^+ + CO_3^{2-}$ logK = -10.33	(30)
$> Fe_wOH + H^+ + CO => Fe_wOH_2^+$ logK = 6.51	(31)
$> Fe_wOH => Fe_wO^- + H^+ + CO$ logK = -9.13	(32)
$> Fe_wOH + H_2CO_3 => Fe_wCO_3H + H_2O$ logK = 2.90	(33)
$> Fe_wOH + H_2CO_3 => Fe_wCO_3^- + H_2O + H^+ + CO$ logK = -5.09	(34)
$0 \cdot Fe(OH)_3 = 0 \cdot [> Fe_sOH_2^+ + > Fe_sO^- + > Fe_sCO_3H + > Fe_sCO_3^- + (> Fe_sO_2)UO_2 + (> Fe_sO_2)UO_2CO_3^{2-}] +$ $> Fe_sOH$, $0.0018C_{Fe(OH)_3} = C_{>Fe_sOH} + C_{>Fe_sOH_2^+} + C_{>Fe_sO^-} + C_{>Fe_sCO_3H} + C_{>Fe_sCO_3^-} + 2(C_{(>Fe_sO_2)UO_2} + C_{(>Fe_sO_2)UO_2CO_3^{2-}})$	(35)
$0 \cdot Fe(OH)_3 = 0 \cdot [> Fe_wOH_2^+ + > Fe_wO^- + > Fe_wCO_3H + > Fe_wCO_3^- + (> Fe_wO_2)UO_2 + (> Fe_wO_2)UO_2CO_3^{2-}] +$ $> Fe_wOH$, $0.8732C_{Fe(OH)_3} = C_{>Fe_wOH} + C_{>Fe_wOH_2^+} + C_{>Fe_wO^-} + C_{>Fe_wCO_3H} + C_{>Fe_wCO_3^-} + 2(C_{(>Fe_wO_2)UO_2} + C_{(>Fe_wO_2)UO_2CO_3^{2-}})$	(36)
$0 \cdot > Fe_sOH => Fe_s(OH)_2$ $C_{Fe_sOH} = 2C_{Fe_s(OH)_2}$	(37)
$0 \cdot > Fe_wOH => Fe_w(OH)_2$ $C_{Fe_wOH} = 2C_{Fe_w(OH)_2}$	(38)
$UO_2^{2+} + NO_3^- = UO_2NO_3^+$ logK = -0.300	(39)

Table 5.3-2 Kinetic-variable Transport Equations Solved in Example 5.3.1

Kinetic-Variable Transport Equations	No.
$\dfrac{\partial(\theta E_1)}{\partial t} + L(E_1^{\ m}) = 0$ $E_1 = \rho_w \begin{bmatrix} H^+ - HCO_3^- - 2CO_3^{2-} - UO_2OH^+ - 2UO_2(OH)_{2(aq)} - 3UO_2(OH)_3^- - 4UO_2(OH)_4^{2-} - (UO_2)_2OH^{3+} \\ -2(UO_2)_2(OH)_2^{2+} - 4(UO_2)_3(OH)_4^{2+} - 5(UO_2)_3(OH)_5^+ - 7(UO_2)_3(OH)_7^- - 2UO_2CO_{3(aq)} - FeOH^{2+} \\ -4UO_2(CO_3)_2^{2-} - 6UO_2(CO_3)_3^{3-} - 12(UO_2)_3(CO_3)_6^{6-} - 5(UO_2)_2CO_3(OH)_3^- - 2Fe(OH)_2^+ - 3Fe(OH)_3^0 \end{bmatrix}$ $-3\rho_w Fe(OH)_3 + \rho_S \begin{bmatrix} > Fe_sOH_2^+ - > Fe_sO^- - 2(> Fe_sO_2)UO_2 - 2(> Fe_wO_2)UO_2 - 4(> Fe_sO_2)UO_2CO_3^{2-} \\ -4(> Fe_wO_2)UO_2CO_3^{2-} - > Fe_sO_3^- - 4Fe(OH)_4^- + > Fe_wOH_2^+ - > Fe_wO^- - > Fe_wCO_3^- \end{bmatrix}$ $E_1^{\ m} = \rho_w \begin{bmatrix} H^+ - HCO_3^- - 2CO_3^{2-} - UO_2OH^+ - 2UO_2(OH)_{2(aq)} - 3UO_2(OH)_3^- - 4UO_2(OH)_4^{2-} - (UO_2)_2OH^{3+} \\ -2(UO_2)_2(OH)_2^{2+} - 4(UO_2)_3(OH)_4^{2+} - 5(UO_2)_3(OH)_5^+ - 7(UO_2)_3(OH)_7^- - 2UO_2CO_{3(aq)} - FeOH^{2+} \\ -4UO_2(CO_3)_2^{2-} - 6UO_2(CO_3)_3^{3-} - 12(UO_2)_3(CO_3)_6^{6-} - 5(UO_2)_2CO_3(OH)_3^- - 2Fe(OH)_2^+ - 3Fe(OH)_3^0 \end{bmatrix}$	(1)
$\dfrac{\partial(\theta E_2)}{\partial t} + L(E_2^{\ m}) = 0 \qquad E_2 = \rho_w \left[Fe^{3+} + FeOH^{2+} + Fe(OH)_2^+ + Fe(OH)_3^0 + Fe(OH)_4^- \right] + \rho_P Fe(OH)_3$ $E_2^{\ m} = \rho_w \left[Fe^{3+} + FeOH^{2+} + Fe(OH)_2^+ + Fe(OH)_3^0 + Fe(OH)_4^- \right]$	(2)
$\dfrac{\partial(\theta E_3)}{\partial t} + L(E_3^{\ m}) = 0$ $E_3 = \rho_w \begin{bmatrix} UO_2^{2+} + UO_2OH^+ + UO_2(OH)_{2(aq)} + UO_2(OH)_3^- + UO_2(OH)_4^{2-} + 2(UO_2)_2OH^{3+} \\ +2(UO_2)_2(OH)_2^{2+} + 3(UO_2)_3(OH)_4^{2+} + 3(UO_2)_3(OH)_5^+ + 3(UO_2)_3(OH)_7^- \\ +UO_2CO_{3(aq)} + UO_2(CO_3)_2^{2-} + UO_2(CO_3)_3^{3-} + 3(UO_2)_3(CO_3)_6^{6-} + 2(UO_2)_2CO_3(OH)_3^- \end{bmatrix}$ $+\rho_S \left[(> Fe_sO_2)UO_2 + (> Fe_wO_2)UO_2 + (> Fe_sO_2)UO_2CO_3^{2-} + (> Fe_wO_2)UO_2CO_3^{2-} \right]$ $E_3^{\ m} = \rho_w \begin{bmatrix} UO_2^{2+} + UO_2OH^+ + UO_2(OH)_{2(aq)} + UO_2(OH)_3^- + UO_2(OH)_4^{2-} + 2(UO_2)_2OH^{3+} \\ +2(UO_2)_2(OH)_2^{2+} + 3(UO_2)_3(OH)_4^{2+} + 3(UO_2)_3(OH)_5^+ + 3(UO_2)_3(OH)_7^- \\ +UO_2CO_{3(aq)} + UO_2(CO_3)_2^{2-} + UO_2(CO_3)_3^{3-} + 3(UO_2)_3(CO_3)_6^{6-} + 2(UO_2)_2CO_3(OH)_3^- \end{bmatrix}$	(3)
$\dfrac{\partial(\theta E_4)}{\partial t} + L(E_4^{\ m}) = 0 \qquad E_4^{\ m} = \rho_w \begin{bmatrix} CO_{2(g)} + H_2CO_3 + HCO_3^- + CO_3^{2-} + UO_2CO_{3(aq)} + 2UO_2(CO_3)_2^{2-} \\ +3UO_2(CO_3)_3^{3-} + 6(UO_2)_3(CO_3)_6^{6-} + (UO_2)_2CO_3(OH)_3^- \end{bmatrix}$ $E_4 = \rho_w \begin{bmatrix} CO_{2(g)} + H_2CO_3 + HCO_3^- + CO_3^{2-} + \\ UO_2CO_{3(aq)} + 2UO_2(CO_3)_2^{2-} + 3UO_2(CO_3)_3^{3-} \\ +6(UO_2)_3(CO_3)_6^{6-} + (UO_2)_2CO_3(OH)_3^- \end{bmatrix} + \rho_S \begin{bmatrix} > Fe_sCO_3H + (> Fe_sO_2)UO_2CO_3^{2-} \\ +(> Fe_wO_2)UO_2CO_3^{2-} + > Fe_sCO_3^- \\ + > Fe_wCO_3H + > Fe_wCO_3^- \end{bmatrix}$	(4)
$\dfrac{\partial(\theta E_5)}{\partial t} + L(E_5^{\ m}) = 0 \qquad E_5 = \rho_S \begin{bmatrix} > Fe_sOH_2^+ - > Fe_sO^- - 2(> Fe_sO_2)UO_2CO_3^{2-} - > Fe_sO_3^- + CO \\ -2(> Fe_wO_2)UO_2CO_3^{2-} + > Fe_wOH_2^+ - > Fe_wO^- - > Fe_wCO_3^- \end{bmatrix} \qquad E_5^{\ m} = 0$	(5)
$\dfrac{\partial(\theta E_6)}{\partial t} + L(E_6^{\ m}) = 0 \qquad E_6 = E_6^{\ m} = \rho_w (NO_3^- + UO_2NO_3^+)$	(6)

Note: as defined in Eq. (2.5.7.4), $\rho_s = \rho_b S_A/\theta$.

Table 5.3-3   Equilibrium Reaction Algebraic Equations Solved in Example 5.3.1

Equilibrium Reaction Algebraic Equations	No.	Equilibrium Reaction Algebraic Equations	No.
$0.0018C_{Fe(OH)_3} = C_{>Fe_sOH} + C_{>Fe_sOH_2^+}$ $+ C_{>Fe_sO^-} + C_{>Fe_sCO_3H} + C_{>Fe_sCO_3^-}$ $+ 2C_{(>Fe_sO_2)UO_2} + 2C_{(>Fe_sO_2)UO_2CO_3^{2-}}$	(1)	$0.8732C_{Fe(OH)_3} = C_{>Fe_wOH} + C_{>Fe_wOH_2^+}$ $+ C_{>Fe_wO^-} + C_{>Fe_wCO_3H} + C_{>Fe_wCO_3^-}$ $+ 2C_{(>Fe_wO_2)UO_2} + 2C_{(>Fe_wO_2)UO_2CO_3^{2-}}$	(2)
$C_{(>Fe_sO_2)UO_2CO_3^{2-}} = \dfrac{10^{-13.0}C_{>Fe_s(OH)_2}C_{UO_2^{2+}}C_{H_2CO_3}}{C_{H^+}{}^4 C_{CO}{}^2}$	(3)	$C_{(>Fe_wO_2)UO_2CO_3^{2-}} = \dfrac{10^{-17.10}C_{>Fe_w(OH)_2}C_{UO_2^{2+}}C_{H_2CO_3}}{C_{H^+}{}^4 C_{CO}{}^2}$	(4)
$C_{(UO_2)_2(OH)_2^{2+}} = 10^{-5.62}C_{UO_2^{2+}}{}^2 / C_{H^+}{}^2$	(5)	$C_{(UO_2)_3(OH)_4^{2+}} = 10^{-11.9}C_{UO_2^{2+}}{}^3 / C_{H^+}{}^4$	(6)
$C_{(UO_2)_3(OH)_5^+} = 10^{-15.5}C_{UO_2^{2+}}{}^3 / C_{H^+}{}^5$	(7)	$C_{(UO_2)_3(OH)_7^-} = 10^{-31.0}C_{UO_2^{2+}}{}^3 / C_{H^+}{}^7$	(8)
$C_{UO_2CO_{3(aq)}} = 10^{-7}C_{UO_2^{2+}}C_{H_2CO_3} / C_{H^+}$	(9)	$C_{UO_2(CO_3)_2^{2-}} = 10^{-16.42}C_{UO_2^{2+}}C_{H_2CO_3}{}^2 / C_{H^+}{}^4$	(10)
$C_{UO_2(CO_3)_3^{4-}} = 10^{-28.44}C_{UO_2^{2+}}C_{H_2CO_3}{}^3 / C_{H^+}{}^6$	(11)	$C_{>Fe_sO^-} = 10^{-9.13}C_{>Fe_sOH} / C_{H^+}C_{CO}$	(12)
$C_{(>Fe_sO_2)UO_2} = 10^{-2.57}C_{>Fe_s(OH)_2}C_{UO_2^{2+}} / C_{H^+}{}^2$	(13)	$C_{(>Fe_wO_2)UO_2} = 10^{-6.28}C_{>Fe_w(OH)_2}C_{UO_2^{2+}} / C_{H^+}{}^2$	(14)
$C_{>Fe_sCO_3^-} = 10^{-5.09}C_{>Fe_sOH}C_{H_2CO_3} / C_{H^+}C_{CO}$	(15)	$C_{(UO_2)_2CO_3(OH)_3^-} = 10^{-17.54}C_{UO_2^{2+}}{}^2C_{H_2CO_3} / C_{H^+}{}^5$	(16)
$C_{(UO_2)_3(CO_3)_6^{6-}} = 10^{-46.08}C_{UO_2^{2+}}{}^3C_{H_2CO_3}{}^6 / C_{H^+}{}^{12}$	(17)	$C_{>Fe_wO^-} = 10^{-9.13}C_{>Fe_wOH} / (C_{H^+}C_{CO})$	(18)
$C_{>Fe_wCO_3^-} = 10^{-5.09}C_{>Fe_wOH}C_{H_2CO_3} / (C_{H^+}C_{CO})$	(19)	$C_{Fe_sOH} = 2C_{Fe_s(OH)_2}$	(20)
$C_{Fe(OH)_3} = 10^{-2.7}C_{Fe^{3+}} / C_{H^+}{}^3$	(21)	$C_{Fe_wOH} = 2C_{Fe_w(OH)_2}$	(22)
$C_{UO_2OH^+} = 10^{-5.2}C_{UO_2^{2+}} / C_{H^+}$	(23)	$C_{UO_2(OH)_{2(aq)}} = 10^{-10.3}C_{UO_2^{2+}} / C_{H^+}{}^2$	(24)
$C_{UO_2(OH)_3^-} = 10^{-19.2}C_{UO_2^{2+}} / C_{H^+}{}^3$	(25)	$C_{UO_2(OH)_4^{2-}} = 10^{-33.0}C_{UO_2^{2+}} / C_{H^+}{}^4$	(26)
$C_{(UO_2)_2OH^{3+}} = 10^{-2.7}C_{UO_2^{2+}}{}^2 / C_{H^+}$	(27)	$C_{CO_3^{2-}} = 10^{-16.68}C_{H_2CO_3} / C_{H^+}{}^2$	(28)
$C_{>Fe_sOH_2^+} = 10^{6.51}C_{>Fe_sOH}C_{H^+}C_{CO}$	(29)	$C_{CO_{2(g)}} = 10^{1.47}C_{H_2CO_3}{}^0$	(30)
$C_{>Fe_sCO_3H} = 10^{2.90}C_{>Fe_sOH}C_{H_2CO_3}$	(31)	$C_{FeOH^{2+}} = 10^{-2.19}C_{Fe^{3+}} / C_{H^+}$	(32)
$C_{Fe(OH)_2^+} = 10^{-5.67}C_{Fe^{3+}} / C_{H^+}{}^2$	(33)	$C_{Fe(OH)_3^0} = 10^{-12.56}C_{Fe^{3+}} / C_{H^+}{}^3$	(34)
$C_{HCO_3^-} = 10^{-6.35}C_{H_2CO_3^0} / C_{H^+}$	(35)	$C_{Fe(OH)_4^-} = 10^{-21.6}C_{Fe^{3+}} / C_{H^+}{}^4$	(36)
$C_{>Fe_wOH_2^+} = 10^{6.51}C_{>Fe_wOH}C_{H^+}C_{CO}$	(37)	$C_{>Fe_wCO_3H} = 10^{2.90}C_{>Fe_wOH}C_{H_2CO_3}$	(38)
$C_{NO_3^-} = 10^{0.3}C_{UO_2NO_3^+} / C_{UO_2^{2+}}$	(39)		

5.3.2   Undisturbed Column Breakthrough Curve Simulation for Uranium (VI) Sorption

This problem involves similar geochemistry to that of the packed column, but involves an undisturbed soil core. A miscible displacement experiment was conducted at pH 4 under atmospheric $CO_2(g)$. The core was 15.2 cm in length and 6.19 cm in diameter and was water-saturated from the bottom at 0.1 ml/h to ensure the removal of trapped air. A non-pulsing medical pump was used to deliver a flush solution to the bottom of the column. Approximately 10 L of 50 mM $CaCl_2$ was used to flush the core. Upon completion of the flush, the influent solution consisted of 50 mg/L U(VI) in 50 mM $CaCl_2$ was pumped through the column at a flow rate of 7 ml/h. The residence time of U(VI) in the column was 26.5 h. The pH of the carrier solution was adjusted to 4 with HCl. Uranium (VI) analysis was conducted using an Inductively Coupled Plasma Mass Spectrometer (ICPMS) (Brooks et al, 2005).

The column was numerically discretized with a simulation grid of 20 nodes and 4 equal sized elements (5.49 cm × 5.49 cm × 3.8 cm each) (Fig. 5.3-3). The experiment duration was 2,448 hours, which was simulated with a constant time-step size of 12 hours. Simulations were initially performed assuming the same equilibrium reactions as in Example 5.3.1. The equilibrium sorption simulation results (upper part of Figure 5.3-4) did not accurately predict U(VI) transport through the undisturbed column, indicating that some of the sorption sites may be kinetically hindered resulting in less sorption. Reactions 18 and 19 (Table 5.3-1) are considered to be the most kinetically limiting reactions. Therefore, a second simulation was performed with these two reactions as rate-limited.

Undisturbed Column Parameters

Total volume: 458 cm^3
Cross section area: 30.1 cm^2
Total length: 15.2 cm
Pore volume (PV): 183 cm^3
Porosity: 0.4 cm^3/cm^3
Mass of solids: 728 g
Bulk Density: 1.59 g/cm^3
Flow rate: 7 cm^3/hour
Darcy velocity: 0.232 cm/hour
Pulse duration: 46.8 PV
Total duration: 93.6 PV
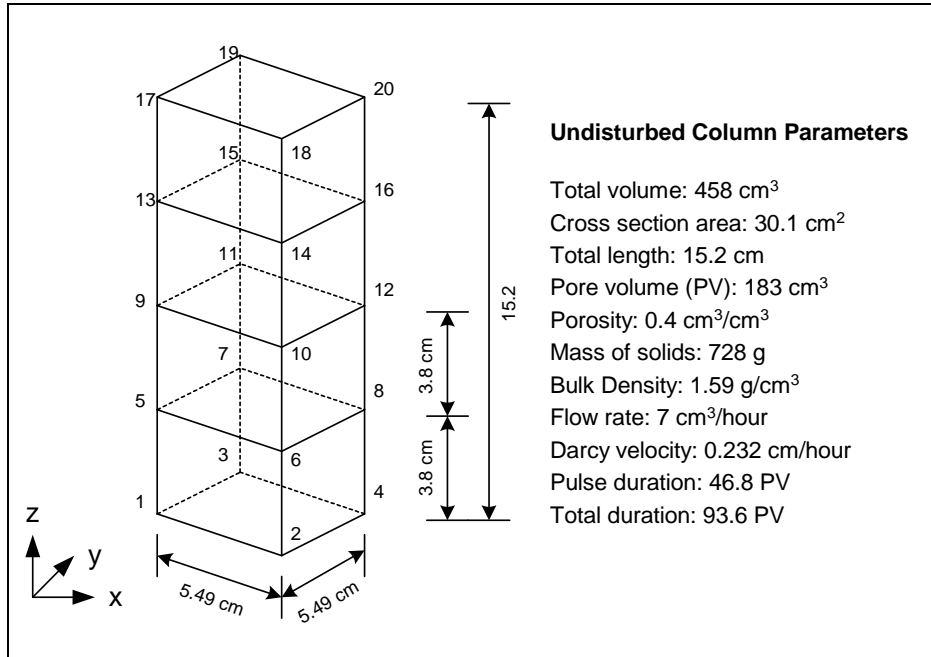
Fig. 5.3-3.   Simulation Domain and Descretization for Example 5.3.2
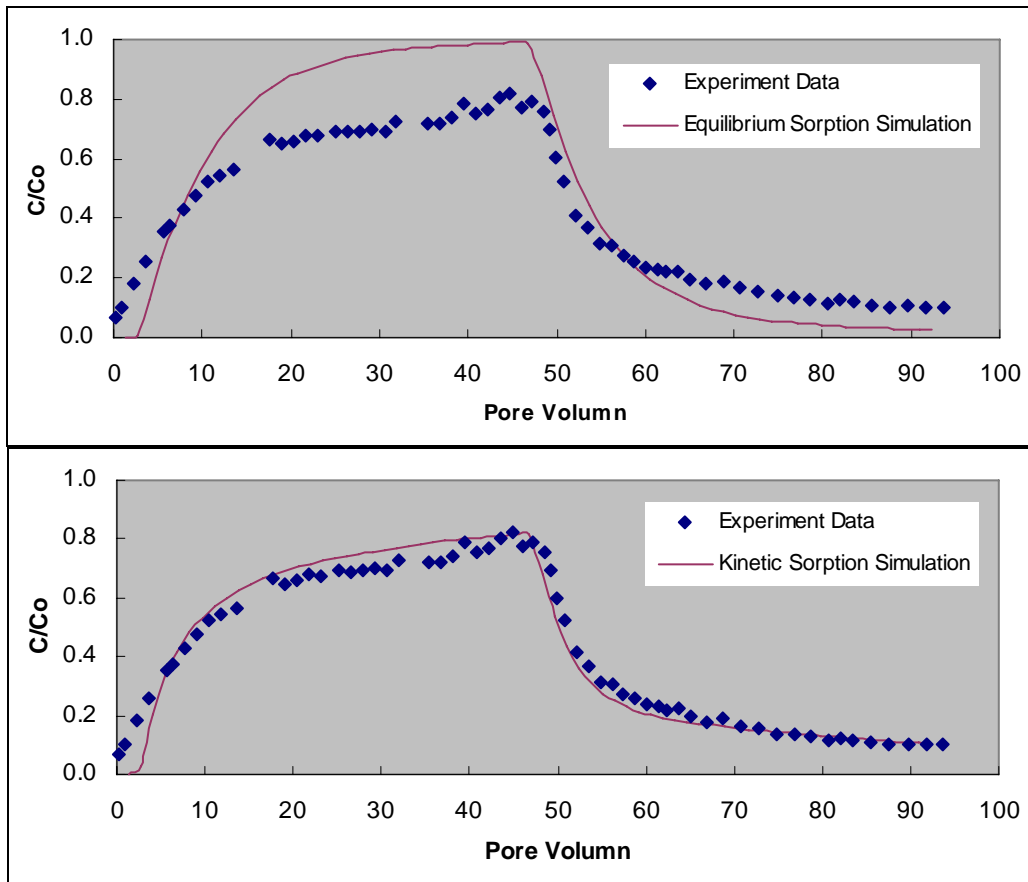
Fig. 5.3-4. U(VI) Breakthrough Curve for the Undisturbed Column
Note: the experiment data are from Brooks et al. (2005)

For the kinetic simulation, we have 46 species, 37 equilibrium reactions and 2 kinetic reactions. As in the previous example, H_2O activity is assumed constant and hence eliminated from the simulation leaving 8 kinetic-variable transport equations (Table 5.3-4) and 37 equilibrium reaction nonlinear algebraic equations (Table 5.3-5) obtained through decomposition.

Among the 8 kinetic-variables, the fifth and the last two involve only immobile species, so that no advection-dispersion equations are needed to solve for them. Therefore, instead of solving 27 mobile species advection-dispersion transport equations, we only need to solve 5 kinetic-variable advection-dispersion transport equations, and the reaction terms related to these kinetic-variables are all simplified. Compared to the previous example, two additional kinetic-variables result from the two linearly independent kinetic reactions. As with the previous example, E_6 can be solved outside the nonlinear iteration loop between hydrologic transport and reactive chemistry when the fully-implicit scheme is used.

Table 5.3-4   Kinetic-variable Transport Equations Solved in Example 5.3.2

Kinetic-Variable Transport Equations	No.
$\dfrac{\partial(\theta E_1)}{\partial t} + L(E_1{}^m) = 0$ $E_1 = \rho_w \begin{bmatrix} H^+ - HCO_3^- - 2CO_3^{2-} - UO_2OH^+ - 2UO_2(OH)_{2(aq)} - 3UO_2(OH)_3^- - 4UO_2(OH)_4^{2-} - (UO_2)_2OH^{3+} \\ -2(UO_2)_2(OH)_2^{2+} - 4(UO_2)_3(OH)_4^{2+} - 5(UO_2)_3(OH)_5^+ - 7(UO_2)_3(OH)_7^- - 2UO_2CO_{3(aq)} - FeOH^{2+} \\ -4UO_2(CO_3)_2^{2-} - 6UO_2(CO_3)_3^{3-} - 12(UO_2)_3(CO_3)_6^{6-} - 5(UO_2)_2CO_3(OH)_3^- - 2Fe(OH)_2^+ - 3Fe(OH)_3^0 \end{bmatrix}$ $-3\rho_w Fe(OH)_3 + \rho_S \begin{bmatrix} > Fe_sOH_2^+ - > Fe_sO^- - 2(> Fe_sO_2)UO_2 - 2(> Fe_wO_2)UO_2 - 4(> Fe_sO_2)UO_2CO_3^{2-} \\ -4(> Fe_wO_2)UO_2CO_3^{2-} - > Fe_sO_3^- - 4Fe(OH)_4^- + > Fe_wOH_2^+ - > Fe_wO^- - > Fe_wCO_3^- \end{bmatrix}$ $E_1{}^m = \rho_w \begin{bmatrix} H^+ - HCO_3^- - 2CO_3^{2-} - UO_2OH^+ - 2UO_2(OH)_{2(aq)} - 3UO_2(OH)_3^- - 4UO_2(OH)_4^{2-} - (UO_2)_2OH^{3+} \\ -2(UO_2)_2(OH)_2^{2+} - 4(UO_2)_3(OH)_4^{2+} - 5(UO_2)_3(OH)_5^+ - 7(UO_2)_3(OH)_7^- - 2UO_2CO_{3(aq)} - FeOH^{2+} \\ -4UO_2(CO_3)_2^{2-} - 6UO_2(CO_3)_3^{3-} - 12(UO_2)_3(CO_3)_6^{6-} - 5(UO_2)_2CO_3(OH)_3^- - 2Fe(OH)_2^+ - 3Fe(OH)_3^0 \end{bmatrix}$	(1)
$\dfrac{\partial(\theta E_2)}{\partial t} + L(E_2{}^m) = 0 \qquad E_2 = \rho_w\left[Fe^{3+} + FeOH^{2+} + Fe(OH)_2^+ + Fe(OH)_3^0 + Fe(OH)_4^- \right] + \rho_P Fe(OH)_3$ $E_2{}^m = \rho_w\left[Fe^{3+} + FeOH^{2+} + Fe(OH)_2^+ + Fe(OH)_3^0 + Fe(OH)_4^- \right]$	(2)
$\dfrac{\partial(\theta E_3)}{\partial t} + L(E_3{}^m) = 0$ $E_3 = \rho_w \begin{bmatrix} UO_2^{2+} + UO_2OH^+ + UO_2(OH)_{2(aq)} + UO_2(OH)_3^- + UO_2(OH)_4^{2-} + 2(UO_2)_2OH^{3+} \\ +2(UO_2)_2(OH)_2^{2+} + 3(UO_2)_3(OH)_4^{2+} + 3(UO_2)_3(OH)_5^+ + 3(UO_2)_3(OH)_7^- \\ +UO_2CO_{3(aq)} + UO_2(CO_3)_2^{2-} + UO_2(CO_3)_3^{3-} + 3(UO_2)_3(CO_3)_6^{6-} + 2(UO_2)_2CO_3(OH)_3^- \end{bmatrix}$ $+\rho_S\left[(> Fe_sO_2)UO_2 + (> Fe_wO_2)UO_2 + (> Fe_sO_2)UO_2CO_3^{2-} + (> Fe_wO_2)UO_2CO_3^{2-} \right]$ $E_3{}^m = \rho_w \begin{bmatrix} UO_2^{2+} + UO_2OH^+ + UO_2(OH)_{2(aq)} + UO_2(OH)_3^- + UO_2(OH)_4^{2-} + 2(UO_2)_2OH^{3+} \\ +2(UO_2)_2(OH)_2^{2+} + 3(UO_2)_3(OH)_4^{2+} + 3(UO_2)_3(OH)_5^+ + 3(UO_2)_3(OH)_7^- \\ +UO_2CO_{3(aq)} + UO_2(CO_3)_2^{2-} + UO_2(CO_3)_3^{3-} + 3(UO_2)_3(CO_3)_6^{6-} + 2(UO_2)_2CO_3(OH)_3^- \end{bmatrix}$	(3)
$\dfrac{\partial(\theta E_4)}{\partial t} + L(E_4{}^m) = 0 \qquad E_4{}^m = \rho_w \begin{bmatrix} CO_{2(g)} + H_2CO_3 + HCO_3^- + CO_3^{2-} + UO_2CO_{3(aq)} + 2UO_2(CO_3)_2^{2-} \\ +3UO_2(CO_3)_3^{3-} + 6(UO_2)_3(CO_3)_6^{6-} + (UO_2)_2CO_3(OH)_3^- \end{bmatrix}$ $E_4 = \rho_w \begin{bmatrix} CO_{2(g)} + H_2CO_3 + HCO_3^- + CO_3^{2-} + \\ UO_2CO_{3(aq)} + 2UO_2(CO_3)_2^{2-} + 3UO_2(CO_3)_3^{3-} \\ +6(UO_2)_3(CO_3)_6^{6-} + (UO_2)_2CO_3(OH)_3^- \end{bmatrix} + \rho_S \begin{bmatrix} > Fe_sCO_3H + (> Fe_sO_2)UO_2CO_3^{2-} \\ +(> Fe_wO_2)UO_2CO_3^{2-} + > Fe_sCO_3^- \\ + > Fe_wCO_3H + > Fe_wCO_3^- \end{bmatrix}$	(4)
$\dfrac{\partial(\theta E_5)}{\partial t} + L(E_5{}^m) = 0 \qquad E_5 = \rho_S \begin{bmatrix} > Fe_sOH_2^+ - > Fe_sO^- - 2(> Fe_sO_2)UO_2CO_3^{2-} - > Fe_sO_3^- + CO \\ -2(> Fe_wO_2)UO_2CO_3^{2-} + > Fe_wOH_2^+ - > Fe_wO^- - > Fe_wCO_3^- \end{bmatrix} \qquad E_5{}^m = 0$	(5)
$\dfrac{\partial(\theta E_6)}{\partial t} + L(E_6{}^m) = 0 \qquad E_6 = E_6{}^m = \rho_w(NO_3^- + UO_2NO_3^+)$	(6)
$\dfrac{\partial(\theta E_7)}{\partial t} + L(E_7{}^m) = R_{18} \qquad E_7 = \rho_S(> Fe_sO_2)UO_2 \qquad E_7{}^m = 0$	(7)
$\dfrac{\partial(\theta E_8)}{\partial t} + L(E_8{}^m) = R_{19} \qquad E_8 = \rho_S(> Fe_wO_2)UO_2 \qquad E_8{}^m = 0$	(8)

Note: as defined in equation (5.4), $\rho_s = \rho_b S_A/\theta$.

Table 5.3-5 Equilibrium Reaction Algebraic Equations Solved in Example 5.3.2

Equilibrium Reaction Algebraic Equations	No.	Equilibrium Reaction Algebraic Equations	No.
$0.0018C_{Fe(OH)_3} = C_{>Fe_sOH} + C_{>Fe_sOH_2^+}$ $+ C_{>Fe_sO^-} + C_{>Fe_sCO_3H} + C_{>Fe_sCO_3^-}$ $+ 2C_{(>Fe_sO_2)UO_2} + 2C_{(>Fe_sO_2)UO_2CO_3^{2-}}$	(1)	$0.8732C_{Fe(OH)_3} = C_{>Fe_wOH} + C_{>Fe_wOH_2^+}$ $+ C_{>Fe_wO^-} + C_{>Fe_wCO_3H} + C_{>Fe_wCO_3^-}$ $+ 2C_{(>Fe_wO_2)UO_2} + 2C_{(>Fe_wO_2)UO_2CO_3^{2-}}$	(2)
$C_{(>Fe_sO_2)UO_2CO_3^{2-}} = \dfrac{10^{-13.0}C_{>Fe_s(OH)_2}C_{UO_2^{2+}}C_{H_2CO_3}}{C_{H^+}^4 C_{CO}^2}$	(3)	$C_{(>Fe_wO_2)UO_2CO_3^{2-}} = \dfrac{10^{-17.10}C_{>Fe_w(OH)_2}C_{UO_2^{2+}}C_{H_2CO_3}}{C_{H^+}^4 C_{CO}^2}$	(4)
$C_{(UO_2)_2(OH)_2^{2+}} = 10^{-5.62}C_{UO_2^{2+}}^2 / C_{H^+}^2$	(5)	$C_{(UO_2)_3(OH)_4^{2+}} = 10^{-11.9}C_{UO_2^{2+}}^3 / C_{H^+}^4$	(6)
$C_{(UO_2)_3(OH)_5^+} = 10^{-15.5}C_{UO_2^{2+}}^3 / C_{H^+}^5$	(7)	$C_{(UO_2)_3(OH)_7^-} = 10^{-31.0}C_{UO_2^{2+}}^3 / C_{H^+}^7$	(8)
$C_{UO_2CO_{3(aq)}} = 10^{-7}C_{UO_2^{2+}}C_{H_2CO_3} / C_{H^+}$	(9)	$C_{UO_2(CO_3)_2^{2-}} = 10^{-16.42}C_{UO_2^{2+}}C_{H_2CO_3}^2 / C_{H^+}^4$	(10)
$C_{UO_2(CO_3)_3^{4-}} = 10^{-28.44}C_{UO_2^{2+}}C_{H_2CO_3}^3 / C_{H^+}^6$	(11)	$C_{>Fe_sO^-} = 10^{-9.13}C_{>Fe_sOH} / C_{H^+}C_{CO}$	(12)
$C_{>Fe_sCO_3^-} = 10^{-5.09}C_{>Fe_sOH}C_{H_2CO_3} / C_{H^+}C_{CO}$	(13)	$C_{(UO_2)_2CO_3(OH)_3^-} = 10^{-17.54}C_{UO_2^{2+}}^2 C_{H_2CO_3} / C_{H^+}^5$	(14)
$C_{(UO_2)_3(CO_3)_6^{6-}} = 10^{-46.08}C_{UO_2^{2+}}^3 C_{H_2CO_3}^6 / C_{H^+}^{12}$	(15)	$C_{>Fe_wO^-} = 10^{-9.13}C_{>Fe_wOH} / (C_{H^+}C_{CO})$	(16)
$C_{>Fe_wCO_3^-} = 10^{-5.09}C_{>Fe_wOH}C_{H_2CO_3} / (C_{H^+}C_{CO})$	(17)	$C_{Fe_sOH} = 2C_{Fe_s(OH)_2}$	(18)
$C_{Fe(OH)_3} = 10^{-2.7}C_{Fe^{3+}} / C_{H^+}^3$	(19)	$C_{Fe_wOH} = 2C_{Fe_w(OH)_2}$	(20)
$C_{UO_2OH^+} = 10^{-5.2}C_{UO_2^{2+}} / C_{H^+}$	(21)	$C_{UO_2(OH)_{2(aq)}} = 10^{-10.3}C_{UO_2^{2+}} / C_{H^+}^2$	(22)
$C_{UO_2(OH)_3^-} = 10^{-19.2}C_{UO_2^{2+}} / C_{H^+}^3$	(23)	$C_{UO_2(OH)_4^{2-}} = 10^{-33.0}C_{UO_2^{2+}} / C_{H^+}^4$	(24)
$C_{(UO_2)_2OH^{3+}} = 10^{-2.7}C_{UO_2^{2+}}^2 / C_{H^+}$	(25)	$C_{CO_3^{2-}} = 10^{-16.68}C_{H_2CO_3} / C_{H^+}^2$	(26)
$C_{>Fe_sOH_2^+} = 10^{6.51}C_{>Fe_sOH}C_{H^+}C_{CO}$	(27)	$C_{CO_{2(g)}} = 10^{1.47}C_{H_2CO_3^0}$	(28)
$C_{>Fe_sCO_3H} = 10^{2.90}C_{>Fe_sOH}C_{H_2CO_3}$	(29)	$C_{FeOH^{2+}} = 10^{-2.19}C_{Fe^{3+}} / C_{H^+}$	(30)
$C_{Fe(OH)_2^+} = 10^{-5.67}C_{Fe^{3+}} / C_{H^+}^2$	(31)	$C_{Fe(OH)_3^0} = 10^{-12.56}C_{Fe^{3+}} / C_{H^+}^3$	(32)
$C_{HCO_3^-} = 10^{-6.35}C_{H_2CO_3^0} / C_{H^+}$	(33)	$C_{Fe(OH)_4^-} = 10^{-21.6}C_{Fe^{3+}} / C_{H^+}^4$	(34)
$C_{>Fe_wOH_2^+} = 10^{6.51}C_{>Fe_wOH}C_{H^+}C_{CO}$	(35)	$C_{>Fe_wCO_3H} = 10^{2.90}C_{>Fe_wOH}C_{H_2CO_3}$	(36)
$C_{NO_3^-} = 10^{0.3}C_{UO_2NO_3^+} / C_{UO_2^{2+}}$	(37)		

Forward and backward kinetic rate coefficients for U(VI) sorption reactions 18 and 19 of the reaction network (Table 5.1) were fitted to the U(VI) breakthrough curve data using a nonlinear parameter estimation procedure yielding

$$> Fe_s(OH)_2 + UO_2^{2+} = (> Fe_sO_2)UO_2 + 2H^+ \quad \log K_f = 3.04,\ \log K_b = -10.1 \qquad \textbf{(5.1.9)}$$

$$> Fe_w(OH)_2 + UO_2^{2+} = (> Fe_wO_2)UO_2 + 2H^+ \quad \log K_f = -0.494,\ \log K_b = 4.5 \qquad \textbf{(5.1.10)}$$

Simulations of U(VI) transport using kinetic parameters (lower part of Figure 5.3-4) yielded good agreement with the measured results indicating that U(VI) transport may be kinetically controlled in naturally heterogeneous media.

5.3.3   Three-dimensional Reactive Uranium Transport Simulation

This example was undertaken to assess the model capability to handle complex geochemistry within a three-dimensional subsurface domain. A 600 m long, 400 m wide, and 200 m deep region is considered (Figure 5.3-5) and discretized with uniform hexahedral elements with size of 60 m × 50 m × 40 m. A steady state flow field was simulated with the subsurface flow module.
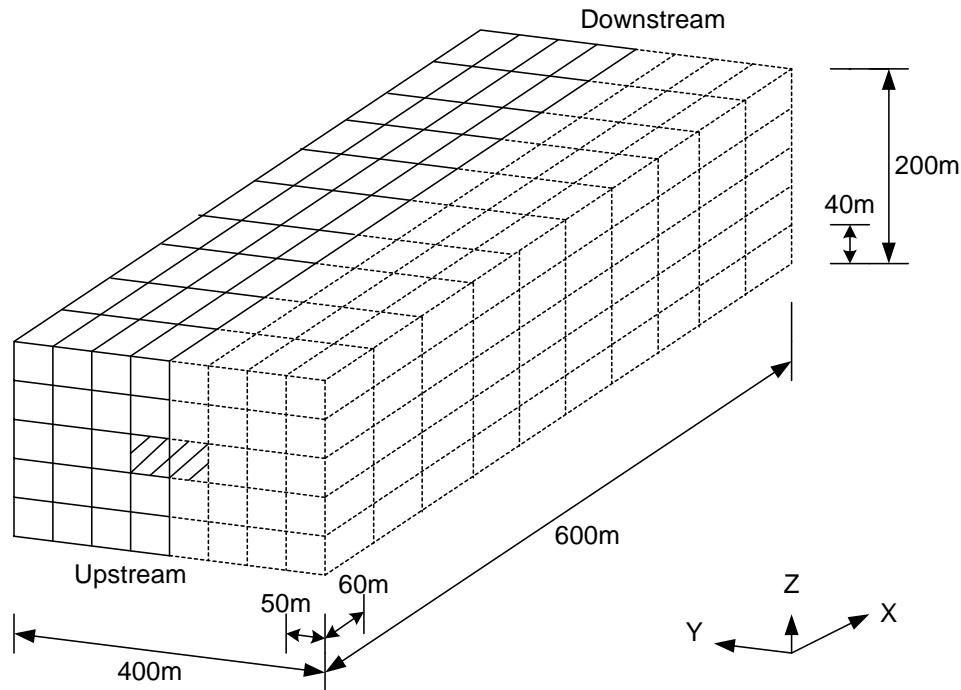
Fig. 5.3-5.   Simulation Domain and Descretization for Example 5.3.3

For flow simulations, Dirichlet boundary conditions were applied to the upstream boundary (x = 0 m) with total head of 190 m and to the downstream boundary (x = 600 m) with total head of 180 m. Variable boundary conditions were applied to the top boundary (z = 200 m) with flux of 0.0015 m/d. We assumed a constant effective porosity of 0.3 and saturated hydraulic conductivity of $K_{xx} = K_{yy} =$ 1.0 and $K_{zz} = 0.1$ m/d. The following two equations were employed to describe the unsaturated hydraulic properties.

$$\theta = 0.1 + (0.3 - 0.1)/(1 + 4h^2) \qquad\qquad (5.1.11)$$

$$Kr = \left[0.1 + (0.3 - 0.1)/(1 + 4h^2)\right]/0.3 \qquad\qquad (5.1.12)$$

where θ is the moisture content and Kr is the relative conductivity. The calculated moisture content is between 0.1 and 0.3 and Darcy velocity is between 0.0014 and 0.021 m/day.

In addition to the chemical species and reactions considered in Example 5.3.2, one more dissolved

species A is assumed to undergo a hypothetic kinetic reduction/oxidation reaction

$$UO_2{}^{2+} = A \quad \log K_f = -10.0, \ \log K_b = -5.0 \tag{5.1.13}$$
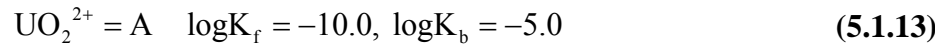
Initial aqueous and adsorbed concentrations are assumed to be zero. The initial concentration of $Fe(OH)_3$ is assumed to be 0.0523 mol/L and the pH is 4.6 throughout the region. The boundary conditions for the transient simulation are: no flux at the bottom ($z = 0$ m), the front ($y = 0$ m) and the back ($y = 400$ m) boundaries; flow-out variable boundary condition for the downstream boundary ($x = 600$ m); flow-in variable boundary condition for the top ($z = 200$ m) and the upstream boundary ($x = 0$ m) with zero concentration for each mobile species except at the two shaded boundary faces shown in Figure 5.3-5, where the inflow contains $UO_2{}^{2+}$ of 1.15×10^{-5} mol/L, NO_3^- of 0.05 mol/L, and a nonreactive tracer of 1.15×10^{-5} mol/L. The longitudinal dispersivity is 60 m, the transverse dispersivity is 6 m, and the molecular diffusion coefficient is assumed to be zero. A 100 years simulation is performed with a fixed time-step size of 1 year.

Simulation results within the bisected simulation domain are illustrated in Figure 5.3-6 for nonreactive tracer, aqueous uranium, and sorbed uranium. The two variable boundary faces on the upstream boundary (Shaded in Figure 5.3-5) represent the source of tracer and aqueous uranium. The nonreactive tracer is transported into the domain along with subsurface flow. However, due to the sorption reactions, most of the mobile aqueous uranium is transformed into immobile sorbed uranium in the region close to the two boundary faces. Therefore, uranium plume migration is much slower than that of the nonreactive tracer. The calculated percentage of sorbed uranium ranges from 56% to 96%, which illustrates that a single value of the distribution coefficient is not able to simulate the spatially variable retardation under the condition set for this example.

Using the fully-implicit scheme to deal with reactive chemistry, it took Option 1 (the FEM applied to the conservative form of the transport equations) 611 seconds to perform the simulation with a fixed time-step size of 1 year (maximum Courant number of 0.6). The same accurate simulation could be obtained through Option 3 (the modified LE approach) with a much larger time-step size of 5 years taking CPU time of 156 seconds. Comparison of CPU time verified the efficiency of Option 3.
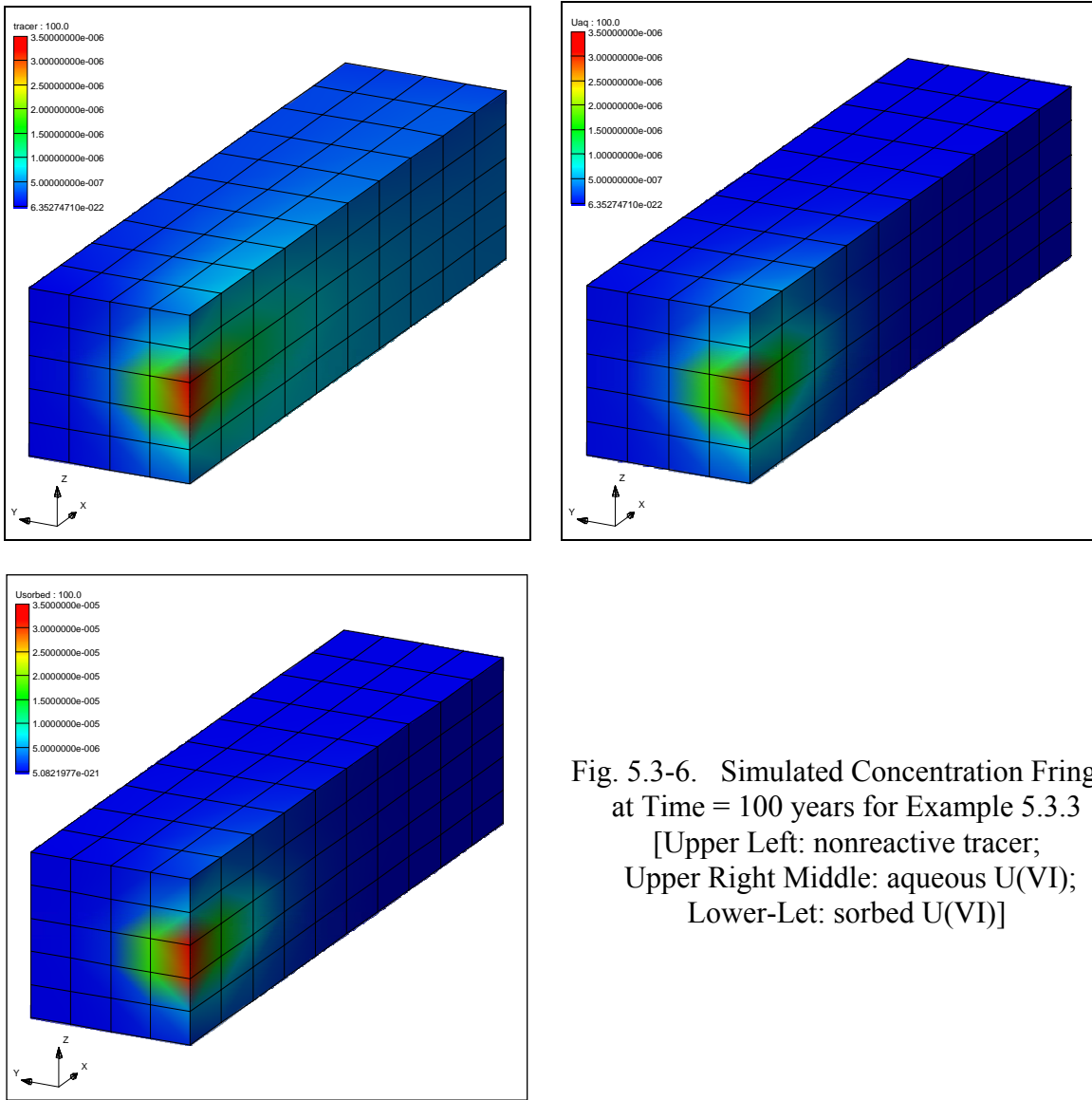
Fig. 5.3-6.   Simulated Concentration Fringes
at Time = 100 years for Example 5.3.3
[Upper Left: nonreactive tracer;
Upper Right Middle: aqueous U(VI);
Lower-Let: sorbed U(VI)]

Animations showing the spatial-temporal distribution of tracer (File Name: Figure 5.3-6 Tracer.avi), sorbed uranium (File Name: Figure 5.3-6 Uranium sorbed.avi), and aqueous uranium (File Name: Figure 5.3-6 Uranium Aqueous.avi), respectively, are attached in Appendix A.   Readers can visualize these moves by clicking the file contained in the attached CD.